Experimental and numerical investigation of liquid and two-phase refrigerant flow through capillary tubes capturing complex flow phenomena

vorgelegt von
Xenia Yvonne Wilhelm, M.Sc. (geb. Gabrisch)
geb. in Braunschweig

von der Fakultät III – Prozesswissenschaften
der Technischen Universität Berlin
zur Erlangung des akademischen Grades

Doktorin der Ingenieurwissenschaften
- Dr.-Ing. -

genehmigte Dissertation

Promotionsausschuss:

Vorsitzender:	Prof. Dr.-Ing. habil. Rudibert King
1. Gutachter:	Prof. Dr.-Ing. habil. Jens-Uwe Repke
2. Gutachter:	Prof. Dr.-Ing. Felix Ziegler
3. Gutachter:	Dr.-Ing. Tommy Grunert

Tag der wissenschaftlichen Aussprache: 23. März 2021

Berlin, 2021

In liebevollem Andenken an Dziadek.

Affidavit

Hiermit erkläre ich an Eides statt, dass ich die vorliegende Arbeit selbstständig und eigenhändig sowie ausschließlich unter Verwendung der aufgeführten Quellen und Hilfsmittel angefertigt habe.

Xenia Yvonne Wilhelm, M.Sc. (geb. Gabrisch)
Berlin, 23. März 2021

I hereby confirm that I prepared this thesis independently and by exclusive reliance on literature or tools indicated herein.

Xenia Yvonne Wilhelm, M.Sc. (geb. Gabrisch)
Berlin, 23rd March 2021

Acknowledgements

Für die Betreuung meiner Doktorarbeit möchte ich mich herzlich bei Prof. Repke bedanken. Ich möchte die Zeit und die damit verbundene fachliche sowie persönliche Weiterentwicklung nicht missen! Besonderer Dank gebührt Tommy, der mich bereits während der Masterarbeit auf den Doktor-Kurs gelotst hat und mir stets ein Mentor und Förderer gewesen ist. Meinen Eltern danke ich dafür, dass sie mich auf meinem Bildungsweg immer unterstützt und an mich geglaubt haben und mir die besten Vorbilder sind. Für die fachliche Zuarbeit danke ich allen studentischen Hilfskräften, die mich während der Promotion unterstützt haben. Ganz besonders danke ich Jelena, nicht nur für ihre Unterstützung als studentische Hilfskraft, sondern insbesondere für ihre Freundschaft, die schönen Kaffee- und Mittagspausen und vieles mehr. Bei dem gesamten Fachgebiet und allen Kolleginnen und Kollegen, die meinen Weg am dbta geteilt haben, möchte ich mich bedanken, dafür, dass ich mit euch eine unvergessliche Zeit hatte. Danke vor allem an Hannes und Johannes, dass ihr mich damals überredet habt, unser späteres Büro zu renovieren und mit euch zu beziehen! Ich weiß nicht, ob ich jemals wieder so viel Spaß im Büro haben werde. Aber ich denke, das ist unmöglich. Zum Schluss bin ich am meisten dankbar dafür, dass ich am Fachgebiet meinen Ehemann Robert kennenlernen durfte. Ohne dich wäre ich nicht wo und wer ich bin! Ich danke dir für alles.

Abstract

English

Capillaries are used as throttle devices in rather small heat pump applications. They meter the refrigerant mass flow in the system and therefore play a decisive role regarding the heat pump performance. In order to exploit the optimization potential that lies in the capillary design with respect to the energy efficiency of the heat pump, computer-aided design is a valuable tool. A valid and predictive capillary model within a valid overall heat pump model is indispensable for robust and reliable results of the optimization of the capillary design.

Modelling the capillary inside a heat pump application means modelling the single liquid and the two-phase flow of refrigerants in a long tube with a small diameter. Researchers are dealing with the modelling of the two-phase flow of refrigerants for many decades. Yet, it is not satisfactorily described until now. Especially, when it comes to natural refrigerants as e.g. the refrigerant propane, only little experimental data is avaiable against which the flow model can be validated. Further, it is essential to capture the change of single to two-phase flow within the flow model as this corresponds to the real operation of the capillary inside the heat pump. However, there are complex flow phenomena that occur at phase change. Researchers e.g. have observed a hysteresis effect that leads to different mass flows or pressure drops in the capillary for the same operating conditions.

As the database on propane is generally limited and the hysteresis effect is barely recorded at all in the available literature, this thesis provides an extensive database on the propane flow in a copper capillary. The database covers a wide range of operating conditions ranging from 16 to 25 bar inlet pressure, subcoolings from

5 to 9 K at the capillary inlet and mass flux from 3430 to 4573 kg/m^{2}s. The characteristics of the hysteresis effect are evaluated quantitatively and qualitatively. The hysteresis effect shows differences in the measured pressure drop of around 20 % for the same flow conditions depending on the previously investigated subcooling at the capillary inlet. Systematic experiments that have been carried out support the hypothesis that the wetting of the capillary tube entails the hysteresis effect as it lowers the friction of the two-phase flow along a previously wetted capillary. These findings were transferred into a mathematical description which were supplemented to a common homogeneous flow approach. The homogeneous flow approach requires a suitable two-phase viscosity correlation. Among the commonly known correlations, the one that leads to the best match between the experimental and numerical data is identified and calibrated to improve the prediction quality of the flow model. The adapted viscosity correlation together with the extended model approach to capture the hysteresis of the flow leads to a high prediction quality of the homogeneous flow model. Around 70 % of the experimental data is predicted within an error band of only 5 % resulting in a mean relative error of 4 %. The basic homogeneous flow model that is not able to capture hysteresis together with the application of the unmodified viscosity correlation, predicts only around 40 % of the experimental data within an error band of 5 % and yields a mean relative error of 7 %. The accuracy of the developed model could be proven for experimental investigations in a steel capillary. A systematic procedure for the investigation of refrigerant flow in a capillary tube including a guideline for the parametrization of the flow model is proposed.

Keywords: *two-phase flow; propane flow; hysteresis effect; metastable flow; capillary tube*

Deutsch

Kapillare werden in eher kleinen Wärmepumpen als Drosselorgane eingesetzt. Da sie den Kältemittelmassenstrom im System regulieren, wirken sie sich maßgeblich auf den Betrieb und die Leistungsfähigkeit der Wärmepumpe aus. Eine modellbasierte Betrachtung stellt eine wertvolle Möglichkeit dar, das Optimierungspotenzial des Kapillardesigns hinsichtlich einer gesteigerten Energieeffizienz der

Wärmepumpe auszuschöpfen. Ein valides und prädiktives Kapillarmodell innerhalb eines validen Gesamtmodells der Wärmepumpe ist dabei unabdingbar, um sich auf die Ergebnisse der Optimierung bzgl. des Kapillardesigns verlassen zu können.

Die Modellierung der Kapillare in der Literatur entspricht der Modellierung des einphasigen flüssigen und zweiphasigen Kältemittels in einem langen Rohr mit sehr kleinem Durchmesser. Wissenschaftler beschäftigen sich seit Jahrzehnten mit der Modellierung von Kältemittelströmung durch Kapillare, jedoch wurden bis zu diesem Zeitpunkt keine zufriedenstellenden Ergebnisse erzielt. Insbesondere natürliche Kältemittel sind weniger umfangreich untersucht. Propan stellt ein Beispiel dar, zu welchem Kältemittel besonders wenige Experimentaldaten verfügbar sind, sodass eine zuverlässige Validierung von Strömungsmodellen schwierig ist. Überdies ist es wichtig den Phasenübergang von flüssig zu zweiphasig in der Kapillare zu erfassen, da dies der gängige Betriebszustand der Kapillare innerhalb der Wärmepumpe ist. Viele Experimente befassen sich jedoch ausschließlich mit der zweiphasigen Strömung von Kältemitteln in Kapillaren. Jedoch treten beim Phasenübergang komplexe Strömungsphänomene, wie z.B. ein Hysterese-Effekt, auf. Der Hysterese-Effekt bewirkt, dass bei gleichen Strömungsbedingungen in der Kapillare unterschiedliche Massenströme oder Druckverluste gemessen werden, abhängig davon welche Zustände zuvor herrschten.

Da die Datengrundlage von Propan grundsätzlich sehr dünn ist und der Hysterese-Effekt in der Literatur kaum dokumentiert ist, liefert diese Arbeit umfangreiche experimentelle Daten von Propanströmen durch eine Kupferkapillare. Die experimentellen Daten decken einen breiten Bereich an Strömungszuständen ab, die von 16 bis 25 bar Eintrittsdruck, Unterkühlungstemperaturen von 5 bis 9 K am Kapillareintritt und Massenstromdichten von 3430 bis 4573 kg/m^2s reichen. Die charakteristischen Ausprägungen der vermessenen Hysteresekurven wurden quantitativ und qualitativ bewertet und zusammengefasst. Durch den Hysterese-Effekt kann es zu einem Unterschied im gemessenen Druckverlust in der Kapillare von 20 % bei gleichen Eintrittsbedingungen kommen, abhängig von der Historie der vermessenen Unterkühlungstemperaturen im Kapillareintritt. Es wurden systematische Untersuchungen durchgeführt, welche die Hypothese unterstützen, dass eine veränderte Benetzung der Kapillare einen Hystere-Effekt hervorrufen kann. Zweiphasige Strömung, die über einen zuvor benetzten Teil der Kapillare

strömt, erfährt weniger Reibung, wodurch es zu einem geringeren Druckverlust in der Kapillare kommt. Diese Erkenntnisse wurden in einen mathematischen Modellansatz überführt, durch welchen ein gängiges homogenes Strömungsmodell weiter entwickelt wurde. Homogene Strömungsmodelle bedürfen einer Korrelation zur Berechnung der zweiphasigen Viskosität des Kältemittels. Unter den gängigen zweiphasigen Viskositätsansätzen wurde ermittelt, welcher Ansatz zusammen mit dem homogenen Strömungsmodell die Experimentaldaten am besten prädiziert. Der identifizierte Ansatz wurde im Vergleich mit den Experimentaldaten kalibriert, sodass die Prädiktionsgüte des Modells weiter gesteigert werden konnte. Das homogenen Strömungsmodell zusammen mit dem adaptierten Viskositätsansatz und dem Modellansatz zur Beschreibung des Hysterese-Effekts prädiziert 70 % der Experimentaldaten innerhalb eines Fehlerbandes von 5 % und resultiert in einem mittleren relativen Fehler von 4 %. Das herkömmliche homogene Strömungsmodell, welches den Hysterese-Effekt nicht modelliert, zusammen mit dem unmodifizierten Viskositätsansatz, prädiziert verglichen damit lediglich 40 % der Experimentaldaten innerhalb eines Fehlerbandes von 5 % und resultiert in einem mittleren relativen Fehler von 7 %. Die Prädiktionsgüte des entwickelten Strömungsmodells konnte im Vergleich mit weiteren Experimentaldaten in einer Stahlkapillare nachgewiesen werden. Die experimentellen Untersuchungen dieser Arbeiten wurden in einer systematischen Prozedur für die generelle Untersuchung von Kältemittelströmen in Kapillarrohren zusammengefasst und um einen Leitfaden für die Parametrierung des entwickelten Strömungsmodells ergänzt.

Schlüsselwörter: *zweiphasige Strömung; Propanströmung; Hysterese; Metastabile Strömung; Kapillarrohr*

Publications

This thesis is partially based on already published contributions. In the following, the contributions are divided into Journal articles and papers within conference proceedings and a supervised thesis.

Journal Articles

- X. Gabrisch and J.-U. Repke (2020): Modelling the two-phase flow of propane in a capillary tube: Determination of the two-phase viscosity based on detailed experiments. *International Journal of Refrigeration* 118, 427–442. ISSN: 0140-7007. DOI: https://doi.org/10.1016/j.ijrefrig.2020.05.018. URL: https://www.sciencedirect.com/science/article/pii/S0140700720302279

- X. Gabrisch and J.-U. Repke (2021): Modelling the two-phase flow of propane in a capillary tube: Investigating and modelling the metastable flow and hysteresis effect. *International Journal of Refrigeration* 121, 126–135. ISSN: 0140-7007. DOI: https://doi.org/10.1016/j.ijrefrig.2020.10.030. URL: https://www.sciencedirect.com/science/article/pii/S0140700720304497

Conference Papers

- X. Gabrisch, T. Grunert, and J.-U. Repke (2017): Dynamische Modellierung einer Kältemittel-Luft-Wärmepumpe - Analyse des Einflusses der Drosselmodellierung auf die Betriebspunktsimulation. In: *Deutsche Kälte- und Klimatagung*. Ed. by X. Gabrisch, T. Grunert, and J.-U. Repke. Bremen: Deutscher Kälte- und Klimatechnischer Verein

- X. Gabrisch and J.-U. Repke (2019c): Experiments of the Pressure Drop of Propane Considering Hysteresis and Metastability. In: *Proceedings of the 4th World Congress on Momentum, Heat and Mass Transfer*. Rome. DOI: 10.11159/icmfht19.106

- X. Gabrisch and J.-U. Repke (2019b): Evaluation of the Two-Phase Pressure Drop of Propane on the Basis of Detailed Experiments Considering Metastability and Hysteresis. In: *10th Internation Conference on Multiphase Flow*. Rio de Janeiro

- X. Gabrisch and J.-U. Repke (2019a): Computer-Assisted Experiments for the Identification of the Two-Phase Viscosity of Fluids. In: *29th European Symposium on Computer Aided Process Engineering*. Eindhoven, 631–636. DOI: 10.1016/B978-0-12-818634-3.50106-5

Supervised Thesis

- J. Deichl (2019): Stationäre und dynamische Simulation von Gegenstrom-Wärmeübertragern. *Master Thesis*. Technische Universität Berlin

Contents

List of Figures

List of Tables

List of Symbols

Greek Symbols

Symbol	Description	Unit
α	void fraction	-
ΔL	discretized length	m
Δp	pressure drop	Pa
ΔT_{SC}	subcooling	K
ΔT_{SH}	superheating	K
δ	differential operator	
η	data within specific error band	%
μ	dynamic viscosity	Pa·s
$\overline{\rho}$	averaged density	kg/m^3
ψ	scaling factor	-
ρ	density	kg/m^3
σ	standard deviation	specific
τ	shear stress	Pa
Θ	wetting ratio of the capillary	
ξ	entrance pressure drop coefficient	

Indices

Symbol	Description
i	index for the discretized pressure drop calculation
j	index for the operating condition of the considered investigated operating conditions

Latin Symbols

Symbol	Description	Unit
$\dot{m}$	mass flow rate	kg/s
$\dot{Q}$	heat rate	W
$\dot{W}$	(electrical) power	W
$\overline{f}$	averaged Darcy friction factor	
A	(cross-sectional) area	m^2
B	auxiliary term within the calculation of the Darcy friction factor following the correlation of Serghides (1984)	-
C	auxiliary term within the calculation of the Darcy friction factor following the correlation of Serghides (1984)	-
c	speed of sound	m/s
d	(inner) diameter of the capillary	m
dp	discretized pressure drop	Pa
dv	discretized change in velocity	m/s
dz	discretized length	m
e	roughness of the inner surface of the capillary tube	m
e	specific energy (only in section 2.2)	J/(kg)
f	Darcy friction factor	
G	mass flux	$kg/(m^2 \cdot s)$
h	specific enthalpy	J/kg
L	length of the capillary	m
Ma	Mach-Number	-
MAE	Mean Absolute Error	bar
MRE	Mean Relative Error	%
Ra	average roughness value	m
Re	Reynolds-Number	-
Rz	average roughness depth	m
S	Sensitivity Matrix	
s	specific entropy	$J/(kg \cdot K)$
SSE	Sum of Square Errors	bar^2
v	(flow) velocity	m/s
x	position in a profile line (applies only in section 3.3.4)	m
x	vapour quality	-
Z	height of a measured profile line (surface profile)	m
z	exemplary parameter	

Superscripts

Symbol	Description
-1	previous condition
0	initial condition
down	lower bound/condition
up	upper bound/condition)

Subscripts

Symbol	Description
Δp	related to the pressure drop
a.entr.	after the entrance of the capillary
acc	accelerational
Copper	related to the copper capillary
d	related to the inner diameter
e	related to the roughness of the inner surface of the capillary
entr.	entrance of the capillary
exp	experimental
fric	frictional
in	at the inlet of the capillary
inlet	at the inlet of the capillary
l	liquid phase
lateral	lateral (area)
liq	liquid flow
out	at the outlet of the capillary
p	peak in a profile line
Ra	related to the average roughness value *Ra*
Rz	related to the average roughness depth *Rz*
sat	at saturation
sim	simulated/predicted
Steel	related to the steel capillary
sum	summarized/accumulated
tp	two-phase
v	valley in a profile line (applies only in section 3.3.4)
v	vapour phase

wetted	related to wetted part of the capillary

List of Abbreviations

Numerics

B&W	**B**eattie **&** **W**halley
COP	**C**oefficient **O**f **P**erformance
MAE	**M**ean **A**bsolute **E**rror
MRE	**M**ean **R**elative **E**rror
SC	**S**ub**c**ooling

1 Introduction

The design of modern heat pumps underlies the global environmental trend of being as resource-saving and having as little impact on the environment as possible. In terms of energy supply, electricity can be saved by optimizing the performance of the heat pump and reducing the required compressor power. A thermostatic or electric expansion valve provides the possibility to implement control strategies and effectively influence the performance of the heat pump. However, these throttle devices are rather costly, especially within small heat pump applications as e.g. heat pump tumble driers. Besides the energy efficiency, an important sale criteria for those devices is the price efficiency. In order to keep the costs to a minimum, capillary tubes are preferably applied as throttle device within smaller heat pump applications.

A capillary is a long tube with a comparably small inner diameter. It can hardly be generalized, yet, usual diameters range from 0.5 to 2 mm and the length from 1 to 6 m (Dubba and Kumar, 2017). For space reasons they are often coiled. Being the counterpart of the compressor in the heat pump, the capillary controls the refrigerant mass flow in the cooling circuit. Consequently, it has a major influence on the performance of the heat pump. Capillaries can be operated diabatically, i.e. exchanging heat with a different medium, or adiabatically, i.e. without heat exchange. A capillary is not able to react on (changing) operating conditions of the heat pump as it is a static throttle device. Its design is not modifiable during the operation. It is therefore all the more important to know how the capillary behaves within the overall system in order to derive the optimal capillary design and improve the energy efficiency of the heat pump.

If the capillary design is to be determined via hardware tests, for given operating conditions of the heat pump (e.g. refrigerant charge, heat loads, heat exchanger specifications, . . .) the capillary design (inner diameter, material, length, . . .) has to

be iteratively changed and tested within the system. This can be time-consuming and expensive. A model-based approach is a more economic way to derive the optimal design of the capillary for given operating conditions. This requires a predictive capillary model within a predictive overall heat pump model. However, modelling the refrigerant flow through a capillary is complex and although it is a subject of research for many decades, researchers have still not come up with a satisfactorily predictive model. On the one hand, this can be traced back to insufficient model assumptions - on the other hand, imprecise and not completely comprehensible experimental data as a validation base can be one reason.

Typically, the refrigerant enters the capillary in a subcooled condition and flashes downstream the capillary inlet. Hence, the refrigerant flow covers a part of the capillary tube in liquid and a part in two-phase condition. Obviously, it is more complex to model the two-phase flow than the single liquid flow of refrigerants. Many researchers therefore focus on the experimental investigation of two-phase flow *only* and are neglecting the liquid phase and phase change effects inside the capillary. However, complex phenomena are observed when investigating the liquid refrigerant flow with phase change in a capillary. Cooper, Chu, and Brisken (1957) discovered the metastable flow phenomena which is referred to as the "underpressure of vaporization". They observed that refrigerant flow remained subcooled at pressures that are below the actual saturation pressure. Z. H. Chen, R. Y. Li, and Z. Y. Chen (1990) developed an empirical correlation to predict the underpressure of vaporization which is mostly referred to when modelling the metastable flow. Meyer and Dunn (1998) discovered the presence of a hysteresis effect that yielded different mass flows for the same flow conditions at the inlet of the capillary depending on the previous flow conditions. More precisely: they discovered that the previous subcooling of the refrigerant at the capillary inlet lead to different measured mass flows depending on whether the subcooling was increased or decreased. Guobing and Yufeng (2006) indicated that there is an interrelation between the metastable flow and the hysteresis effect which is supported by the research of Gao, Eguchi, and Tatara (2015). As the refrigerant usually enters the capillary in a subcooled condition within the heat pump process, those flow phenomena may impact the heat pump performance. However, to the best of the author's knowledge, so far no model approach that is available in the literature interrelates both flow phenomena. Instead, applying the correlations

proposed by Z. H. Chen, R. Y. Li, and Z. Y. Chen (1990) and/or Feburie et al. (1993) which are widely used, the metastable flow is not calculated depending on any previous flow conditions. Therefore, the hysteresis effect is not captured within the available model approaches.

The hysteresis effect leads to ambiguity within the experimental data gathered on the liquid and two-phase flow of refrigerant in a capillary tube. If this ambiguity is not particularly worked out in the experimental database, the numerical results of predicting the flow will at least deviate from the experimental results by the amount the experimental results deviate due to the hysteresis effect. However, a systematic documentation on the history of investigated flow conditions in order to comprehend the hysteresis effect is very rare in the available literature. If a flow model shall capture the hysteresis effect in order to predict the overall experimental database including ambiguous data, the prerequisite for that is a comprehensive experimental database that discloses the hysteresis effect.

Besides unconsidered flow phenomena, imprecise parameters that specify the capillary design within the flow model, such as the inner diameter and the roughness of the inner surface of the capillary, entail a discrepancy between the prediction and the experimental results. Ribatski (2013) criticized that many researchers do not thoroughly specify the design of the investigated capillary tube. Consequently, wrong conclusions can be drawn concerning the structure or correlations the flow model is based on when observing a deviation between the experimental and numerical results.

Referring to Dubba and Kumar (2017) most experimental data on the flow of refrigerants in capillary tubes exists on hydrofluorocarbons. However, those refrigerants are gradually replaced by more environmental-friendly refrigerants in terms of a lower global warming potential. Consequently, there is a lack of sufficient and reliable experimental data on natural refrigerants which explicitly document the history of investigated flow conditions in order to interrelate the metastable flow and the observed hysteresis effect (see (Meyer and Dunn, 1998) and (Guobing and Yufeng, 2006)). Further, the experimental databases additionally often lack a precise capillary specification that is essential for an appropriate parametrization of a model that describes the flow of the refrigerant in the capillary.

Against the background of the outlined lack in the research above, this thesis has the following major targets:

- to generate a comprehensive database on the single liquid and two-phase flow of propane flow through a capillary tube that captures the hysteresis effect
- to determine and disclose precise specifications of the inner diameter and the roughness of the inner surface of the investigated capillary
- to explore the root and the interrelation between the occurrence of metastable flow and the hysteresis effect
- to develop a flow model that is able to precisely predict the investigated flow and capture the metastable flow and hysteresis effect, respectively

In chapter 2 the role of the capillary as expansion device is embedded into the theoretical background of a heat pump operation and the principles of tube flow are derived as a basis for the development of the flow model that describes the refrigerant flow in the capillary.

The developed experimental apparatus and the necessary experimental investigations on the refrigerant flow in order to systematically record the hysteresis effect are presented in chapter 3. Therefore, it is thoroughly distinguished between increasing and decreasing subcoolings in the pre-defined measurement series of flow conditions that are to be investigated. Further, specific investigations that are carried out to explore the root and the characteristics of the hysteresis effect are shown and discussed. The experimental investigations comprise the propane flow in a copper and a steel capillary that are specified to an inner diameter of 1.1 mm, a length of 1 m. Both capillary tubes are horizontally applied in the experimental apparatus. After the experiments are accomplished, the inner diameter and roughness of the capillaries are determined.

In chapter 4 the mathematical model that is used to predict the refrigerant flow is described in detail. It is based on the homogeneous flow approach in order to keep the model as simple as necessary and computational effort as low as possible. The findings concerning the development of metastable flow and the

hysteresis effect in chapter 3 are transformed into a mathematical description and supplemented to the basic homogeneous model approach.

In chapter 5 the prediction of the flow based on the developed flow model is compared and evaluated against the gathered experimental data. Common two-phase viscosity correlations that are applied within the homogeneous flow model are evaluated against the experimental database concerning the copper capillary tube. An adapted viscosity correlation is proposed to better predict the experimental database on propane. The flow model requires the determination of three empirical parameters which are determined via parameter estimation. The parameters are related to the entrance pressure drop of the propane flow that enters the narrow cross-sectional area of the capillary coming from a wider tube, the proposed viscosity correlation and the modelling of the hysteresis effect and are determined against the experimental data obtained in the copper capillary. The fully parametrized flow model is consecutively used to predict the gathered experimental data in the steel capillary. This serves to verify the prediction accuracy of the flow model.

Finally, the findings of the thesis are summarized in chapter 6 and future directions are discussed.

2 Theoretical Background and State of the Art

As this work deals with the investigation of capillary tubes which are considered to be part of a heat pump system, the principles of the heat pump technology are outlined and the role of the capillary is highlighted. The principles of the heat pump operation in section 2.1 help to comprehend the design of the experimental apparatus in chapter 3 and the overall background of the capillary application. Further, it is important to understand the peculiarities of the capillary operation within a heat pump operation in order to follow the modelling of the capillary in chapter 4 which is explained in section 2.2. The principles of tube flow are derived in section 2.3 and serve as a basis for the modelling of refrigerant flow through the capillary. Section 2.4 reveals the state of the art with regard to experiments of flow phenomena that influence the capillary operation. Further, the model attempts to predict these flow phenomena are pointed out. Finally, the determination of the refrigerant properties needed for the modelling is explained in section 2.5.

2.1 Principles of a Heat Pump Operation

"A heat pump, in the common thermodynamic sense, is a system in which refrigeration components (compressors, condensers, evaporators, and expansion devices) are used in such a manner as to take heat from a source (air, water ground, etc.) and give it up to a heat sink (air, water, ground etc.) that is at a higher temperature than the source." (Sauer and Howell, 1983)

Fig. 2.1 depicts the process of the heat pump cycle with its basic components. The compressor and the throttle are counterparts in the process: the compressor

generates the refrigerant mass flow in the cycle; it increases the pressure of the refrigerant as the throttle blocks the refrigerant. Usually, the refrigerant is in gas phase at the inlet of the compressor. By increasing the pressure of the gas, the temperature and the specific enthalpy of the refrigerant rise. Hence, the refrigerant is brought to a higher level of temperature for which the compressor requires the electrical power $\dot{W}_{1-2}$. Considering the heat loss Q_{1-2} in the compressor, the energy balance of the compressor results in:

$$\dot{W}_{1-2} = \dot{m} \cdot (h_2 - h_1) + \dot{Q}_{1-2} \tag{2.1}$$

where $\dot{m}$ denotes the mass flow and h the specific enthalpy of the refrigerant at the specified state in the cycle (see Fig. 2.1). The according change of state of the refrigerant can be traced in an exemplary heat pump cycle in the p,h-diagram of propane as an example for natural refrigerants in Fig. 2.2. Upstream the compressor, the refrigerant enters the condenser in gas phase where it is liquefied and subcooled and transfers heat ($\dot{Q}_{2-3}$) to the heat sink:

$$\dot{Q}_{2-3} = \dot{m} \cdot (h_3 - h_2) \tag{2.2}$$

Subsequently, the subcooled refrigerant is expanded by the throttle device whereby the pressure and temperature decrease. The expansion of the refrigerant is regarded as adiabatic and isenthalpic, hence it follows:

$$h_4 = h_3 \tag{2.3}$$

In the last change of state of the heat pump cycle, the two-phase refrigerant that results from the expansion enters the evaporator where it is evaporated and superheated. For this it requires the heat $\dot{Q}_{4-1}$ from the heat source:

$$\dot{Q}_{4-1} = \dot{m} \cdot (h_4 - h_1) \tag{2.4}$$

The coefficient of performance (COP) of a heat pump relates the provided heat $\dot{Q}_{2-3}$ and the required electrical power $\dot{W}_{1-2}$ and is defined as follows:

$$COP = \frac{\dot{Q}_{2-3}}{\dot{W}_{1-2}} \tag{2.5}$$

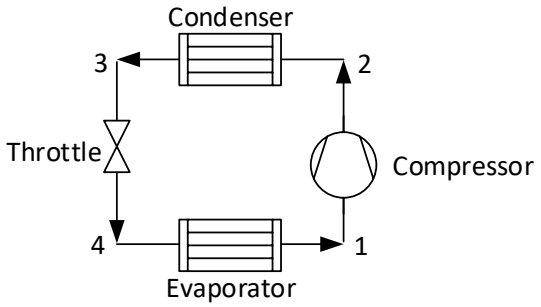

Fig. 2.1: *Basic components of the heat pump process.*

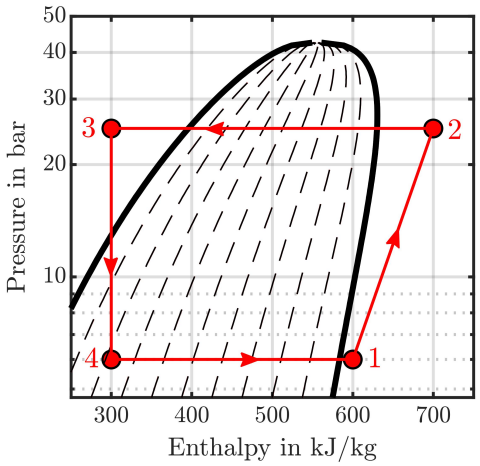

Fig. 2.2: *Exemplary simplified and idealized heat pump process in the p,h-diagram of propane.*

The superheating and subcooling are reference conditions of the heat pump process that have an influence on the COP. The superheating ΔT_{SH} is calculated subtracting the saturation temperature $T_{sat,1}$ for the present pressure p_1 at the compressor inlet from the temperature at the compressor inlet T_1 (compare Fig. 2.2):

$$\Delta T_{SH} = T_1 - T_{sat,1} \tag{2.6}$$

A safe compressor operation requires refrigerant in gas phase at the suction line, thus, a certain amount of superheating ΔT_{SH} is desired within the heat pump operation.

The subcooling ΔT_{SC} is defined by the difference between the saturation temperature $T_{sat,3}$ according to the high pressure p_3 and the temperature at the inlet of the expansion valve T_3 (compare Fig. 2.2):

$$\Delta T_{SC} = T_{sat,3} - T_3 \tag{2.7}$$

Other than the superheating, a larger degree of subcooling has a positive effect on the heat pump performance, as it increases the mass flow rate. As the heat pump process is a closed cycle, a larger degree of subcooling has an impact on the superheating, too. Consequently, both properties need to be coordinated within the heat pump operation. (Dinçer and Kanoglu, 2010)

2.2 Peculiarities of the Operation of a Capillary within a Heat Pump

"The control, expansion, or metering device must match the flow of refrigerant on the load on the evaporator, the pumping capacity of the compressor, and the ability of the condenser to reject heat. It determines the capacity of the system, which is probably the most important function in the entire system." (Sauer and Howell, 1983)

Capillary tubes are applied as expansion device in rather small heat pump applications due to cost advantages. Whereas thermostatic or electric expansion valves dynamically control the mass flow in a heat pump system, the capillary is a static expansion device. It is therefore designed to perform within a pre-defined temperature range between the evaporating temperature T_1 and the condensing temperature T_3 (see Fig. 2.2). (Pohlmann, 2010) Hence, the heat pump system and the influence of the capillary tube on its performance must be very well understood when designing the capillary. With the desired refrigerant condition at the capillary inlet being subcooled, see section 2.1, the refrigerant is subject to a phase change from liquid to two-phase (vapour-liquid) flow in the usual operation. The pressure rapidly drops due to the friction and the acceleration pressure drop of the two-phase flow. The capillary tube meters the mass flow such that the refrigerant at the outlet of the capillary is choked. This means that the Mach-Number

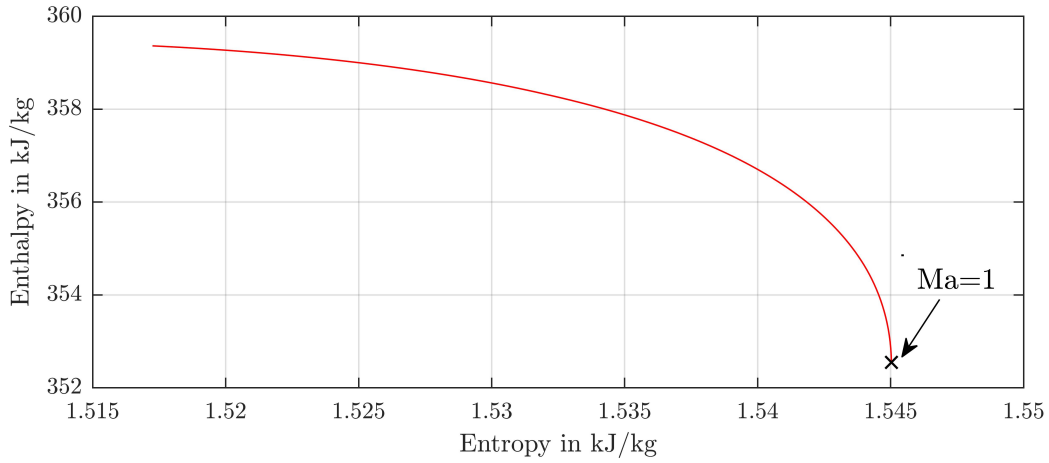

Fig. 2.3: *Exemplary Fanno line for an exemplary two-phase refrigerant flow subject to friction.*

equals 1 in maximum (see (Bansal and G. Wang, 2004)). The Mach-Number is defined as the fraction of the velocity v and the speed of sound c:

$$Ma = \frac{v}{c} \tag{2.8}$$

For the two-phase flow through a capillary with a constant cross-sectional area A that is regarded to be a one-dimensional, steady-state, compressible and adiabatic flow, the continuity equation applies:

$$v \cdot \rho = \frac{\dot{m}}{A} = const. \tag{2.9}$$

where ρ is the density of the refrigerant and v is the flow velocity. Without the impact of any external forces, neglecting the potential energy and applying the continuity equation, the energy balance of the above characterized flow results in:

$$h + \frac{1}{2} \cdot v^2 = h + \frac{1}{2} \cdot \left(\frac{\dot{m}}{A \cdot \rho} \right)^2 = e = const. \tag{2.10}$$

where e denotes the specific energy of the flow. For an exemplary two-phase flow of propane with Ma<1, the resulting Fanno line is drawn in the h,s-diagram in Fig. 2.2 which means that the depicted pairs of specific enthalpy and specific entropy comply with Eq. (2.10). The line in Fig. 2.2 depicts the expansion of a two-phase propane flow with a constant specific energy of e=359.4 kJ/kg and a

mass flow of $\dot{m}$=15 kg/h in a capillary tube with a diameter of d=1.1799e-3 m. Decreasing the pressure leads to an increase of the entropy until the maximum of entropy is reached (see Fig. 2.2). At this point, the Mach-Number becomes unity. Accordingly, the capillary meters the mass flow such that the entropy of the flow through the capillary reaches its maximum at the outlet of the capillary where the Mach-Number becomes unity.

2.3 Principles of Tube Flow

In this section, the principles of two-phase flow of a refrigerant through a capillary tube are derived which serve as a basis for the model described in chapter 4. The two-phase flow is considered to consist of a vapour phase (denoted by the subscript v) and a liquid phase (denoted by the subscript l). The void fraction α of the two-phase flow is the ratio of the cross-sectional area of the tube A that is occupied by the vapour phase A_v:

$$\alpha = \frac{A_v}{A} \tag{2.11}$$

The cross-sectional area that is occupied by the vapour phase A_v and the cross-sectional area that is occupied by the liquid phase A_l sum up to the cross-sectional area of the capillary tube A.

$$A = A_v + A_l \tag{2.12}$$

The vapour quality x is defined by the ratio of the vapour mass flow $\dot{m}_v$ of the total mass flow $\dot{m}$:

$$x = \frac{\dot{m}_v}{\dot{m}} \tag{2.13}$$

For the sum of the vapour mass flow $\dot{m}_v$ and the liquid mass flow $\dot{m}_l$ applies:

$$\dot{m} = \dot{m}_v + \dot{m}_l \tag{2.14}$$

From Eq. (2.9) the mass flux G is defined as follows:

$$G = \frac{\dot{m}}{A} \tag{2.15}$$

Inserting Eq. (2.13) and the correlation in Eq. (2.14) into Eq. (2.15) it follows:

$$\dot{m}_v = G \cdot A \cdot x \tag{2.16}$$

and

$$\dot{m}_l = G \cdot A \cdot (1 - x) \tag{2.17}$$

Eq. (2.9) applies for the vapour mass flow $\dot{m}_v$ and accordingly the velocity of the vapour phase v_v can be calculated:

$$v_v = \frac{\dot{m}_v}{\rho_v \cdot A_v} \tag{2.18}$$

and accordingly for the liquid mass flow $\dot{m}_l$ so that

$$v_l = \frac{\dot{m}_l}{\rho_l \cdot A_l} \tag{2.19}$$

With Eq. (2.11), Eq. (2.16), Eq. (2.17), Eq. (2.18) and Eq. (2.19) follows:

$$v_v = \frac{G \cdot x}{\rho_v \cdot \alpha} \tag{2.20}$$

the same applies for the liquid mass flow $\dot{m}_l$ so that the velocity of the liquid phase v_l can be calculateds:

$$v_l = \frac{G \cdot (1 - x)}{\rho_l \cdot (1 - \alpha)} \tag{2.21}$$

The capillary tube is considered to be straight and of a constant diameter d. The two-phase (i.e. compressible) flow of a refrigerant through the capillary tube is considered to be one-dimensional in the direction of the capillary length L, steady-state, adiabatic and subject to friction. The gravitational force is neglected. Fig. 2.4 depicts the flow of one single phase along a discretized tube element of the discretized length dz. The refrigerant flow enters the discretized tube element at the velocity v whereby the pressure drops from p at the inlet of the tube element to $(p - dp)$ at the outlet of the tube element due to the wall shear stress τ. If the flow is compressible, the density decreases with decreasing pressure and consequently the velocity increases to $(v + dv)$ at the outlet of the tube element. For steady-state flow the continuity equation in Eq. (2.9) applies. Applying the momentum

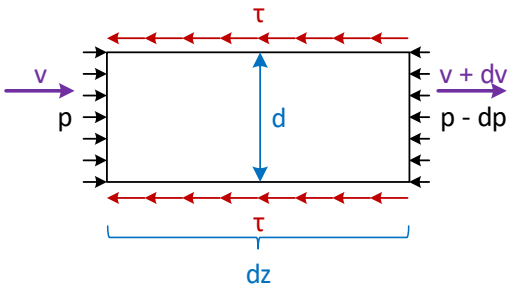

Fig. 2.4: *Schematic flow through a discretized length of a tube ΔL.*

balance for the depicted flow in Fig. 2.4 delivers:

$$\dot{m} \cdot v + p \cdot A = v \cdot \dot{m} + d\left(\dot{m} \cdot v\right) + \tau \cdot A_{lateral} + p \cdot A - dp \cdot A \tag{2.22}$$

For a two-phase flow, the impulse of the total mass flow sums up from the impulse of the liquid and the gas flow. Eq. (2.22) is transformed to:

$$dp = \frac{1}{A} \cdot d\left(\dot{m}_v \cdot v_v + \dot{m}_l \cdot v_l\right) + \frac{1}{A} \cdot \tau \cdot A_{lateral} \tag{2.23}$$

Inserting Eq. (2.16), Eq. (2.17), Eq. (2.20) and Eq. (2.21) results in:

$$dp = G^2 \cdot d\left(\frac{x^2}{\rho_v \cdot \alpha} + \frac{1 - x^2}{\rho_l \cdot (1 - \alpha)}\right) + \frac{1}{A} \cdot \tau \cdot A_{lateral} \tag{2.24}$$

with $A_{lateral}$, the lateral area of the discretized tube element:

$$A_{lateral} = \pi \cdot d \cdot dz \tag{2.25}$$

and the cross-sectional area of the tube A:

$$A = \pi \cdot d^2/4 \tag{2.26}$$

Eq. (2.24) transforms to:

$$dp = G^2 \cdot d \left(\frac{x^2}{\rho_v \cdot \alpha} + \frac{(1-x)^2}{\rho_l \cdot (1-\alpha)} \right) + \frac{4}{d} \cdot \tau \cdot dz \tag{2.27}$$

The Darcy friction factor f is used in order to describe the wall shear stress τ:

$$\tau = \frac{1}{8} \cdot f \cdot \rho \cdot v^2 \tag{2.28}$$

with f the Darcy friction factor, Eq. (2.27) turns into:

$$dp = G^2 \cdot d \left(\frac{x^2}{\rho_v \cdot \alpha} + \frac{(1-x)^2}{\rho_l \cdot (1-\alpha)} \right) + \frac{f}{2 \cdot d} \cdot \rho \cdot v^2 \cdot dz \tag{2.29}$$

For laminar flows in circular pipes the friction factor f is calculated depending on the Reynolds-Number Re as follows:

$$f = \frac{64}{Re} \tag{2.30}$$

For hydraulic rough pipes in turbulent flow regimes the friction factor is calculated solving the implicit Colebrook-White equation (Schade and Kunz, 2007a):

$$\frac{1}{\sqrt{f}} = -2 \log \left(\frac{2.51}{Re \cdot \sqrt{f}} + 0.27 \cdot \frac{e}{d} \right) \tag{2.31}$$

where e corresponds to the sand grain roughness (see (Colebrook, 1939)). In this work, the average roughness value Ra and the average roughness depth Rz are applied in order to substitute the sand grain roughness e. The average roughness value Ra comes closest to the definition of the sand grain roughness e by Nikuradse (1933). However, Rz is considered in order to investigate if the measure which determines a rougher tube surface better predicts the refrigerant flow and the observed flow phenomena. The definition of both roughness measures is attached in section 3.3.4.

When it comes to modelling the refrigerant flow through a capillary tube, it is significantly simpler to describe the liquid than the two-phase flow as most thermodynamic and transport properties are available for single phase conditions

(see section 2.5). There are two elementary model approaches for modelling the two-phase flow in pipes which are of a comparably low calculation effort but still deliver reliable results: the separated and the homogeneous flow approach. (Collier and Thome, 1994b) There are further modelling approaches that describe the two-phase flow in more detail but involve increasing computational effort. Since the flow model that is derived in this work shall be applicable in overall heat pump models, the computational effort is to be kept at a low level in order to afford the simulation of the overall heat pump model. Consequently, the attempt is to start with a simple model that is complex enough to capture relevant flow phenomena that may influence the operation of the heat pump.

The homogeneous flow model considers the two-phase flow as a single flow with properties that follow certain averaging correlations depending on the vapour fraction. For the two-phase density ρ_{tp} of the vapour-liquid flow applies:

$$\frac{1}{\rho_{tp}} = \frac{x}{\rho_v} + \frac{1-x}{\rho_l} \tag{2.32}$$

which satisfies the consistency conditions of ρ_{tp}=ρ_l for x=0 and ρ_{tp}=ρ_v for x=1. The vapour and liquid phase are assumed to be in thermodynamic equilibrium and the vapour and liquid phase are assumed to travel at the same velocity, hence:

$$v = v_v = v_l \tag{2.33}$$

From Eq. (2.20), Eq. (2.21) and Eq. (2.3) follows the correlation for the homogeneous void fraction α:

$$\alpha = \frac{x \cdot \rho_l}{x \cdot \rho_l + (1-x) \cdot \rho_v} \tag{2.34}$$

The calculation of the friction factor f follows defined correlations for the single-phase friction factor. One possible option is to regard the flow as total liquid flow and obtain the according liquid friction factor f_{liq}. Another option is to calculate the friction factor for the homogeneous flow of vapour and liquid f_{tp} by using e.g. Eq. (2.31) and calculating the Reynolds-Number Re_{tp} assuming a homogeneous two-phase dynamic viscosity μ_{tp}. (Collier and Thome, 1994b) There a various correlations available in the literature that determine the homogeneous two-phase dynamic viscosity μ_{tp} which are summarized by Awad and Muzychka (2008). The correlations follow different analogies and averaging methods. For the

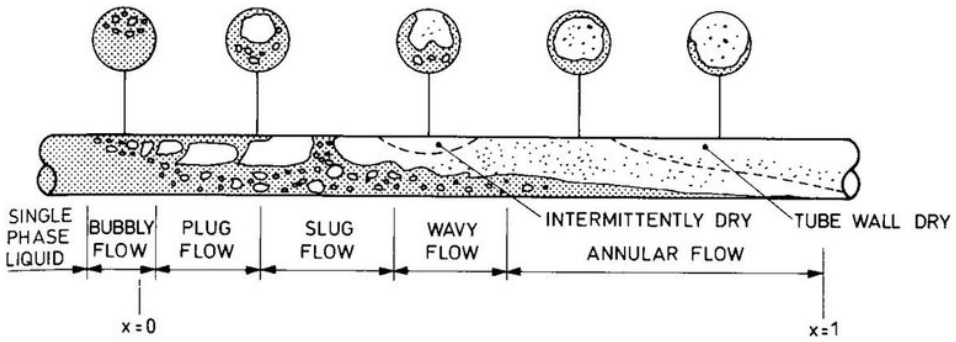

Fig. 2.5: *Two-phase flow patterns in horizontal tubes (evaporation) (Source: (Collier and Thome, 1994a)).*

homogeneous viscosity correlations the same consistency conditions as for the homogeneous density apply. At the saturation conditions the two-phase viscosity μ_{tp} therefore has to equal the liquid viscosity μ_l for x=0 and the vapour viscosity μ_v for x=1.

In contrast, in the separated model approach, the two-phase flow is separated into a vapour and a liquid stream that travel at mean velocities. If the velocities are considered to be the same, the separated model is equal to the homogeneous model. The separated flow approach can become complex since, compared to the homogeneous flow approach, more parameters need to be identified (see (Collier and Thome, 1994b) for more detailed description).

For two-phase flow in horizontal tubes, the flow patterns illustrated in Fig. 2.5 are observed. However, the flow patterns for high flow velocities rather correspond to those observed in vertical tubes (see Fig. 2.6). (Collier and Thome, 1994a) The separated flow approach is regarded to better predict the two-phase flow at higher void fractions which is reasonable regarding the observed flow patterns where the two-phase flow can be regarded as two segregated streams of vapour and liquid. However, Collier and Thome (1994b) state that the homogeneous approach is more suitable for mass fluxes higher than 2000 $\mathrm{kg/ms^2}$ which applies for the experimental data considered in this paper. Finally, in this work, the homogeneous flow approach is chosen due to its simplicity. If simulation results indicate that the simpler approach is not able to predict the experimental data, the logical consequence is to apply a more precise (and complex) approach.

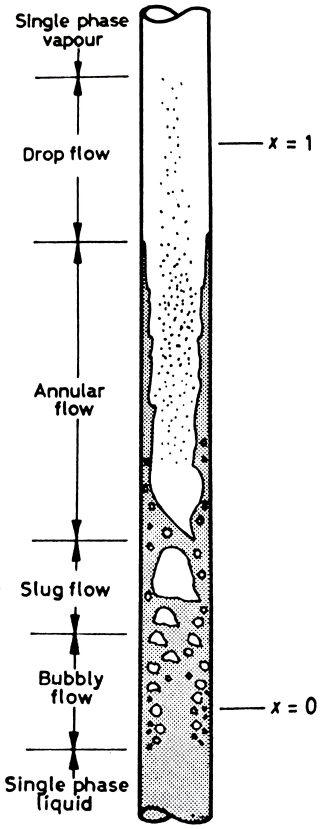

Fig. 2.6: *Flow patterns in a vertical evaporator tube (Source: (Collier and Thome, 1994a)).*

2.4 Experimental Investigations and Modelling of Two-Phase Flow in a Capillary Tube

This section deals with the experimental investigations and the modelling attempts of two-phase flow of refrigerants in capillary tubes. It focuses on the research that has been done on straight and adiabatic capillary tubes. The experimental database of (two-phase) refrigerant flow is discussed whereby the focus lies on experimental data that include occurring flow phenomena concerning the phase change inside the capillary tube.[1] Researchers have been striving to predict the two-phase flow of refrigerants through capillary tubes for many decades, as reviewed by Ribatski (2013). Up to now, the predictions are still unsatisfactory, which the author attributes to many reasons. Inaccurate experimental data and imprecise capillary specifications are two examples. Furthermore, it is discussed how far the available models of the refrigerant flow in capillary tubes are able to capture the observed flow phenomena. The negligence of the mentioned flow phenomena are a further reason for the deviation of predictions and experiments as elaborated in this work (see e.g. chapter 3).

When it comes to natural refrigerants there is a lack of experimental data especially with respect to propane (see (Dubba and Kumar, 2017)). Sempértegui-Tapia and Ribatski (2017) found that most predictive methods that describe the flow through capillaries have been proposed for hydrofluorocarbons, but the appropriateness for natural refrigerants is still not proven. However, the interest in natural refrigerants has increased due to global environmental goals which results in the gradual replacement of hydrofluorocarbons due to their global warming potential. For this reason, the experimental and numerical investigations of this work focus on the natural refrigerant propane.

Complex flow phenomena occur at the phase change from liquid to two-phase flow of the refrigerant in the capillary tube. So-called "metastable flow" can be developed at certain operating conditions that can grow up to the previous point of nucleation where originally it would be two-phase for the current inlet condition. Hence, the flow is liquid at pressures below the actual saturation pressure as researchers have investigated experimentally (see e.g. (R.-Y. Li et al., 1990),

[1] Parts of this section are adopted from (Gabrisch and Repke, 2020) and (Gabrisch and Repke, 2021)

(Chang and Ro, 1996), (Meyer and Dunn, 1998) and (Guobing and Yufeng, 2006)). A further flow phenomenon that has been discovered, is the occurrence of a hysteresis effect: for the same inlet conditions of the refrigerant flow through the capillary tube, different outlet conditions are observed (e.g. different resulting mass flows or pressure drops). The difference in the outlet condition depends on the history of inlet conditions (see (Meyer and Dunn, 1998) and (Guobing and Yufeng, 2006)).

The two-phase flow of refrigerants in capillary tubes has been subject of experimental investigations for many decades, as Dubba and Kumar (2017) reflect in their work. However, very little research exists that include the above mentioned flow phenomena. Up to now, it is not well understood how exactly both phenomena are interrelated. Further, the cause for the development of metastable flow and the root of the hysteresis effect is not clarified to the best of the author's knowledge. Therefore, this section highlights the work that has previously been done on the examination of the metastable flow and the hysteresis effect.

Research on the metastable flow of refrigerants has been done before 1990 as R.-Y. Li et al. (1990) have summarized and was discovered by Cooper, Chu, and Brisken (1957). The metastable flow phenomenon is characterized by a delay on vaporization. The refrigerant does not flash at the actual saturation pressure p_{sat} but further downstream the capillary at p_{vap}. The difference $\left(p_{sat} - p_{vap}\right)$ is referred to as the *underpressure of vaporization* (R.-Y. Li et al., 1990). The length of the capillary that corresponds to this pressure difference is referred to as *metastable length*. R.-Y. Li et al. (1990) investigated the flow of R12 through a capillary tube and highlighted the presence of metastable flow. They conclude their experimental investigations on R12 with the findings that the metastable length decreases for increasing inlet subcoolings (i.e. the inlet temperature, see Eq. (2.7)) and increasing diameter of the capillary tube and increases for increasing mass flux.

Z. H. Chen, R. Y. Li, and Z. Y. Chen (1990) proposed a correlation that predicts the underpressure of vaporization. The correlation is fitted to the experimental investigations of R.-Y. Li et al. (1990) and, hence, is limited in its range of application. The correlation by Z. H. Chen, R. Y. Li, and Z. Y. Chen (1990) is often used when modelling the flow of refrigerants through capillary tubes considering the metastable flow (see (Dirik et al., 1994), (Melo et al., 1998), (García-Valladares,

2007), (Mittal, Kumar, and Gupta, 2009), (Kim et al., 2011), (Rasti and Jeong, 2018) and (Lee and Jeong, 2019)). Although Melo et al. (1998) already indicated that it is not appropriate for other refrigerants than R12 and a wider operation range than the correlation was fitted to.

Feburie et al. (1993) developed a model to predict the metastable flow which is divided into a metastable liquid and a metastable two-phase flow. The metastable liquid flow, i.e. the actual vaporization pressure p_{vap} is calculated using a simple correlation. The metastable two-phase flow is regarded to consist of a superheated liquid flow, a saturated liquid and a saturated vapour flow. Feburie et al. (1993) proposed a correlation to calculate the ratio of the saturated flow depending on the pressure.

Chang and Ro (1996) set up a correlation to predict the underpressure of vaporization that depends on the subcooling at the inlet of the capillary and the mass flux. The correlation is fitted by parameters derived from experiments they carried out with HFC mixtures.

Meyer and Dunn (1998) investigated the refrigerant R22, as they found the existing database on the metastable flow to be unsatisfactory. They discovered that the metastable length grew for decreasing inlet subcoolings. The increased metastable length results in lower pressure drops than expected (and higher mass fluxes, respectively). At a certain point, however, the metastable region can collapse and the pressure drop increases (or the mass flux decreases). They expected a hysteresis effect due to the development of the metastable flow and performed experiments with the refrigerant R134a in order to verify. The inlet pressure was kept constant while the subcooling was changed from 13.9 °C to 0 °C and back. Experimental results proved the presence of a hysteresis on the resulting mass flow through the capillary depending on the previous flow through the capillary. Meyer and Dunn (1998) strongly advised further research on the hysteresis of the flow through a capillary which requires a systematic measurement technique to capture the history of measurements and, thus, be able to document the hysteresis course.

Bittle, Carter, and Oliver (2001) conducted experiments on the mass flow hysteresis of R134a and concluded that the direction of the performed operating conditions (increasing and decreasing subcooling) has an influence on the metastable flow

and, hence, entails a hysteresis effect. They modified the capillary by inserting a thin wire or thrilling holes into the capillary wall and showed that thereby the metastability of the flow is reduced and the flow behaviour becomes better predictable.

Guobing and Yufeng (2006) examined the mechanism of the mass flow hysteresis of R22 in coiled capillary tubes. They repeated the measurements of increasing and decreasing subcooling paths with different initial flow conditions. They recognized that, in general, the metastable length is longer for the decreasing subcooling paths and that the length depends on the initial flow condition. For the increasing subcooling paths, however, the metastable flow length is remarkably shorter and may even disappear.

The findings of Guobing and Yufeng (2006) allow the conclusion that there may not even be a metastable flow at all for increasing subcooling paths. If that is true, metastable flow is developed when changing the direction from increasing to decreasing inlet subcooling.

The correlations by Z. H. Chen, R. Y. Li, and Z. Y. Chen (1990) and Chang and Ro (1996) calculate a constant underpressure of vaporization for specific operating conditions, regardless of how the current condition was reached (e.g. increasing or decreasing subcooling). With these correlations it is not possible to distinguish between increasing and decreasing subcooling. The history of previous inlet conditions needs to be considered within the flow model in order to predict hysteresis effects.

Gao, Eguchi, and Tatara (2015) conducted experiments on the hysteresis effect of the flow of R134a through a capillary. They showed that being able to predict the underpressure of vaporization that is different for increasing and decreasing subcooling paths, a homogeneous flow model can predict the flow very well. Yet, they did not present a correlation to predict the underpressure of vaporization but referred to the experimental data.

Although Guobing and Yufeng (2006) indicated that the underpressure of vaporization can not be predicted without the knowledge of previous flow conditions, researchers still applied the correlation by Z. H. Chen, R. Y. Li, and Z. Y. Chen (1990) or similar ones (see (García-Valladares, 2007),(Kim et al., 2011), (J. Wang

et al., 2012), (Fiorelli, Silva, and Huerta, 2013), (Rasti and Jeong, 2018), (Lee and Jeong, 2019)). To the best of the author's knowledge, no research has been done to predict any experimental hysteresis curves presented by researchers, such as by Meyer and Dunn (1998) or Guobing and Yufeng (2006). Hence, up to now, there is no correlation available that predicts the metastable flow depending on previous flow conditions.

Additionally, to the best of the author's knowledge, all investigations on the metastable flow are based on the experimental data of hydrofluorcarbons. However, nowadays, natural refrigerants are of major importance for environmental reasons as stated before. There is research done on the flow of propane through capillaries (see (Pamitran et al., 2010), (Maqbool, Palm, and Khodabandeh, 2013), (Del Col, Bortolato, and Bortolin, 2014), (S. Wang et al., 2014), (Longo et al., 2017), (Novianto et al., 2018), (Lillo et al., 2018),(Simon Fries, Severin Skusa, 2019)); yet, it does not treat metastable flow phenomena and hysteresis.

This work aims to thoroughly examine the root and the interrelation of the metastable flow and hysteresis occurrence observed for the flow of refrigerants in capillary tubes. The discoveries are consecutively transferred into a mathematical model and supplement the common homogeneous flow model in order to predict the propane flow in a capillary tube. Special attention is further paid to the determination of the capillary geometry and material characteristics (i.e. the inner diameter and the roughness of the inner surface of the capillary) as Ribatski (2013) attributes unsatisfactory prediction, among others, to inaccurate capillary specification. Consequently, the research of this work contributes to a reliable and extensive experimental database of propane flow through capillary tubes capturing the metastable flow and hysteresis phenomena experimentally and numerically.

2.5 Refrigerant Properties

For the calculation of the refrigerant flow through a capillary tube, refrigerant properties are needed. Within this work, the NIST Standard Reference Fluid Thermodynamic and Transport Properties Database (REFPROP) is used (see (Lemmon,

Bell, et al., 2013)). REFPROP is a program that is based on three models for the calculation of thermodynamic and transport properties, which are: equation of state explicit in Helmholtz energy, the modified Benedict-Webb-Rubin equation of state, and an extended corresponding states model. In this work, the following thermodynamic and transport properties (accordingly within the sketched area of temperature and pressure) of the pure vapour and liquid state are needed for the calculation of propane flow through a capillary tube:

- temperature T (0-100°C)
- pressure p (2-40 bar)
- specific enthalpy h
- density ρ
- specific entropy s
- the speed of sound c
- the dynamic viscosity μ

REFPROP provides an interface for MATLAB that works via a function call. The single phase thermodynamic properties are calculated given two thermodynamic properties of the first five properties of the list above using the equation of state provided by Lemmon, McLinden, and Wagner (2009). The single phase dynamic viscosity μ is calculated using the viscosity model by Quiñones-Cisneros and Deiters (2006). As REFPROP does not provide the calculation of most two-phase properties, the two-phase dynamic viscosity needs to be self-implemented following chosen correlations (see section 4.1).

3 Experimental Investigations

In this chapter, the propane flow through a copper and a steel capillary tube is examined. The experimental set-up that serves to carry out the investigations is explained in section 3.1. In section 3.2, the measurement procedure is described in detail. Section 3.3 and section 3.4 then outline the design on experiments, discuss the experimental results and refine the capillary specifications of both - the copper and steel capillary tube.

3.1 Experimental Set-Up

Fig. 3.1 depicts the experimental apparatus which was developed to investigate the single and two-phase pressure drop of refrigerants in a capillary tube with a designated inlet condition of the flow at the capillary inlet. The purpose is to independently adjust the temperature (TRC-1), the pressure (PRC-1) and the mass flow (FIRC-1) at the inlet of the capillary and measure the resulting pressure drop (DPR-1) in the capillary. The thermodynamic condition is fully defined by the specification of PRC-1 and TRC-1 in case that the refrigerant is liquid, i.e. subcooled or saturated. Thus, the specification of TRC-1 follows the specification of a desired subcooling. The resulting temperature is determined via calculation of the saturation temperature according to the desired inlet pressure PRC-1 and subtracting the specified subcooling. The calculation of the desired temperature TRC-1 is executed in the process control system that refers to the REFPROP database and is implemented using the software *LabVIEW*.

The apparatus represents a heat pump in terms of the operation principle. A rotary compressor transports the refrigerant through the closed cycle and increases the pressure as the refrigerant is blocked at the capillary inlet. Depending on the

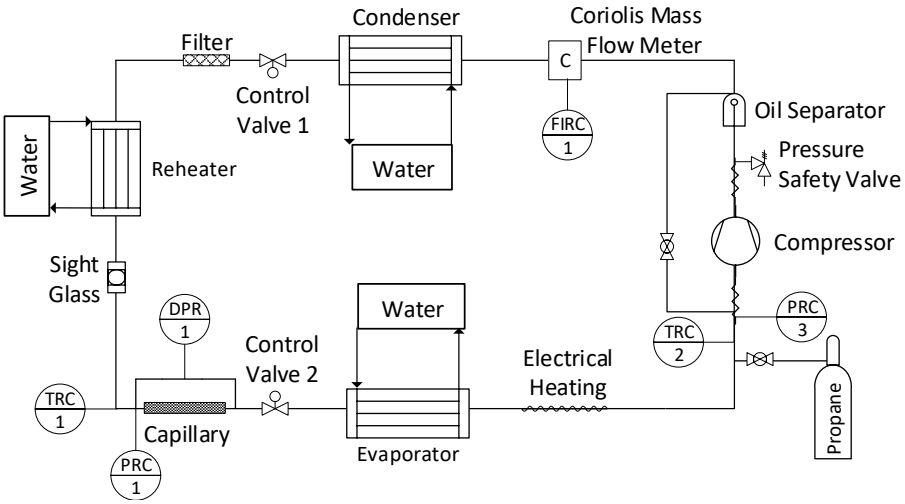

Fig. 3.1: *Experimental apparatus (Source: (Gabrisch and Repke, 2020)).*

refrigerant charge in the system and the operating condition of the heat pump, the pressure on the high-pressure side reaches a maximum of about 36 bar (see sensor accuracies in Tab. 3.1). The gas at the outlet of the compressor flows through a coriolis mass flow meter, where the mass flow (FIRC-1) is registered and then passes the condenser where the refrigerant is fully liquefied. The reheater is used to control the designated refrigerant temperature (TRC-1) at the capillary inlet. The designated inlet pressure (PRC-1) is achieved by manipulating Control Valve 1 and thereby lowering the pressure on the high-pressure side to the desired value.

Within a conventional heat pump cycle without any addition pressure valves, the capillary outlet is directly affecting the inlet of the compressor. Together with the evaporator it determines the thermodynamic condition of the refrigerant at the compressor inlet and is thereby influencing the mass flow of refrigerant that is transported by the compressor. In the experimental apparatus, shown in Fig. 3.1, downstream the capillary tube a second control valve (Control Valve 2) is installed in order to decouple the capillary outlet from the compressor inlet and adjust mass flows independently from the capillary outlet condition. However, this control concept is restricted to the pressure difference between the pressure at the outlet of the capillary and the pressure at the inlet of the compressor which is needed to adjust the desired mass flow. Fig. 3.2 illustrates this relation. In the left diagram

in Fig. 3.2, a flow condition at the inlet of the capillary tube is given (with PRC-1^1, TRC-1^1, FIRC-1^1). It results in a pressure at the outlet of the capillary (PRC-1^1-DPR-1^1) which is assumed to equal the pressure at the inlet of the compressor PRC-3^1 when the Control Valve 2 is fully opened. PRC-3^1 causes the mass flow FIRC-1^1. At this point, the manipulated variable (opening of Control Valve 2) can not effect any higher mass flow. It can only lower the mass flow by reducing the cross-sectional area of the valve and adjust a lower PRC-3^1. On the right diagram in Fig. 3.2 the desired temperature TRC-$1^{\text{des}\,2}$ is lower than TRC-1^1 and, consequently, the pressure drop DPR-1^2 is lower than DPR-1^1. In this scenario, Control Valve 2 is able to adjust the desired mass flow FIRC-$1^{\text{des}\,2}$ by reducing the cross-sectional area so that a pressure drop of $\Delta p_{Control\ Valve\,2}$ is induced. The maximum mass flow at the desired inlet conditions PRC-$1^{\text{des}\,2}$ and TRC-$1^{\text{des}\,2}$ would be the mass flow that results from the pressure at the capillary outlet (which equals the pressure at the compressor inlet) when the Control Valve 2 is fully opened.

As oil is likely to circulate within the refrigerant cycle due to the compressor design, an oil separator is installed upstream the compressor to prevent oil distorting the pressure drop experiments of the refrigerant in the capillary. The oil seperator (manufacturer: ESK Schultze, type: OS-16-CD) is specified to work with a separation ratio of 97-99 %. Remaining oil residues are neglected.

Preliminary model-based investigations of the pressure drop of propane in a capillary tube by Gabrisch, Grunert, and Repke (2017) revealed a high sensitivity of the calculated pressure drop especially depending on the inner diameter. Consequently, within the experimental setup specific attention has been paid to keep the impact of the sensor installation on the change in capillary geometry as low as possible. Fig. 3.3 sketches the measuring section of the capillary tube within the experimental apparatus in Fig. 3.1. Custom-built ferule fittings have been used in order to install the pressure (PRC-1) and differential pressure (DPR-1) with marginal flow disturbance. At the inlet of the capillary the ferule fitting connects the capillary tube with the high-pressure side. The pressure tab is located in the middle of the ferule fitting where the inner diameter is 6 mm which corresponds to the connection tube between reheater and capillary (see Fig. 3.1). At the outlet of the capillary it connects the capillary with the low-pressure side. The through-hole of the ferule fitting at the capillary outlet has an inner diameter of 1.1 mm

Tab. 3.1: Sensor accuracies.

Sensor Name	PRC-1, PRC-3	TRC-1	FIRC-1	DPR
Manufacturer	Keller	TCdirect	Endress&Hauser	Endress&Hauser
Type of Sensor	piezoresistive pressure sensor	thermocouple type T	coriolis flow meter	piezoresistive differential pressure sensor
Measurement Range	0-40 bar	-200-400 °C	0-100 kg/h	0-30 bar
Accuracy	0.28 bar	0.5 K	0.3 %	0.03 bar

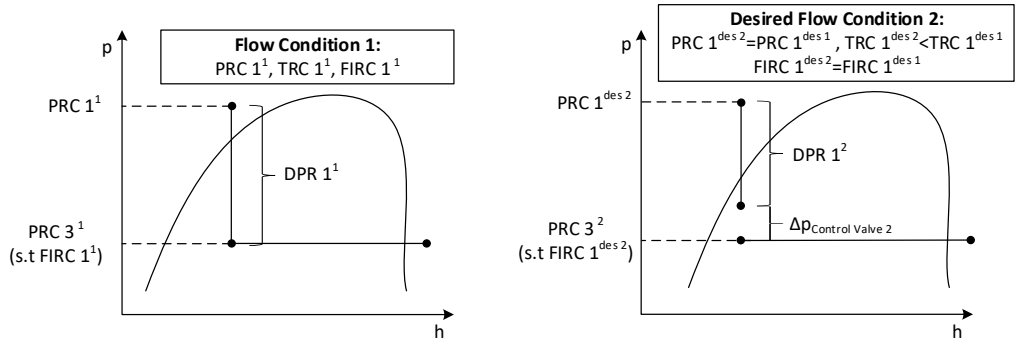

Fig. 3.2: Limit of the mass flow control in the experimental apparatus.

which equals the inner diameter of the capillary tube. Consequently, the measurement of the pressure drop in the capillary (DPR-1) includes the entrance pressure drop due to sudden contraction at the inlet of the capillary. However, it excludes the influence of the cross-sectional widening at the outlet of the capillary as the sensor taps at the inner diameter of the capillary tube.

Tab. 3.1 lists the installed sensors for the pressure at the capillary inlet (PRC-1), the temperature at the inlet of the capillary (TRC-1), the mass flow through the capillary (FIRC-1) and the pressure drop in the capillary (DPR-1) and further specifies their measurement range and accuracy.

3.2 Measurement Procedure

The homogeneous flow model that is presented in chapter 4 aims to be representative for the operation of a capillary tube in overall heat pump simulations. In order to validate the model, an experimental database is needed that comprises

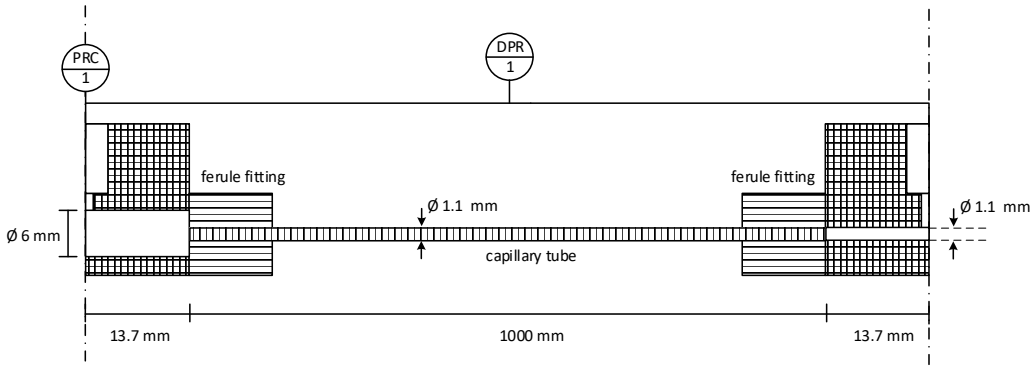

Fig. 3.3: *Dimensions of the capillary tube and distances of pressure taps to inlet and outlet of the capillary tube.*

a large operational range that is typical for capillaries within heat pump applications. The chosen refrigerant that is investigated in this work is propane due to its relevance in terms of environmental compatibility. As Dubba and Kumar (2017) have outlined there is also the general desire of more data on natural refrigerants. It is decided to choose the refrigerant condition at the inlet of the capillary to be subcooled in order to capture phase change effects inside the capillary tube. For inlet pressures that range from 16 to 25 bar, the subcooling is to be varied from 5 to 9 K; mass flows are investigated from 13.5 to 18 kg/h. Experiments are carried out using a copper capillary first. In a second experimental phase a steel capillary with the same geometry specification is investigated.

Guobing and Yufeng (2006) have indicated that the metastable length of the flow in a capillary is longer for decreasing subcoolings and shorter for increasing subcoolings where it may even fully disappear depending on the initial subcooling. It is reasonable to conclude that the occurence of metastable flow is negligible for measurement series of increasing subcoolings starting with a very low subcooling. Hence, for the start-up of the experimental apparatus shown in Fig. 3.1 a target subcooling of 2 K is specified at the capillary inlet. Subcoolings that are too low result in very high pressure drops in the capillary followed by very low realizable mass flows. It is difficult to drive the heat pump process towards the desired inlet pressures and mass flows from this condition. Hence, 2 K subcooling is a compromise of having a low subcooling and keeping the operation in a stable condition.

For investigating the range of the desired flow conditions at the capillary inlet, measurement series are defined. One measurement series comprises the subsequent investigation of one *increasing subcooling path* and a directly followed *decreasing subcooling path* while keeping the inlet pressure and mass flow at a constant level. It is necessary to define these series since the measured pressure drops depend on the previous flow condition in the capillary. One measurement series, thus, corresponds to one *hysteresis curve* depending on the series of investigated subcoolings. The increasing subcooling path is specified by the sequence of 5 to 9 K in 1 K-steps whereas the decreasing subcooling path is specified by the backward sequence. One measurement series is carried out as follows:

1. start up the process in the experimental apparatus until it reaches the desired inlet pressure at 2 K subcooling and the desired mass flow
2. drive towards the first subcooling of the increasing subcooling path (here: 5 K)
3. remain steady-state for at least 10 minutes
4. proceed to the next subcooling of the increasing subcooling path
5. repeat 2. and 3. until the last subcooling of the increasing subcooling path is reached (here: 9 K which is likewise the first subcooling of the decreasing subcooling path) and remain steady-state for at least 10 minutes)
6. proceed to the next subcooling of the decreasing subcooling path
7. remain steady-state for at least 10 minutes
8. repeat 5. and 6. until the first subcooling of the increasing subcooling path is reached (here: 5 K) and remain steady-state for at least 10 minutes

Steady-state conditions are determined by analysing the time-resolved measurement data. The following requirements need to be fulfilled in order to obtain steady-state conditions for PRC-1, TRC-1, FIRC-1 and DPR-1:

– for each sensor: steady-state duration must last for a certain period of time; here it is set to at least 3 minutes

- one sensor is in steady-state if within the defined period of time the deviation around the mean value is not larger than the sensor accuracy (see Tab. 3.1). The accuracy of FIRC-1 is set to ± 1 % as the mass flow fluctuation in the closed cycle is generally too large to reach a steady-state condition for FIRC-1 that deviates by only ± 0.3 %.

- steady-state condition for all four sensors must be given at the same time

Before start-up, the capillary may be fully wetted by the refrigerant. Accordingly, the very first initial condition of the capillary may be regarded as very high subcooling so that metastable flow may occur for the increasing subcooling path already. Section 4.2 explains in more detail the assumption for the occurence of metastable flow, namely the wetting of the capillary tube. It is assumed that a wetted capillary evokes a lower pressure drop than a dry capillary tube. By starting-up the process with 2 K subcooling the purpose is to reduce the length of the capillary that is fully wetted to a low level. As the measurement series of the experimental data start at the lowest subcooling of 5 K, the start-up condition of 2 K ensures an initial wetting of the capillary that is lower than the first recorded operating condition of the series. It is therefore assumed that the increasing subcooling paths do not (or only to a small extend) entail a metastable flow. However, deviations in the redundant measurements of the measured hysteresis curves, especially concerning the increasing subcooling paths, may be explained by the presence of metastable flow.

3.3 Experiments on the Propane Flow Through a Copper Capillary Tube

This section treats the experimental investigation of the propane flow through the copper capillary tube that is specified to an inner diameter of 1.1 mm and a length of 1 m. The design on experiments is presented and the results on the measured pressure drops is shown and discussed. The presence of the hysteresis effect depending on the subcooling is highlighted and a thesis for the cause of the hysteresis effect is derived based on systematic experiments.

Tab. 3.2: *Investigated flow conditions at the (copper) capillary inlet with liquid flow through capillary tube.*

PRC-1 in bar	**FIRC-1** in kg/h	**Subcooling** in K
16	12	20
16	15	20
16	18	20
20	13	30
20	14	30
20	15	30
20	16	30
20	17	30
24	12	39
24	18	33
24	22	33

As preliminary sensitivity studies by Gabrisch, Grunert, and Repke (2017) based on the homogeneous flow model have shown, the sensitivity of the inner diameter is immense. Consequently, the inner diameter of the investigated capillary is refined by measurements using a light microscope which is elaborated in section 3.3.4. Additionally, the roughness of the inner surface of the capillary tube is determined. Both - the inner diameter and the roughness - are needed to parametrize the homogeneous flow model that is presented in chapter 4.

3.3.1 Design on experiments

Tab. 3.2 displays the investigated flow conditions of propane at the capillary inlet that result in pure liquid flow through the capillary. The liquid flow experiments are used in section 5.1.1 for the parametrization of the homogeneous flow model.

Tab. 3.3 contains the investigated inlet conditions of propane that result in a liquid and two-phase flow in the capillary. Each flow condition is investigated twice in order to check on the reproducibility of the measured pressure drops.

As described in section 3.2, one measurement or one hysteresis curve is performed for each listed combination of inlet pressure (PRC-1) and mass flow (FIRC-1) of

Tab. 3.3: *Investigated flow conditions at the (copper) capillary inlet with phase change inside the capillary tube.*

PRC-1 in bar	**FIRC-1** in kg/h	**Subcooling** in K
16	13.5	5, 6, 7, 8, 9
16	14	5, 6, 7, 8, 9
16	14.5	5, 6, 7, 8, 9
16	15	5, 6, 7, 8, 9
17	15	5, 6, 7, 8, 9
18	15	5, 6, 7, 8, 9
19	15	5, 6, 7, 8, 9
20	15	5, 6, 7, 8, 9
20	16.5	5, 6, 7, 8, 9
21	15	5, 6, 7, 8, 9
21	16.5	5, 6, 7, 8, 9
23	15	5, 6, 7, 8, 9
23	16.5	5, 6, 7, 8, 9
23	18	5, 6, 7, 8, 9
25	16	5, 6, 7, 8, 9
25	16.5	5, 6, 7, 8, 9
25	18	5, 6, 7, 8, 9

propane and the according subcoolings from 5 to 9 K. Fig. 3.4 depicts an exemplary measurement series at a constant inlet pressure of 25 bar and constant mass flow of 18 kg/h. For the validation of the homogeneous flow model in chapter 5, only steady-state conditions of the inlet conditions of the propane flow (i.e. PRC-1, TRC-1 and FIRC-1) are needed as input variables of the flow model, as well as the resulting steady-state pressure drop (DPR-1) for the comparison with the pressure drop that is predicted by the flow model. For all measurement series in Tab. 3.3 steady-state conditions are determined. In the further course of this work it will be referred to the steady-state conditions when referring to experimental results in general. The results are listed in Tab. A.2 and Tab. A.3 in the appendix. For the liquid flow experiments in Tab. 3.2 the steady-state conditions are determined in the same way. The experimental results are attached in Tab. A.1. For all conditions in Tab. 3.3 the entrance condition of the refrigerant flow is highly turbulent, ranging from approximately Re=47400 (at PRC-1=16 bar, FIRC-1=13.5 kh/h, 9 K Subcooling) to Re=80400 (at PRC-1=23 bar, FIRC-1=18 kh/h, 5 K Subcooling).

3.3.2 Results and discussion

In this section, the general findings on the pressure drop of propane in the investigated copper capillary tube as well as the findings on the characteristics of the hysteresis curve depending on the subcooling are analysed and discussed.
Fig. 3.5 depicts the gathered pressure drops for the performed increasing and decreasing subcooling paths within the measurement series at a constant mass flow of 15 kg/h and different constant inlet pressures. Only the mean values of the double measured measurement series are depicted in the figure for a clearer appearance of the results. The presence of a hysteresis effect is visible for all shown measurement series: the measured pressure drop depends on the previous measured operating condition (here: subcooling). It can be seen that for all increasing subcooling paths, the measured pressure drop is higher than for the decreasing subcooling paths. Generally, the experimental results in Fig. 3.5 show that the lower the inlet pressure the higher the pressure drop for the same degree of subcooling. This can be explained with the pressure difference from the inlet pressure and the saturation pressure - which is smaller for lower inlet pressures and higher for higher inlet pressures. Hence, for higher inlet pressures a larger

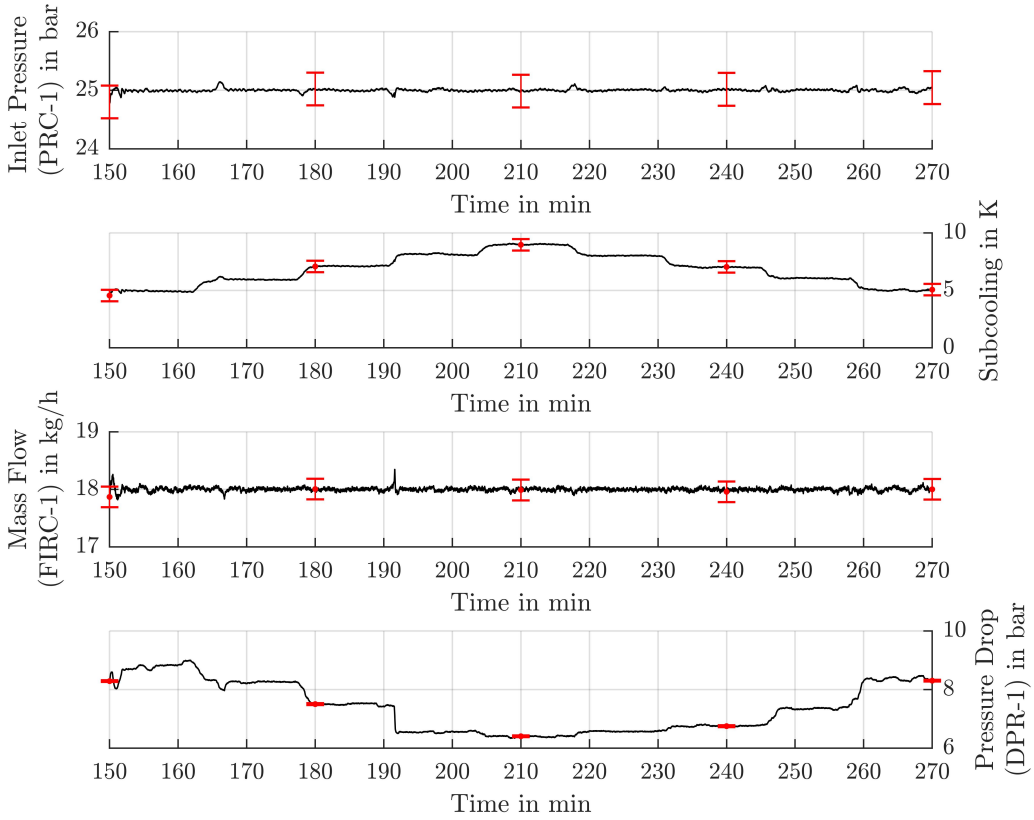

Fig. 3.4: *Exemplary time-resolved measurement series at a constant inlet pressure (PRC-1) of 25 bar and a mass flow (FIRC-1) of 18 kg/h further displaying the change of subcooling at the capillary inlet and the resulting pressure drop (DPR-1).*

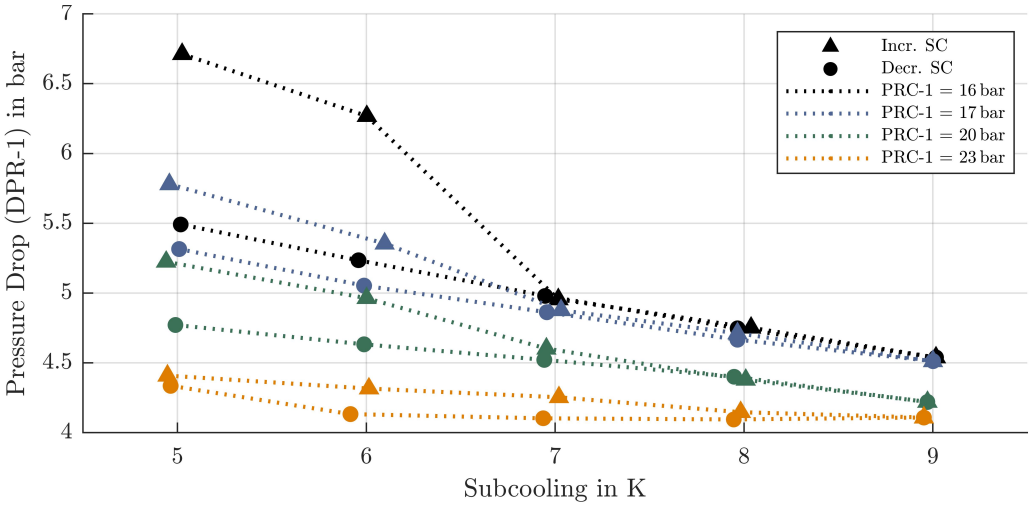

Fig. 3.5: *Experimental results of the measurement series including the increasing (Incr.) and decreasing (Decr.) subcooling path at a constant mass (FIRC-1) flow of 15 kg/h and different inlet pressures (PRC-1) in the copper capillary tube depicting the resulting pressure drop (DPR-1) over the change of the subcooling at the capillary inlet (mean values of the redundant measurements).*

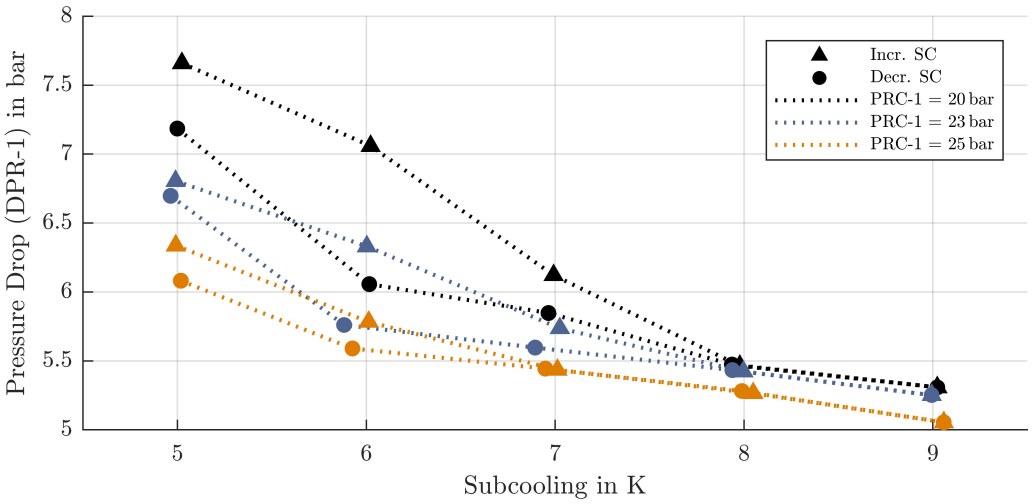

Fig. 3.6: *Experimental results of the measurement series including the increasing (Incr.) and decreasing (Decr.) subcooling path at a constant mass flow (FIRC-1) of 16.5 kg/h and different inlet pressures (PRC-1) in the copper capillary tube depicting the resulting pressure drop (DPR-1) over the change of the subcooling at the capillary inlet (mean values of the redundant measurements).*

part of the capillary tube is occupied with liquid refrigerant and consequently the pressure drop is lower. The flow of propane with a subcooling of 5 K at the inlet of the capillary entails a larger two-phase pressure drop than 9 K subcooling. The higher ratio of two-phase flow in the capillary is the reason why the pressure drop at lower subcoolings is larger than at higher subcoolings. The difference between the pressure drop at 5 K and 9 K subcooling of the increasing subcooling is larger, the lower the inlet pressure is. The decreasing subcooling paths in Fig. 3.5 follow linear courses, approximately. It is remarkable that the slope of the approximated linear graphs is slightly higher for higher inlet pressures.

For an inlet pressure of 20 bar and a subcooling of 5 K the pressure drop is around 47 % higher when increasing the mass flow from 15 kg/h to 16.5 kg/h (increase by 10 %), see Fig. 3.6. For an inlet pressure of 23 bar the pressure drop is even increased by 53 %. Both pressure drop relations refer to the increasing subcooling path. Concerning the decreasing subcooling paths, the slope of the approximate linear correlation is higher in Fig. 3.6 than in Fig. 3.5. The difference between the pressure drop at 5 K and 9 K subcooling is way lower at the decreasing subcooling paths compared to the increasing subcooling paths.

At some point in the decreasing subcooling paths the linear correlation seems to be suddenly disrupted - see e.g. Fig. 3.6 for 20 bar inlet pressure from 6 to 5 K subcooling. The redundant measurements of this specific measurement series is depicted in Fig. 3.7. Two rendundant measurements of the increasing and decreasing subcooling paths are shown. Following the black graph of the decreasing subcooling path it can be seen that there are two measured pressure drops at a subcooling of 5 K. Meyer and Dunn (1998) interpreted the presence of two, or more, possible steady-state pressure drops at the same degree of subcooling as a "collapse of a metastable flow". Such a collapse results in a higher pressure drop or lower mass flow depending on the investigated subject. Fig. 3.8 shows the time-resolved measurement of the black measurement series in Fig. 3.7. Fig. 3.8 represents the time section of measuring the subcooling of 5 K of the decreasing subcooling path. The first three diagrams show the flow condition at the capillary inlet - the inlet pressure, the subcooling and the mass flow of propane - whereas the last diagram plots the course of the resulting pressure drop in the copper capillary. It can be seen that the operation is in steady-state in the time from 218-224 min with a pressure drop of 7 bar. Then suddenly the pressure drop increases

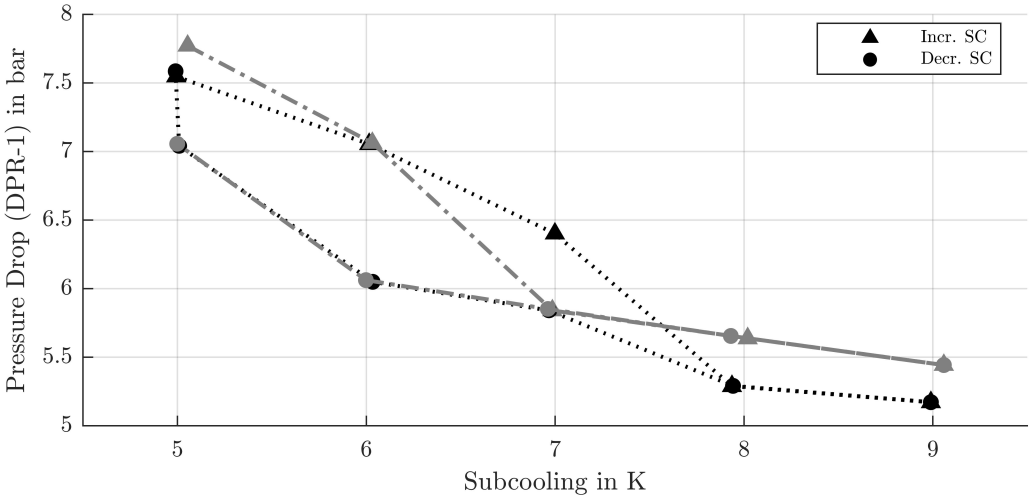

Fig. 3.7: *Experimental results of two redundant measurement series including the increasing (Incr.) and decreasing (Decr.) subcooling path at the constant inlet pressure (PRC-1) of 20 bar and mass flow (FIRC-1) of 16.5 kg/h in the copper capillary tube depicting the resulting pressure drop (DPR-1) over the change of the subcooling at the capillary inlet.*

whereupon the inlet condition of the propane flow is affected and the desired condition of the propane flow at the capillary inlet needs to be adjusted again. At the time of 227 min a new steady-state condition is reached with a pressure drop of around 7.6 bar. The collapse of a metastable flow is assumed to be responsible for the sudden increase in the pressure drop shortly before the time of 225 min. As such collapses of metastable flow only occured in the decreasing subcooling paths, it strengthens the hypothesis that primarily the decreasing subcooling paths entail metastable flow. As after such a collapse, the pressure drops of the decreasing subcooling path approximate the pressure drops of the increasing subcooling paths, it can reasonably be concluded that the metastable flow causes the hysteresis effect. If, however, the metastable flow collapses, the hysteresis effect is lowered in terms that the difference between the increasing and decreasing subcooling path is reduced. Whenever two steady-state pressure drops have been traceable within the measurements, both pressure drops are documented and marked in the experimental results in Tab. A.3.

We may assume that metastable flow is developed when changing from increasing to decreasing subcooling at 9 K in the investigated measurement series in Tab. 3.3. However, it is hard to track within the measurements if a metastable collapse took

place. Presumably, it does not have to be the case that it is as obvious as in Fig. 3.8 where there are two steady-state conditions. In contrast, metastable flow can collapse when changing from one investigated subcooling of the measurement series to another while waiting for the process to become steady-state. Consequently, it may be possible that some of the decreasing subcooling paths (e.g. at 23 bar inlet pressure and 16.5 kg/h in Fig. 3.6) may be subject to a metastable collapse which could explain sudden changes in the slope of the linear courses of the decreasing subcooling paths. Following this assumption, comparing Fig. 3.5 and Fig. 3.6, metastable flow is more likely to collapse at higher mass flows.

Generally, it can be observed that the hysteresis effect is higher (i.e. the difference between the pressure drops of the increasing and decreasing subcooling path for the same degree of subcooling is higher) for lower inlet pressures and for higher mass flows (compare Fig. 3.6 and Fig. 3.5). This statement is valid for low subcoolings (5 and 6 K). The difference in the pressure drop for a subcooling of 5 K, the inlet pressure of 16 bar and mass flow of 15 kg/h is around 22 % comparing the increasing and decreasing subcooling path (see Fig. 3.5). Whereas it is 9.5 % for the same conditions at 17 bar inlet pressure. For higher subcoolings (7-9 K) the increasing and decreasing subcooling curves tend to overlap. The findings on the characteristics of the hysteresis effect can be seen more clearly in Fig. 3.9. Comparing the measurement series at 23 bar and 25 bar for the same mass flow of 16.5 kg/h, it becomes obvious that a lower inlet pressure implies a higher hysteresis effect. This complies with the comparison of the measurement series at 23 bar and 25 bar for the higher mass flow of 18 kg/h. Comparing the measurement series with the mass flow of 16.5 kg/h and the mass flow of 18 kg/h at 23 bar, it is noticeable that for the measurement series with 18 kg/h the linear relation of the decreasing subcooling paths is disrupted at 6 K subcooling. Presumably, there has been a collapse of metastable flow. Concerning the measurement series with 16.5 kg/h mass flow, the disruption takes place at 5 K subcooling. Consequently, the metastable flow/hysteresis effect at higher mass flows seems to be less stable which also corresponds to the measurement series at 25 bar (see Fig. 3.9). The findings on the effects on the charateristics of the hysteresis effect depending on the refrigerant flow condition at the inlet of the capillary is summarized in Tab. 3.4. The observed characteristics are valid for the range of experiments listed

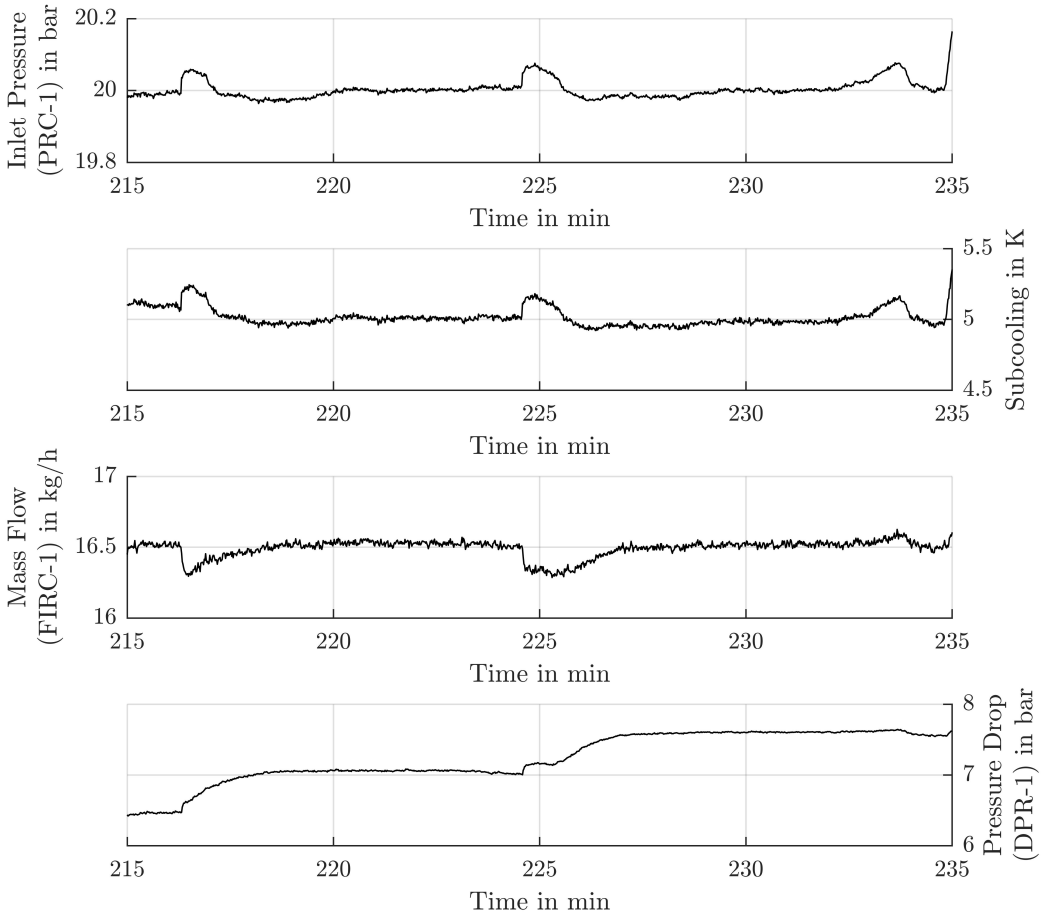

Fig. 3.8: *Extracted time-resolved measurement of the measurement series at a constant inlet pressure (PRC-1) of 20 bar and a mass flow (FIRC-1) of 16.5 kg/h in the copper capillary tube further displaying the subcooling at the capillary inlet and the pressure drop (DPR-1) showing a collapse of a metastable flow (increase in pressure drop).*

Tab. 3.4: *Summarized effects on the hysteresis effect depending on the refrigerant flow condition at the capillary inlet. Valid for the investigated range of flow conditions in Tab. 3.3 for the copper capillary. (*difference between the pressure drops of the increasing and decreasing subcooling paths).*

Refrigerant flow condition			**Effects on the hysteresis effect evoked by the change in subcooling**	
Inlet pressure	**Mass flow**	**Subcooling**	**Quantitative characteristics***	**Stability**
low	low	low	moderate	moderate-high
		high	low	high
	high	low	high	low
		high	moderate	low-moderate
high	low	low	low-moderate	high
		high	low	high
	high	low	high	low
		high	low-moderate	moderate

in Tab. 3.3 and are to be regarded relatively distinguishing between the investigated flow conditions.

3.3.3 Investigation on the cause of the development of metastable flow/hysteresis effect

The metastable flow occurs when changing from high subcoolings to low subcoolings as was seen and discussed at Fig. 3.5 and Fig. 3.6 in the section before. Apparently, some circumstance causes the pressure drop to decrease when changing the direction of the subcooling and going from high to low subcooling. In this section, systematic measurements shall give an answer to which circumstance might cause the development of metastable flow so that a hysteresis effect on the pressure drop appears.

When changing the degree of subcooling while keeping the mass flow and pressure at the inlet of the capillary to a constant level, two obvious changes arise in the flow through the capillary:

- the inlet temperature is changed
- the ratio of the capillary length that is covered by liquid flow is changed

When changing from low subcoolings to high subcoolings, the ratio of the capillary length that is covered by liquid flow is enlarged. This ratio is hereby designated as "wetting ratio". As also experienced by Guobing and Yufeng (2006), the

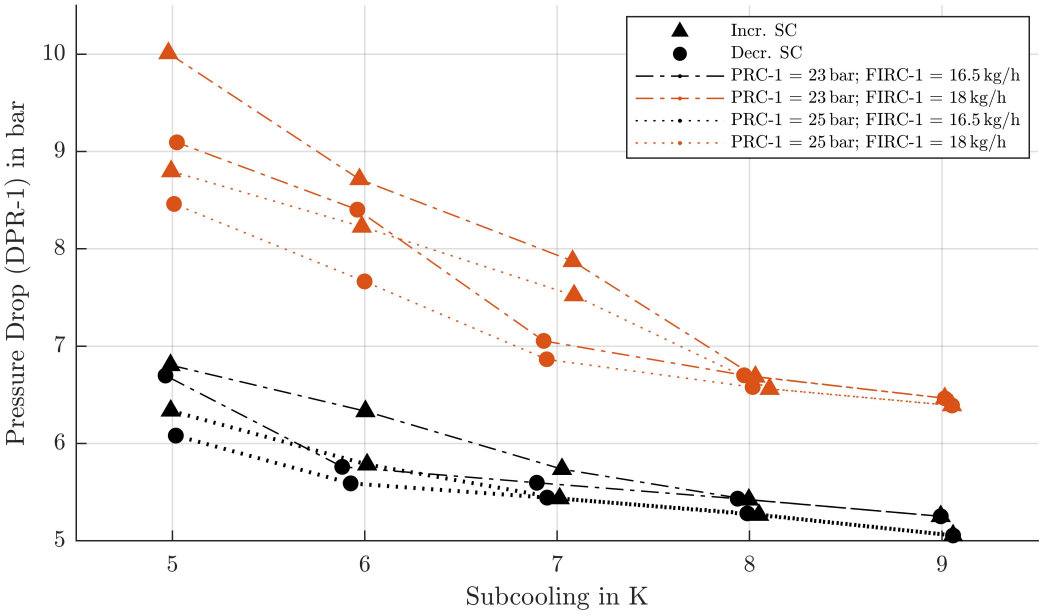

Fig. 3.9: *Comparison of the characteristics of the hysteresis curves including the increasing (Incr.) and decreasing (Decr.) subcooling path at mass flows (FIRC-1) of 16.5 and 18 kg/h and inlet pressures (PRC-1) of 23 and 25 bar in the copper capillary depicting the resulting pressure drop (DPR-1) over the change of the subcooling at the capillary inlet (mean values of the redundant measurements).*

assumption is that metastable flow is negligible for increasing subcooling paths if the initial subcooling is low. Hence, the cause for the development of metastable flow lies in the changing from high to low subcoolings. Consequently, the two possible causes for the development of metastable flow are considered:

1. the change in the inlet temperature from lower to higher temperature

2. the change from a higher wetting ratio to a lower wetting ratio

In order to exclude one of the listed causes, a systematic experiment is carried out. The experiment consists of two parts. In **the first experiment**, an exemplary measurement series at a constant inlet pressure of 16 bar and mass flow of 16 kg/h is performed. The increasing and decreasing subcooling paths are performed consecutively from 5 to 9 K and back to 5 K in 1 K-steps. **The second experiment** is exactly alike in terms of inlet pressure, mass flow and the increasing and decreasing subcooling paths. The difference is that after (and before) each steady-state operation of one adjusted subcooling the capillary is flushed with fully liquid flow. The liquid flow is realized by increasing the pressure at the inlet of the capillary. Fig. 3.10 shows a time section of the second experiments which highlights the

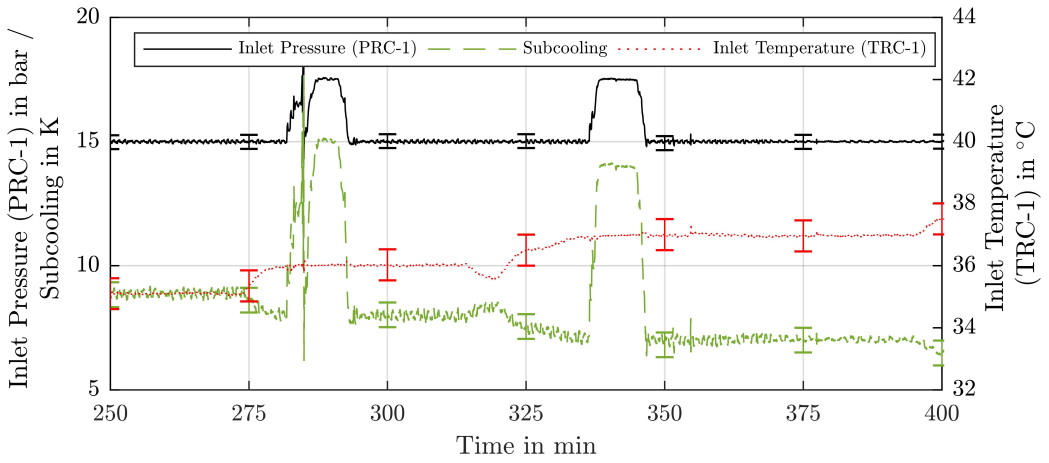

Fig. 3.10: *Representative extract from the time-resolved recordings of the propane flow conditions at the inlet of the copper capillary - flushing the capillary by increasing the inlet pressure (PRC-1). Showing the inlet pressure (PRC-1), the subcooling and the temperature (TRC-1) at the capillary inlet (source: (Gabrisch and Repke, 2021)).*

flushing of the capillary after each steady-state condition of the measurement

series. It can be seen that when the inlet pressure is increased, the subcooling is increased, too. However, the inlet temperature remains constant. This is due to the approximate incompressibility of the refrigerant. It follows that the second experiment includes the temperature change impact of the first experiment but, in contrast, the wetting ratio is not changed. In the second experiment, the capillary is always fully flushed as a precondition for each steady-state measurement point of the increasing and decreasing subcooling path. Thus, in the second experiment, there is no change in the wetting ratio as it remains constant for the whole measurement series. If the wetting ratio does not cause the metastable flow, we expect to not see any difference compared to the first experiment. As the inlet conditions of the flow remain the same in the second experiment, we then could conclude that the temperature change causes the development of the metastable flow and thereby evokes the hysteresis effect on the gathered pressure drop.

Fig. 3.11 depicts the results of the two experiments. The left diagram shows the results of the **first experiment**. The measurement series results in the expected hysteresis curve of the pressure drop with the recorded pressure drops of the decreasing subcooling path being below the pressure drops of the increasing subcooling path. The right diagram in Fig. 3.11 presents the results of the **second**

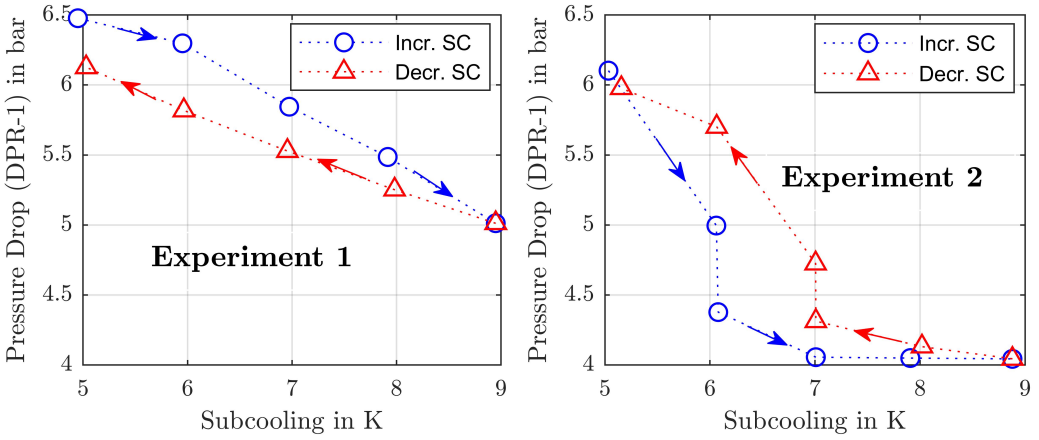

***Fig. 3.11: Left**: Performing increasing (Incr.) and decreasing (Decr.) subcooling paths **without flushing**; **Right**: Performing increasing and decreasing subcooling paths **with flushing**. Both at 15 bar inlet pressure (PRC-1) and a mass flow (FIRC-1) of 16 kg/h in the copper capillary depicting the resulting pressure drop (DPR-1) over the change of the subcooling at the capillary inlet (source: (Gabrisch and Repke, 2021)).*

experiment. The following observations are striking about the second experiment:

- the overall pressure drops in the second experiment are below the pressure drops of the first experiment
- the pressure drops of the decreasing subcooling path lie above those of the increasing subcooling path
- metastable collapse took place at both - the increasing and decreasing subcooling paths

The listed observations suggest that metastable flow was developed not only at the decreasing but also at the increasing subcooling path. Assuming that the increasing subcooling path of the first experiment entails (almost) no metastable flow, the increasing subcooling path of the second experiment has to since the pressure drops are much lower. The observed ambiguous pressure drops at 6 K subcooling of the increasing subcooling path of the second experiment support this assumption. It is an indicator for the collapse of metastable flow - hence, there should have been metastable flow before it collapsed. **It is reasonable to conclude that the flushing of the capillary evoked the development of metastable flow and thereby a lower pressure drop**.

It can be assumed that the higher the wetting ratio the longer the metastable flow and, thus, the lower the measured pressure drop. In the first experiment, the lowest pressure drop is 5 bar at an inlet pressure of 16 bar and a subcooling of 9 K. The according inlet enthalpy can be determined by means of the REFPROP database for propane. Assuming an isenthalpic throttling, the vapour quality at the capillary outlet can be calculated given the outlet pressure (11 bar) and the calculated inlet enthalpy. The calculated vapour quality is at 6.12 %. Hence, within the first experiment, the capillary is never fully flushed if the wetting of the capillary is regarded of the part of the capillary that is covered by pure liquid flow. In the second experiment, in contrast, the capillary is fully flushed before each recording of the pressure drop. As the pressure drops in the second experiments are lower or equal to the first experiment, it is reasonable to assume that the degree of the wetting ratio enhances the development of metastable flow and thereby evokes a lower pressure drop.

As the influence of the change in the inlet temperature in the second experiment is the same as in the first experiment, it is concluded that the wetting of the capillary tube entails the development of metastable flow. In the first experiment, the highest wetting ratio of the capillary tube is reached at 9 K subcooling. Before, it is assumed that there is no metastable flow present and, hence, the pressure drop is as high as possible for the given capillary design and flow condition. Metastable flow is developed when changing back to lower subcoolings. Regarding the 5 K subcooling of the decreasing subcooling path of the first experiment, the capillary tube is partly wetted where it was not wetted at 5 K subcooling for the increasing subcooling path. Consequently, the wetted capillary surface affects the two-phase flow of the refrigerant and lowers the pressure drop.

The following hypotheses conclude the investigations on the cause of the development of metastable flow and the presence of the hysteresis effect on the pressure drop, respectively:

- a wetted capillary lowers the pressure drop of the (two-phase) flow or refrigerant through the capillary
- the higher the previous wetting ratio of the capillary the lower the resulting pressure drop

The hypotheses will be introduced in model assumptions in section 4.2.

3.3.4 Refining measurements of the inner diameter and roughness

In order to precisely determine the inner diameter and the roughness of the inner surface of the capillary, the capillary is excluded from the experimental apparatus after the measurements in the copper capillary tube are accomplished. Five test samples of 1 cm length and are cut out of the capillary tube for the investigation of the inner diameter and 4 test samples of 2 cm length for the investigation of the roughness. In the following, the measurement methods and techniques are explained.

Measuring the inner diameter

The inner diameter of the capillary is measured using a light microscope (Nikon SMZ-U stereo microscope). The test samples that have been cut out of the capillary for the investigation of the inner diameter consist of the outer parts of the capillary (inlet and outlet) and three inner parts that are taken from evenly distributed parts over the capillary length. The 1 cm long tube samples are vertically placed in a PVC cuboid with holes which is shown in Fig. 3.12 and Fig. 3.13. The outer parts of the capillary tube are placed in such way that the inlet and outlet of the capillary tube (as it was installed within the experimental apparatus) are pointing outward of the PVC cuboid. The outer parts of the capillary remain unprepared compared to the application within the experimental apparatus. However, the inner parts of the capillary have been cut out of the capillary tube at both sides. Consequently, both ends of the test samples are deformed compared to the installation within the experimental apparatus. The test samples require a treatment in order to measure the undistorted inner diameter which is described in the following. For the inner test samples it is insignificant in which direction they are put inside the PVC cuboid. The cuboid that contains the inner test samples is framed with tape and the cuboid is poured over with epoxy resin so that the epoxy resin encloses, fills and covers the test samples. After the epoxy resin is hardened, the epoxy surface of the cuboid is grinded with increasingly finer sandpaper until finally it is polished. In this manner, the deformation by the cutting process is eliminated while the epoxy resin prevents burr to arise. The progress is continuously observed under the light microscope until the resulting cross-sectional area of the tube samples appears to be free from burr and the inner diameter is clearly standing out from the filled cross-sectional area of the samples. The inner diameter of the outer and inner parts of the capillary are analysed using an imaging software (Olympus, Stream 2.0) in which circles are drawn via three points that are set at the contour of the inner diameter. The software determines the diameter of the drawn circles. Since the cross-sectional area of the test samples is not perfectly round, five circles are drawn with the three points distributed at different locations on the contour (see Fig. B.1 in the appendix). For each test sample the mean of the diameter of the five circles and the standard deviation is determined and corresponds to the indicated inner diameter of one test sample. For the total capillary the mean inner diameter of all investigated test samples as well as the standard deviation

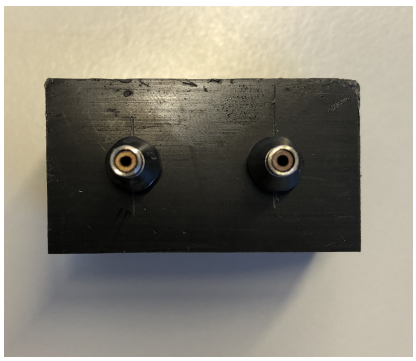

Fig. 3.12: Unembedded test samples of the outer parts of the capillary.

Fig. 3.13: Unembedded test samples of the inner parts of the capillary.

(of the outer and the inner test samples) is averaged. The detailed results are included in the appendix (see Tab. B.1). In this way, the averaged inner diameter of the investigated copper capillary results in d_{Copper}=1.1799e-3 m with a standard deviation of $\sigma_{d,Copper}$=0.01e-3 m .

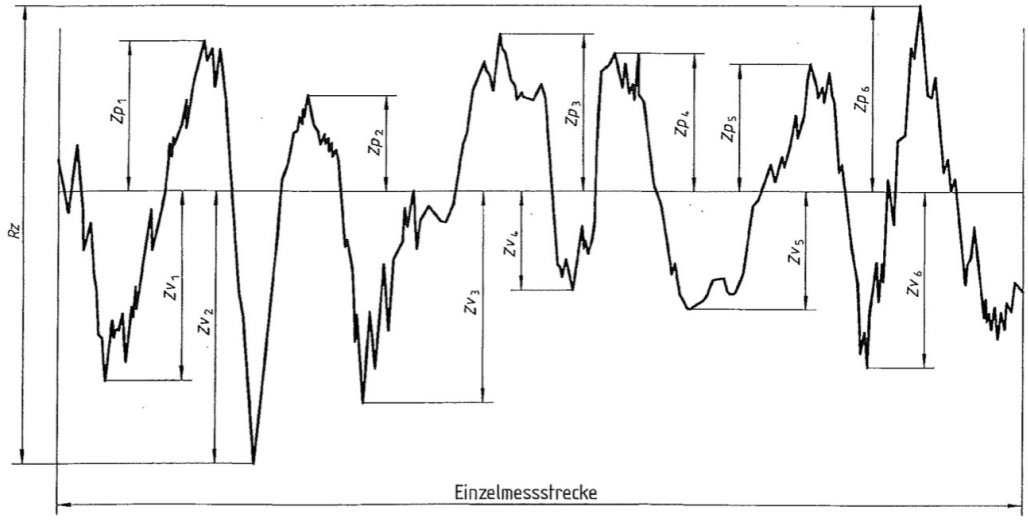

Fig. 3.14: *Illustration of the average roughness depth Rz (source: DIN EN ISO 4287).*

Measuring the roughness

The roughness is measured using a white light interferometer (Axio Imager.Z2m with Laser Scanning Module LSM800). The four test samples (R1-R4) that have been cut out of the capillary for the purpose of measuring the roughness of the inner surface of the capillary are evenly distributed over the length of the capillary. The test samples are prepared for the measurement using the white light interferometer by grinding them longitudinally and thereby create half-pipes (see Fig. B.2). The test samples are cleaned in ethanol in an ultrasonic bath for ten minutes and investigated under the white light interferometer using the software ZEN 2.3 blue edition (Lens: 20x/ NA 0,7, Mastergain 185 VI). The analysis is done using the analysis tool ConfoMap 7.4. The investigation and analysis was carried out by the company BSH Home Appliances Group. 77 to 85 profile curves of the inner surface of the prepared half-pipes are analysed with respect to the average roughness value *Ra* and average roughness depth *Rz* which are chosen to be considered for the parametrization of the roughness e in the flow model presented in chapter 4. According to the DIN EN ISO 4287, the average roughness

value Ra is defined as follows:

$$Ra = \frac{1}{l} \int_0^l |Z(x)| dx \tag{3.1}$$

where $Z(x)$ is the height of a measured profile line at any position x. The average roughness depth Rz is defined as the sum of the largest profile valley Z_v and the largest profile peak Z_p(see Fig. 3.14). The mean values and the standard deviations of the profile curves for each test stample are listed in Tab. B.2.

For the determination of the roughness measures Ra and Ra and the according standard deviations, the mean values and standard deviations of the test samples are averaged and result to: Ra_{Copper}=0.101e-6 m , $\sigma_{Ra,Copper}$=0.016e-6 m , Rz_{Copper}=1.285e-6 m and $\sigma_{Rz,Copper}$=0.391e-6 m .

3.4 Experiments on the Propane Flow Through a Steel Capillary Tube

In this section, the propane flow through a steel capillary tube that has the same manufacturer specification as the copper capillary tube in section 3.3 is examined using the test apparatus in Fig. 3.1. Consequently, the steel capillary is 1 m long and the inner diameter is specified to 1.1 mm. However, the inner diameter is refined in section 3.4.3 after the experiments on the propane flow are accomplished. The experiments on the steel capillary serve as a further validation base in order to check whether the flow model that is adapted based on the experimental results of the capillary tube is valid for the steel capillary as well.

3.4.1 Design on experiments

The roughness of the inner surface of the capillary tube is not specified by the manufacturer. In order to estimate the roughness of the investigated steel capillary (see section 5.2.1), experiments that result in pure liquid flow are performed. The

Tab. 3.5: *Investigated flow conditions at the (steel) capillary inlet with liquid flow through capillary tube.*

PRC-1 in bar	**FIRC-1** in kg/h	**Subcooling** in K
15	8	9
15	9	9.5
16	11	11.5
16.5	13	12
18	15	16.5
18.5	17	18
19	18	19

test plan is shown in Tab. 3.5 [1] and the according experimental results of the steady-state conditions are presented in Tab. A.4 in the appendix.

The experiments of the two-phase pressure drop of propane in the steel capillary are designed to result in comparable pressure drops as in the copper capillary. As a consequence, the experiments result in the same validation range for the flow model as the experiments of the propane flow through the copper capillary. In order to not perform the complete test plan of the experiments that have been carried out in the copper capillary, representative inlet conditions of the propane flow from the test plan related to the copper capillary are chosen. The chosen inlet conditions are listed in Tab. 3.6 and investigated for the propane flow through the steel capillary. The shown conditions result in pressure drops that range from the lowest to the highest achieved pressure drop in the copper capillary tube (compare the experimental range of the experiments in the copper capillary in Tab. A.2). Therefore, the resulting operation range is considered to be comparable with the experiments of the copper capillary if the throttling behaviour is comparable. The listed inlet conditions in Tab. 3.6 result in a liquid and two-phase flow in the capillary. The inlet conditions are performed in increasing subcooling paths which are directly followed up by the decreasing subcooling path as explained in section 3.2. The steady-state conditions are determined as described in section 3.3.1 and the experimental results are listed in Tab. A.5 and Tab. A.6 in the appendix.

[1] It was decided do increase the range of inlet conditions in terms of the mass flow as the inlet pressure and the subcooling for pure liquid flow is rather insensitive with respect to the liquid pressure drop.

Tab. 3.6: *Investigated flow conditions at the (steel) capillary inlet with phase change inside the capillary tube.*

PRC-1 in bar	**FIRC-1** in kg/h	**Subcooling** in K
16	13.5	5, 6, 7, 8, 9
20	15	5, 6, 7, 8, 9
20	16.5	5, 6, 7, 8, 9
23	16.5	5, 6, 7, 8, 9
23	18	5, 6, 7, 8, 9
25	16.5	5, 6, 7, 8, 9
25	18	5, 6, 7, 8, 9

3.4.2 Results and discussion

Fig. 3.15 depicts all gathered measurement series that are listed in Tab. 3.6. Only the mean values of the double measured measurement series are depicted in the figure for a clearer appearance of the results. It can be seen that the general effects of the input variables (mass flow, inlet pressure and subcooling) is the same as observed in the copper capillary (see section 3.3.2): the higher the mass flow and the lower the subcooling and inlet pressure, the higher the resulting pressure drop in the capillary. The highest pressure drop is observed for the increasing subcooling path at 23 bar inlet pressure and 18 kg/h mass flow. However, it is to note that at 5 K the mass flow of 18 kg/h is not properly reached. Consequently, the pressure drop should be higher here. At 6 and 7 kg/h the mass flow is slightly above 18 kg/h (see experimental data in Tab. A.5), so the pressure drop should be slightly lower for the the desired 18 kg/h. Consequently, the course of the pressure drop for the increasing subcooling path at 23 bar and 18 kg/h is slightly misleading.

Tab. A.7 in the appendix contains the mean values of the measurement series of the listed flow conditions in Tab. 3.6 comparing the resulting pressure drops gathered in the copper and steel capillary. It becomes visible that the pressure drop in the steel capillary is significantly higher for all compared flow conditions. The difference between the measured pressure drop in the copper and steel capillary tube increases for decreasing inlet pressures and increasing mass flows. The largest difference is reached for the measurement series ar 23 bar inlet pres-

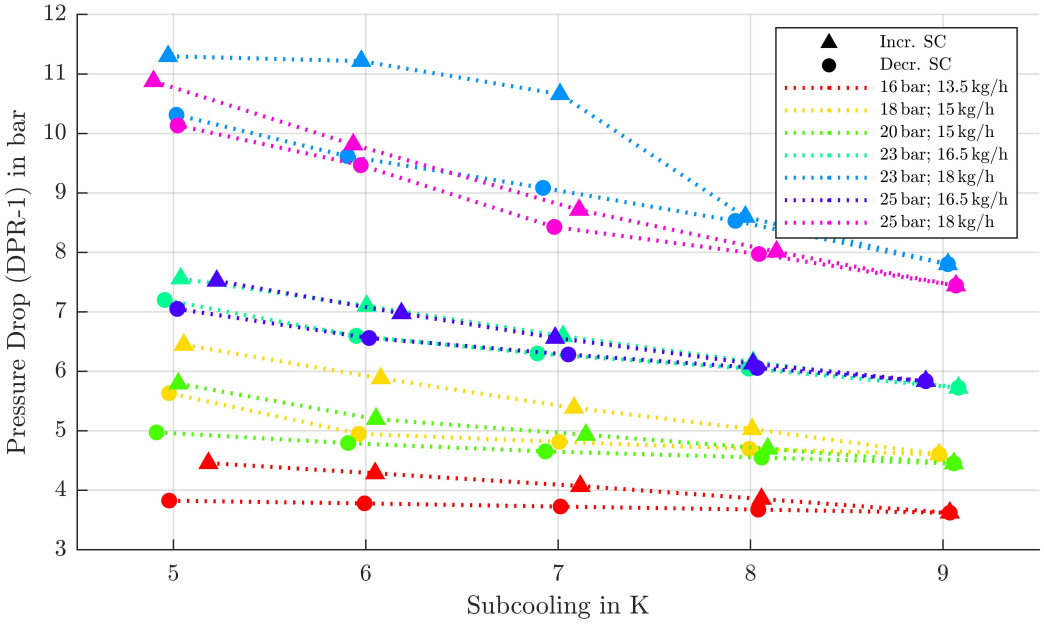

Fig. 3.15: *Experimental results of the measurements series in Tab. 3.6 in the steel capillary tube comprising all increasing (Incr.) and decreasing (Decr.) subcooling paths. The legend displays the measurements at different inlet pressures (PRC-1) and different mass flows (FIRC-1). The diagram shows the resulting pressure drop (DPR-1) over the change of the subcooling at the capillary inlet (mean values of the redundant measurements).*

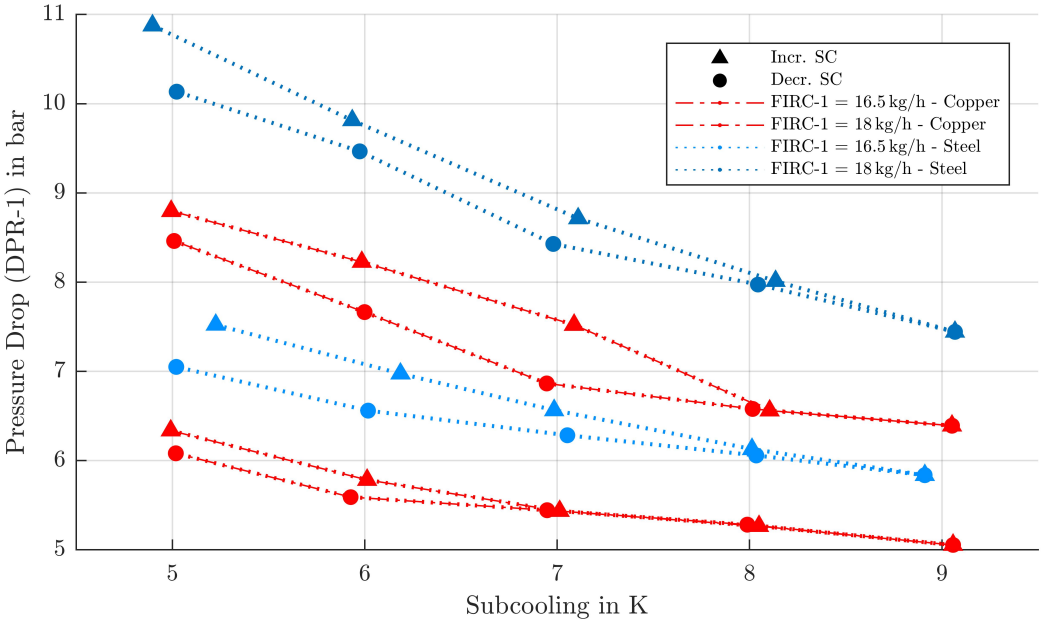

Fig. 3.16: *Comparison of the characteristics of the hysteresis curves including the increasing (Incr.) and decreasing (Decr.) subcooling path at different mass flows (FIRC-1) for an inlet pressure (PRC-1) of 25 bar referring to the experiments in the copper and steel capillary. The diagram shows the resulting pressure drop (DPR-1) over the change of the subcooling at the capillary inlet.*

sure and 18 kg/h mass flow. The difference between both capillary tubes marks a maximum of about 35 % concerning the evoked pressure drop. Generally, the discrepancy between the pressure drops in the two capillaries increases for increasing two-phase flow of the refrigerant which is plausible since the effect of the capillary design (e.g. inner diameter or roughness) is larger for the two-phase flow as for the pure liquid flow due to the acceleration of the flow induced by the friction. The difference in the pressure drop concerning the liquid flow is significantly lower (compare Tab. A.1 and Tab. A.4). As the inner diameter of the steel capillary is specified to be equal to the copper capillary, the difference has to be attributable to the difference of the roughness of the tubes. The inner diameter of the steel capillary is measured in section 3.4.3 in order to confirm the comparability of the inner diameters of the copper and steel capillary. The roughness of the steel capillary is determined based on a model-based approach in section 5.2.1.

Fig. 3.16 compares the pressure drops gathered in the copper and steel capillary tube for the measurement series at 25 bar inlet pressures and the mass flows of 16.5 kg/h and 18 kg/h. Only the mean values of the double measured measurement series are depicted in the figure for a clearer appearance of the results. It can be seen that the steel capillary evokes a clearly higher pressure drop for the depicted measurement series.

Except the measurements at 25 bar inlet pressure and 18 kg/h, the hysteresis effect in the steel capillary appears to be more stable than in the copper capillary tube, which means that the decreasing subcooling paths follow mostly linear graphs without any presumable collapses of metastable flow (see Fig. 3.15).

Fig. 3.16 shows that for a mass flow of 16.5 kg/h the hysteresis effect is higher in the steel capillary than in the copper capillary - i.e. the difference between the pressure drops of the increasing and decreasing subcooling path is larger for the steel capillary. At the mass flow of 18 kg/h both measurement series indicate a collapse of metastable flow as the linear course of the decreasing subcooling paths is disrupted at 6 K (see section 3.3.2 for the classification of an instable hysteresis effect). Consequently, it is not reasonable to compare the quantity of hysteresis effect for these measurement series. However, for all other measurement series the difference between the increasing and decreasing subcooling paths is larger in the steel capillary than in the copper capillary which is obvious when comparing the data in Tab. A.7. Hence, it can be stated that the hysteresis effect has a larger impact in the steel capillary than in the copper capillary. As presumably, the inner diameters of the capillaries are within the same dimension, the reason for that can be related to the different surface structure of both tubes.

3.4.3 Refining measurements of the inner diameter

For the refinement of the steel capillary specification, five test samples are prepared from the investigated steel capillary and the inner diameter is measured analogously as described in section 3.3.4. The detailed statistical results of the measurement of the equivalent five test samples of the steel capillary under the

light microscope is attached in the appendix (see Tab. B.3). The investigation results in an average inner diameter of the steel capillary of d_{Steel}=1.1749e-3 m and a standard deviation of $\sigma_{d,Steel}$=0.01e-3 m .

The roughness measures Ra_{Steel} and Rz_{Steel} are not measured. A model-based approach to determine both values is applied which is described in section 5.2.1 and is a cost-effective alternative based on the equal inner diameters of the copper and steel capillary.

4 Mathematical Model of the Refrigerant Flow Through A Capillary Tube

In this chapter, the mathematical model that describes the single and two-phase flow of a refrigerant through a capillary tube is presented. This chapter basically consists of the published content from (Gabrisch and Repke, 2020) and (Gabrisch and Repke, 2021).

4.1 Homogeneous Flow Model

The modelling of the single phase liquid and two-phase refrigerant flow through the capillary is divided into the calculation of the liquid flow and the two-phase flow. The two-phase flow is considered to be homogeneous. It is a common assumption to predict the overall pressure drop in a capillary by dividing it into the calculation of liquid and two-phase pressure drop where the two-phase flow is considered to be homogeneous (e.g. (Dirik et al., 1994) and (Gao, Eguchi, and Tatara, 2015)). For a detailed derivation of the homogeneous flow approach see section 2.3.

In the following, the applied solution algorithm in terms of the homogeneous flow model is described in detail since different researchers apply different assumptions. A high level of detail is targeted in the description for reproducibility of the numerical data.

The pressure drop in the capillary Δp is calculated as the sum of the pressure drop due to the sudden contraction $\Delta p_{entr.}$ when the refrigerant flow enters the

capillary, the pressure drop of the liquid phase Δp_{liq} and the pressure drop of the two-phase flow Δp_{tp} of the refrigerant:

$$\Delta p = \Delta p_{entr.} + \Delta p_{liq} + \Delta p_{tp} \tag{4.1}$$

The pressure drop at the exit of the capillary tube is not regarded as the pressure at the capillary outlet is measured inside the capillary tube (see Fig. 3.3). The pressure drop that arises due to the sudden contraction at the entrance of the capillary tube is calculated using a simple pressure drop correlation depending on the entrance pressure drop coefficient ξ, the mass flux G and the density at the capillary inlet ρ_{inlet} (compare (Schade and Kunz, 2007b)) :

$$\Delta p_{entr.} = \xi \cdot \frac{G^2}{\rho_{inlet}} \tag{4.2}$$

G denotes the mass flux which is the mass flow $\dot{m}$ per cross-sectional area of the capillary A and equal to the product of density ρ and flow velocity v:

$$G = \frac{\dot{m}}{A} = \rho \cdot v \tag{4.3}$$

$p_{a.entr.}$ is the pressure after the entrance of the capillary, i.e. the inlet pressure p_{inlet} subtracted by the entrance pressure drop $\Delta p_{entr.}$:

$$p_{a.entr.} = p_{inlet} - \Delta p_{entr.} \tag{4.4}$$

In case $p_{a.entr.}$ is still larger than p_{sat} – the saturation pressure according to h_{inlet} assuming an isenthalpic throttling – the length of the capillary that is occupied with liquid flow ΔL_{liq} is calculated next. If $p_{a.entr.}$ is lower or equal to p_{sat} the two-phase pressure drop is calculated (Eq. (4.13) and following). ΔL_{liq} is explicitly calculated by setting the pressure drop of the liquid flow Δp_{liq} in the capillary to the difference $(p_{a.entr.} - p_{sat})$:

$$\Delta p_{liq} = p_{a.entr.} - p_{sat} \tag{4.5}$$

The liquid pressure drop Δp_{liq} is described by the Darcy-Weisbach correlation for the frictional pressure drop (see derivation in section 2.3):

$$\Delta p_{liq} = \Delta L_{liq} \cdot \frac{\overline{f}_{liq}}{2 \cdot d} \cdot \frac{G^2}{\overline{\rho}_{liq}} \tag{4.6}$$

where d denotes the inner diameter of the capillary and $\overline{\rho}_{liq}$ and $\overline{f}_{liq}$ represent the mean values of the friction factor and density for the liquid pressure drop defined by Eq. (4.5) and constant enthalpy, see Eq. (4.7). This is a simplification that follows the assumption that for the liquid flow the refrigerant is considered to be nearly incompressible and the pressure drop is almost isothermal.

$$\overline{f}_{liq} = \frac{f_{inlet} + f_{sat}}{2} \text{ and } \overline{\rho}_{liq} = \frac{\rho_{inlet} + \rho_{sat}}{2} \tag{4.7}$$

Single phase properties are determined using the REFPROP database.

Eq. (4.5) assumes that the liquid flashes inside the capillary. If, for this assumption, the calculation of the liquid length ΔL_{liq} exceeds the actual capillary length L, Eq. (4.6) is used to calculate the pressure drop Δp_{liq} that is evoked by fully liquid flow in the capillary. In this case, ΔL_{liq} is set to the capillary length L.

The friction factor f follows, in each case, the correlation developed by Serghides (1984), described in the equations below, which approximates the implicit correlation by Colebrook (1939) (see Eq. (2.31)):

$$\frac{1}{\sqrt{f}} = AA - \frac{(B - AA)^2}{C - 2 \cdot B + AA} \tag{4.8}$$

$$AA = -2 \cdot \log_{10}\left(\frac{e/d}{3.7} + \frac{12}{Re}\right) \tag{4.9}$$

$$B = -2 \cdot \log_{10}\left(\frac{e/d}{3.7} + \frac{2.51 \cdot AA}{Re}\right) \tag{4.10}$$

$$C = -2 \cdot \log_{10}\left(\frac{e/d}{3.7} + \frac{2.51 \cdot B}{Re}\right) \tag{4.11}$$

The correlation by Serghides was found out to be appropriate for the given relation of the considered relative roughness e and the diameter d of the capillary (generally investigated by Asker, Turgut, and Coban (2014); for the given geome-

try investigated by Gabrisch, Grunert, and Repke (2017)). The Reynolds-Number Re is calculated by the means of the dynamic viscosity μ:

$$Re = \frac{v \cdot d \cdot \rho}{\mu} \tag{4.12}$$

The two-phase pressure drop Δp_{tp} in Eq. (4.1) splits into the acceleration pressure drop $\Delta p_{acc,tp}$ and the frictional pressure drop $\Delta p_{fric,tp}$ (compare Eq. (2.29) and derivation in section 2.3):

$$\Delta p_{tp} = \Delta p_{acc,tp} + \Delta p_{fric,tp} \tag{4.13}$$

The two-phase pressure drop calculation is conducted pressure-discretized, where dp_i, the discretized pressure drop, is a function of the iteration step i:

$$dp_i = 10^5 \cdot \exp\left(-0.2 \cdot i\right) + 500 \tag{4.14}$$

$$\Delta p_{tp,i} = p_{tp,i} - p_{tp,i+1} = dp_i \tag{4.15}$$

The pressure is reduced incrementally, beginning from the saturation pressure:

$$p_1 = p_{sat} \tag{4.16}$$

Subsequently, the two-phase capillary length $\Delta L_{tp,i}$ that corresponds to the pressure drop in Eq. (4.15) is calculated. This requires the calculation of the acceleration pressure drop $\Delta p_{acc,tp,i}$ and the frictional pressure drop $\Delta p_{frict,tp,i}$, see Eq. (4.13):

$$\begin{aligned} \Delta p_{acc,tp,i} = &\left(\frac{G^2 \cdot x_i^2}{\alpha_i \cdot \rho_{v,i}} + \frac{G^2 \cdot (1-x_i)^2}{(1-\alpha_i) \cdot \rho_{l,i}}\right) - \\ &\left(\frac{G^2 \cdot x_{i+1}^2}{\alpha_{i+1} \cdot \rho_{v,i+1}} + \frac{G^2 \cdot (1-x_{i+1})^2}{(1-\alpha_{i+1}) \cdot \rho_{l,i+1}}\right) \end{aligned} \tag{4.17}$$

where x is the vapour quality. The void fraction α_i is calculated using the homogeneous definition (as in Beattie and Whalley (1982)):

$$\alpha_i = \frac{x_i}{x_i + (1-x_i) \cdot \rho_{v,i}/\rho_{l,i}} \tag{4.18}$$

The frictional pressure drop $\Delta p_{fric,tp,i}$ is calculated as follows:

$$\Delta p_{fric,tp,i} = \Delta L_{tp,i} \cdot \frac{\overline{f}_{tp,i}}{2 \cdot d} \cdot \frac{G^2}{\overline{\rho}_{tp,i}} \tag{4.19}$$

The pressure drop in the two-phase region is regarded as non-isenthalpic, which derives from energy conservation for adiabatic and stationary flow with friction, neglecting the potential energy of the flow (see Eq. (2.10) and derivation in section 2.2):

$$\begin{aligned} h_{tp,i} + \frac{1}{2} \cdot \left(\frac{\dot{m}}{A}\right)^2 \cdot \frac{1}{\rho_{tp,i}^2} = \\ h_{l,i+1} + x_{i+1} \cdot \Delta h_{lv,i+1} + \frac{1}{2} \cdot \left(\frac{\dot{m}}{A}\right)^2 \cdot \left(\frac{1}{\rho_{l,i+1}} + x_{i+1} \cdot \frac{1}{\Delta \rho_{lv,i+1}}\right)^{-2} \end{aligned} \tag{4.20}$$

where h_l is the liquid enthalpy and ρ_l the liquid density, Δh_{lv} the enthalpy of vaporization and $\Delta \rho_{lv}$ the difference of liquid and vapour density, accordingly. As the kinetic energy of the refrigerant flow rises due to the density drop of the refrigerant, the enthalpy must decrease. Knowing the current condition of the refrigerant at discretization state i, the vapour quality x_{i+1} can be calculated.
For Eq. (4.19), the mean value $\overline{f}_{tp,i}$ is calculated as follows:

$$\overline{f}_{tp,i} = \frac{f_{tp,i} + f_{tp,i+1}}{2} \tag{4.21}$$

Analoguously to Eq. (4.21) follows the calculation for $\overline{\rho}_{tp,i}$. The friction factor $f_{tp,i}$ follows the correlation of Serghides in Eq. (4.8) to (4.11). This requires the two-phase Reynolds-Number $Re_{tp,i}$, which in turn requires the two-phase density $\rho_{tp,i}$, the two-phase velocity $v_{tp,i}$ and the two-phase dynamic viscosity $\mu_{tp,i}$. The two-phase density $\rho_{tp,i}$ of the refrigerant is determined by the arithmetic mean of the vapour quality x_i corresponding to the homogeneous flow approach:

$$\frac{1}{\rho_{tp,i}} = \frac{x_i}{\rho_{v,i}} + \frac{1 - x_i}{\rho_{l,i}} \tag{4.22}$$

For the homogeneous two-phase dynamic viscosity $\mu_{tp,i}$, several correlations exist that specifically average the vapour viscosity $\mu_{v,i}$ and the liquid viscosity $\mu_{l,i}$,

Tab. 4.1: *Considered two-phase viscosity correlations (homogeneous two-phase flow).*

Author	Two-phase viscosity correlation
McAdams, Woods, and Heroman (1942)	$\mu_{tp,i} = \left(\frac{x_i}{\mu_{v,i}} + \frac{1-x_i}{\mu_{l,i}} \right)^{-1}$
Cicchitti et al. (1959)	$\mu_{tp,i} = x_i \cdot \mu_{v,i} + (1-x_i) \cdot \mu_{l,i}$
Dukler, Wicks III, and Cleveland (1964)	$\mu_{tp,i} = \rho_{tp,i} \cdot \left[x_i \cdot \frac{\mu_{v,i}}{\rho_{v,i}} + (1-x_i) \cdot \frac{\mu_{l,i}}{\rho_{l,i}} \right]$
Beattie and Whalley (1982)	$\mu_{tp,i} = \mu_{l,i} \cdot (1-\beta_i) \cdot (1+2.5 \cdot \beta_i) + \mu_{v,i} \cdot \beta_i$ $\beta_i = \frac{x_i}{x_i + (1-x_i) \cdot \rho_{v,i}/\rho_{l,i}}$
Lin et al. (1991)	$\mu_{tp,i} = \frac{\mu_{l,i} \cdot \mu_{v,i}}{\mu_{v,i} + x^{1.4} \cdot (\mu_{l,i} \cdot \mu_{v,i})}$
Fourar and Bories (1995)	$\mu_{tp,i} = \rho_{tp,i} \cdot \left(\sqrt{\frac{x_i \cdot \mu_{v,i}}{\rho_{v,i}}} + \sqrt{\frac{(1-x_i) \cdot \mu_{l,i}}{\rho_{l,i}}} \right)^2$
Awad and Muzychka (2008)	$\mu_{tp,i} = \mu_{v,i} \cdot \left[\frac{2 \cdot \mu_{v,i} + \mu_{l,i} - 2 \cdot (\mu_{v,i} - \mu_{l,i}) \cdot (1-x_i}{2 \cdot \mu_{v,i} + \mu_{l,i} + (\mu_{v,i} - \mu_{l,i}) \cdot (1-x_i)} \right]$

see Tab. 4.1. The listed viscosity correlations are taken into consideration for the validation of the overall capillary model.

The capillary length $\Delta L_{tp,i}$ that is needed for the current two-phase pressure drop $\Delta p_{tp,i}$ is calculated by solving Eq. (4.13) for $\Delta L_{tp,i}$ applying Eq. (4.14), Eq. (4.15), Eq. (4.17), and Eq. (4.19).

In order to solve for the unknown pressure p_{outlet} and enthalpy h_{outlet} at the capillary outlet, the pressure is incrementally reduced by dp_i as long as the following two conditions are fulfilled:

– The cumulatively calculated length $L_{sum,i}$ is lower than the real capillary length L:

$$L_{sum,i} = \Delta L_{liq} + \sum_i \Delta L_{tp,i} < L \tag{4.23}$$

– The Mach-Number at the current outlet condition is lower than 1 (choked condition: $Ma = 1$,):

$$Ma_{tp,i+1} \left(p_{tp,i+1}, h_{tp,i+1} \right) < 1 \tag{4.24}$$

The Mach-Number is calculated following Eq. (2.8). The speed of sound is calculated as the square root from the fraction of the differential of the pressure δp and

the differential of the density $\delta\rho$ while the entropy is constant and in the limit of $\delta p \to 0$, which is a generally applicable approach for any medium (Schade and Kunz, 2007a):

$$c = \lim_{\delta p \to 0} \sqrt{\frac{\delta p}{\delta \rho}}_{s=const.} \tag{4.25}$$

Consequently, a solution is found when the cumulative length corresponds to the actual capillary length while the Mach-Number is lower or equal to 1. The calculation also terminates when Eq. (4.24) is violated, which can lead to a resulting cumulative length lower than the actual capillary length. This means that there is no physical solution for the given inlet condition of the flow and the capillary design as this is no possible scenario in reality.

4.2 Modelling the Hysteresis Effect on the Pressure Drop

In this section, the findings of the investigations in section 3.3.3 are introduced into model assumptions. The flow model from section 4.1 is extended by the mathematical description of these assumptions.

As concluded in section 3.3.3 the wetting of the capillary tube affects the two-phase flow of the refrigerant through the capillary such that the pressure drop is decreased. It is hypothesised that the roughness of the inner surface of the capillary is decreased when overflowed with liquid. The hypothesis and its consequence on the refrigerant flow through the capillary for changed subcoolings at the inlet of the capillary is depicted in Fig. 4.1. Fig. 4.1 illustrates the changing of the subcooling of a refrigerant flow through a capillary from a low to a high to a low subcooling while the inlet pressure and the mass flow remain the same for all three depicted flows. The first depicted flow condition presupposes that the capillary was dry before or the previous flow condition had a lower subcooling than SC_1 so that the wetting ratio of the capillary was lower than the current. The depicted flow results in a liquid flow and a two-phase flow in the capillary and the outlet pressure $P_{out,1}$. The second illustrated flow condition has a higher subcooling SC_2 and, therefore, the liquid flow occupies a larger part of the capillary compared to the first flow. The third shown flow condition indicates the

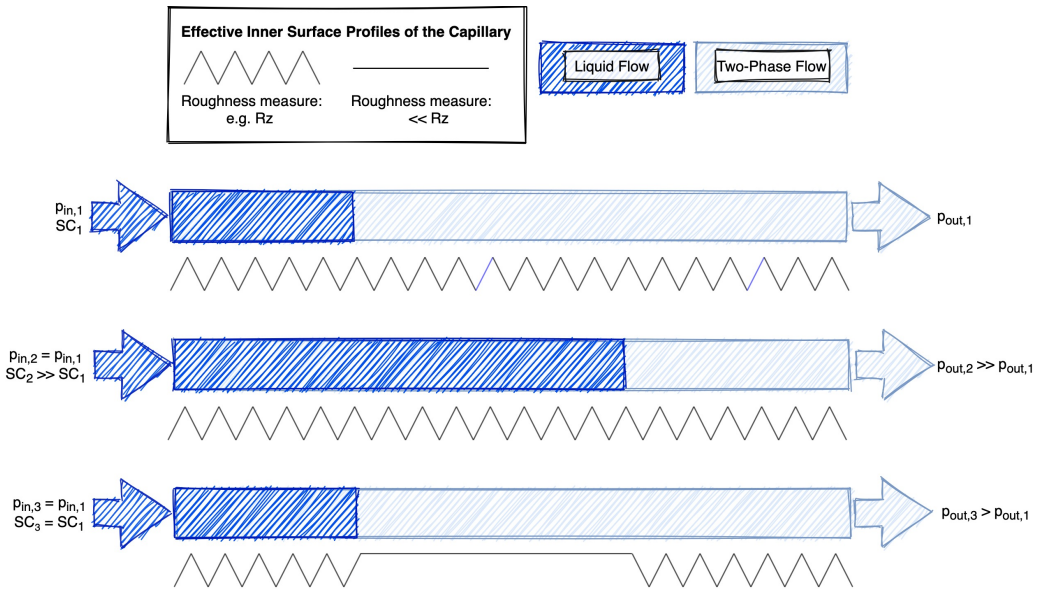

Fig. 4.1: *Effective roughness of the inner surface of the capillary depending on the wetting ratio of the capillary tube (source: (Gabrisch and Repke, 2021)).*

same subcooling as the first flow (SC_3=SC_1) and results in the same liquid flow as the first flow condition. However, it is assumed that the previous flow smoothed the roughness of the inner surface of the capillary where liquid flow overflowed the capillary tube. Up to the point where the liquid flow reached before, the two-phase flow of the third flow is exposed to a lower roughness (and thereby friction) so that the outlet pressure $P_{out,3}$ of the third flow is lower than the outlet pressure $P_{out,1}$ of the first flow. It is assumed that the smoothing only comes into account for the two-phase flow and not for the liquid flow as otherwise it would contradict the Darcy-Weisbach correlation on frictional flow.

Physically, it is possible that the liquid is absorbed in the pores of the roughness profile of the inner surface of the capillary and thereby smoothes the surface. It is presumably an interplay between the roughness profile and the surface tension characteristics of the refrigerant as well as dependant on thermodynamic and flow conditions to which extend the absorption takes place. The complex process of liquid absorption is simplified to the introduction of a scalar variable that is hereinafter referred to as "(effective) wetted surface roughness" e_{wetted}. This variable needs to be empirically determined against the experimental results of

the propane flow through the copper and steel capillary which is elaborated in section 5.1.4 section 5.2.3, independently. Further, the information of the previous wetting ratio is needed in order to determine up to what point the two-phase flow is exposed to the wetted surface roughness e_{wetted}.

The wetting ratio that results from a given flow condition is defined as follows:

$$\Theta = \frac{\Delta L_{liq}}{L} \tag{4.26}$$

The wetting ratio determines the ratio of the liquid flow length ΔL_{liq} to the total capillary length L. ΔL_{liq} is calculated based on Eq. (4.6).

In order to calculate the pressure drop that corresponds to a certain flow condition at the inlet of the capillary, the previous wetting ratio Θ^{-1} is needed as input variable for the flow model in section 4.1. Based on the previous wetting ratio, the capillary length that was previously covered by liquid flow is calculated. The wetted surface roughness e_{wetted} is applied as roughness measure e within the calculation of the two-phase frictional pressure drop $\Delta p_{tp,i}$ in Eq. (4.19) as long as the following condition is valid:

$$L_{sum,i} = \Delta L_{liq} + \sum_i \Delta L_{tp,i} \leq L \cdot \Theta^{-1} \tag{4.27}$$

When Eq. (4.27) is violated, the roughness measure e is either set to the average roughness value Ra or the average roughness depth Rz for the further calculation of the frictional pressure drop of the two-phase flow as long as the conditions in Eq. (4.23) and Eq. (4.24) are fulfilled.

It is obvious that from lower to higher subcoolings, the wetted surface roughness does not influence the calculation of the pressure drop as Eq. (4.27) is never fulfilled.

In the transient simulation of the capillary operation (e.g. when simulating a measurement series, i.e. an increasing and decreasing subcooling path) for the calculation of the first flow condition an initial wetting ratio of the capillary Θ^0 must be given. The flow model is then able to calculate the pressure drop and the wetting ratio Θ^1 for the first flow condition of the measurement series. For the

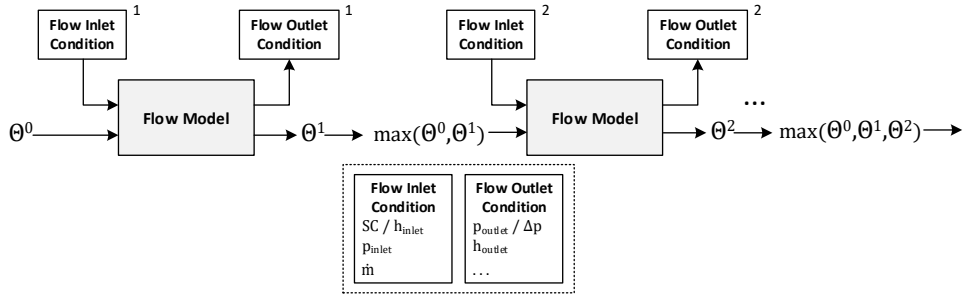

Fig. 4.2: *Calculation scheme of a transient simulation of the flow model for a series of flow conditions.*

calculation of the second flow condition of the measurement series the maximum of all previous wetting ratios is transferred to the flow model and so forth. The procedure of the transient capillary simulation is demonstrated in Fig. 4.2. For the simulation of the increasing subcooling path from 5 to 9 K the current flow condition will result in a higher wetting ratio than the previous flow condition. When simulating the according decreasing subcooling path, the highest wetting ratio is achieved at the subcooling of 9 K. Consequently, for all upcoming flow conditions of the decreasing subcooling path the wetting ratio that resulted from 9 K subcooling is transferred to the flow model.

5 Comparison between Experimental and Numerical Results

The flow model which is presented in chapter 4 can be summarized as a function $F_{Capillary}$ that calculates the pressure drop Δp that arises for a refrigerant flow through a capillary tube given the needed parameters, correlations and input variables:

$$\Delta p = F_{Capillary}\left(\dot{m}, p_{inlet}, h_{inlet}, \Theta^{-1}, d, L, e, e_{wetted}, \xi, \mu_{tp}\right) \tag{5.1}$$

If the inner diameter d, the length L, the relative roughness e of the inner surface and the (effective) wetted surface roughness e_{wetted} as well as the entrance pressure drop coefficient ξ for a specific capillary application and the previous wetting ratio Θ^{-1} are known and the viscosity correlation μ_{tp} is designated, the pressure drop Δp can be calculated for any condition of the refrigerant flow at the inlet of the capillary, where $\dot{m}$ is the mass flow through the capillary, p_{inlet} the pressure and h_{inlet} the enthalpy at the inlet of the capillary tube.

The length of both, the copper and steel capillary, is considered to be $L = L_{Copper} = L_{Steel} = 1.0274\,\mathrm{m}$ (see Fig. 3.3). Whereas the diameter d_{Copper} and the roughness e_{Copper} (here: Ra_{Copper} and Rz_{Copper}) of the copper capillary have been determined via measurements in section 3.3.4, the diameter d_{Steel} has been determined in section 3.4.3.

In the following sections the determination of the entrance pressure drop coefficient ξ, the determination of the best-matching two-phase viscosity correlation μ_{tp} as well as the effective wetted surface roughness $e_{wetted,Copper}$ and $e_{wetted,Steel}$ is presented.

5.1 Experimental and Numerical Results of the Copper Capillary Tube

In this section the flow model is parametrized with respect to:

- the entrance geometry of the capillary (i.e. the ratio of the inner diameter of the connection tube and the inner diameter of the capillary) - hence, identifying the entrance pressure drop coefficient ξ due to sudden contraction

- the investigated refrigerant propane - hence, determining the appropriate two-phase viscosity correlation μ_{tp}

- the investigated capillary material copper - hence, identifying wetted surface roughness $e_{wetted,Copper}$

In section 5.1.1, the entrance pressure drop coefficient ξ is identified based on the experiments of pure liquid flow of propane through the copper capillary tube. Both roughness measures, Ra_{Copper} and Rz_{Copper}, are taken into consideration for the parametrization of e.

Knowing the parameters d, L, e and ξ while setting $e_{wetted} = e$ and choosing a two-phase viscosity correlation μ_{tp}, the flow model that is described in chapter 4 can be used to describe the increasing subcooling paths resulting from the experiments of propane flow through the copper capillary (see Tab. A.2). By setting $e_{wetted} = e$, the hysteresis effect is not taken into account; the flow model is not able to predict ambiguous pressure drops then. However, the pressure drops recorded within the increasing subcooling paths are regarded to be unique and to cause the highest possible pressure drop for the given inlet conditions of the flow (compare findings of (Guobing and Yufeng, 2006) and see section 3.3.3). Consequently, the flow model with $e_{wetted} = e$ aims to predict the increasing subcooling paths of the experimental data.

In section 5.1.2, common two-phase viscosity correlations (listed in Tab. 4.1) are applied within the flow model and compared to the experimental data of the increasing subcooling paths of the propane flow through the copper capillary.

Section 5.1.3 suggests a simple adaption of the viscosity correlation provided by Beattie and Whalley (1982) in order to better match the experimental data of the specifically investigated refrigerant propane.

The two-phase viscosity correlation which results in the best prediction of the experimental data of the increasing subcooling paths is chosen for further calculations. Hence, at this point the only remaining parameter in order to predict the ambiguous pressure drops, i.e. predict the observed hysteresis effect on pressure drop, for the flow through the copper capillary tube is the wetted surface roughness $e_{wetted,Copper}$. The latter one is identified via parameter estimation in section 5.1.4 based on the experimental data of the decreasing subcooling paths of the propane flow through the copper capillary (see Tab. A.3).

The outlined steps of the parametrization of the flow model is summarized in Fig. 5.1. And is a general proposal for the investigation of refrigerant flow in a capillary and the according model adaption/parametrization.

Finally, the overall prediction quality of the parametrized flow model with respect to the experimental data observed in the copper capillary tube is discussed in section 5.1.5 and a model uncertainty analysis is conducted in section 5.3.

5.1.1 Estimation of the entrance pressure drop coefficient

For the determination of the entrance pressure drop coefficient ζ, a parameter estimation using the flow model described in chapter 4 and the liquid flow experiments of propane through the copper capillary (see Tab. A.1) is carried out[1]. As only the liquid flow is considered for the estimation of the parameter, the model is reduced to Eq. (4.6) and the required auxiliary equations. Consequently, ζ remains the only unknown parameter. The parameter estimation is executed in MATLAB using the nonlinear least-squares solver (lsqnonlin) that solves for the parameter ζ that minimizes the error between the calculated and measured liquid pressure drops. Solving for the least squares referring to the comparison between

[1]The content of this section is mainly adopted from (Gabrisch and Repke, 2020)

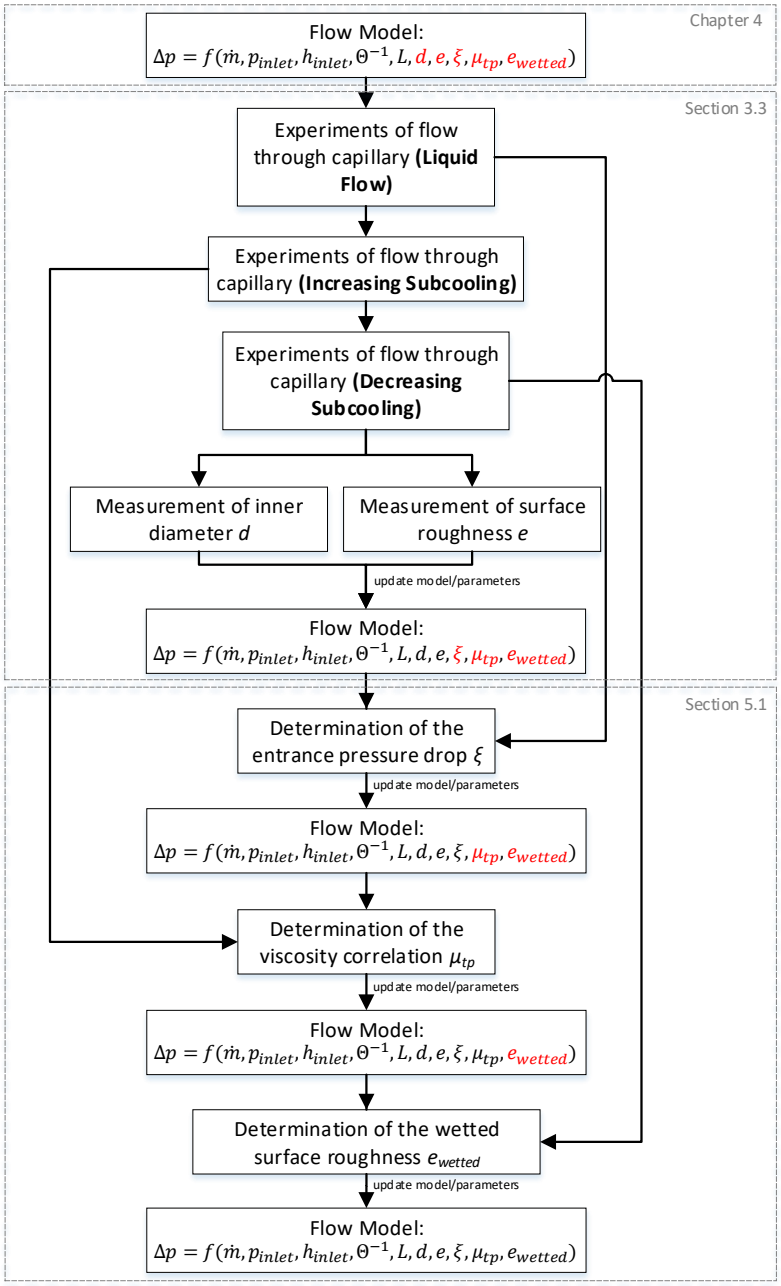

Fig. 5.1: *Systematic approach for the generation of an experimental database on the refrigerant flow in a capillary and the parametrization of the according flow model.*

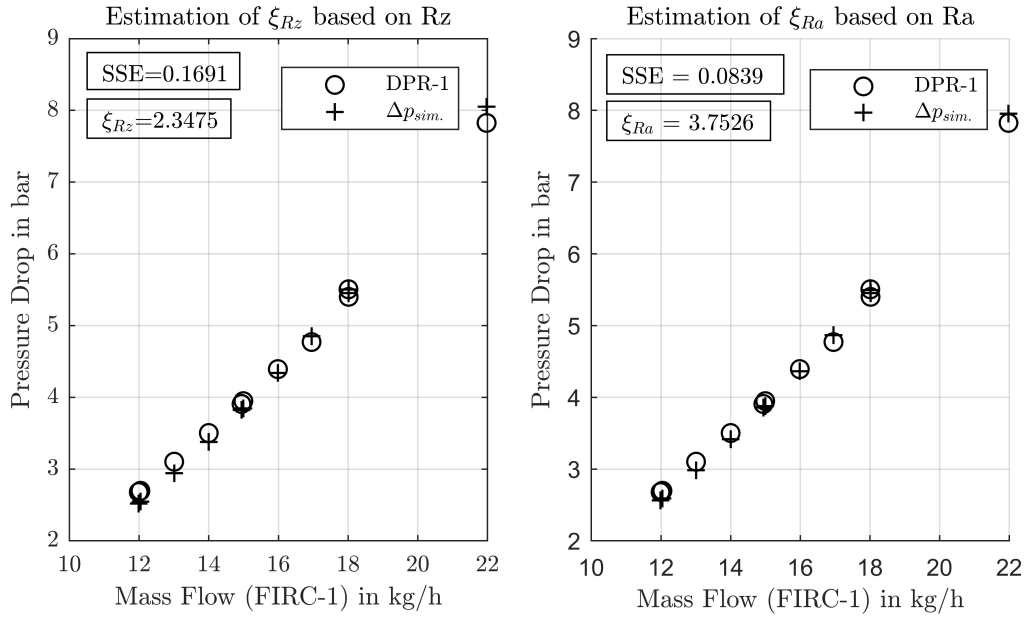

Fig. 5.2: *Estimation of the entrance pressure drop coefficient ξ depending on the parametrization of the roughness e with the averaged roughness value Ra or the averaged roughness depth Rz. The diagram shows the resulting experimental pressure drop (DPR-1) vs. the simulated pressure drop ($\Delta p_{sim.}$) over the different measured mass flows (FIRC-1), see data in Tab. A.1. It further shows the resulting sum of square errors (SSE) and the result of the entrance pressure drop coefficient ξ. source: (Gabrisch and Repke, 2020).*

the predicted pressure drop $\Delta p_{sim.}$ and the experimental pressure drop $\Delta p_{exp.}$ while adjusting a certain parameter z can generally be expressed as follows:

$$\min_{z} \sum_{j} \left(\Delta p_{sim.,j} - \Delta p_{exp.,j} \right)^2 \tag{5.2}$$

In this case, the parameter that is solved for is $z = \xi$ whereas j denotes the the j-th considered operating condition of the experimental investigations on the liquid flow listed in Tab. A.1.

Since the estimated entrance pressure drop coefficient depends on the parametrization of e, it is distinguished between ξ_{Ra} and ξ_{Rz}. The results of the parameter estimation for both - ξ_{Ra} and ξ_{Rz} - are given in Fig. 5.2 including the resulting sum of square errors (SSE) depending on the parametrization. The parameter estimation results in ξ_{Ra}=3.7526 and ξ_{Rz}=2.3475 . As Fig. 5.2 indicates, the parametriza-

tion with e=Ra_{Copper}=0.101e-6 m performs better than the parametrization with e=Rz_{Copper}=1.285e-6 m . However, in general both parametrizations capture the experimental data well so that both are further considered for the parametrization of the flow model in chapter 4. As the roughness measure Rz defines a rougher surface as Ra, the effect of both values should be compared when predicting the two-phase flow in the following sections.

5.1.2 Comparison of common two-phase viscosity correlations

In this section, the investigated increasing subcooling paths in the copper capillary (see Tab. A.2) are predicted using the flow model in chapter 4 following the solution algorithm for the transient simulation of the flow model (see Fig. C.1 in the appendix).[2]

As within the experimental investigation of the increasing subcooling paths it was aimed to keep the subcooling at the capillary inlet constantly below the first subcooling of the measurement series (see Tab. 3.3) the initial wetting ratio for the prediction of each investigated increasing subcooling path is set to zero as the previous wetting ratio for the increasing subcooling paths is not relevant because it is always lower than the current wetting.

Following the model assumptions in section 4.2 there is no influence of the wetted surface roughness e_{wetted} for the prediction of the increasing subcooling paths. Consequently, the wetted surface roughness $e_{wetted,Copper}$ is set to e_{Copper} (either Ra or Rz). Applying the viscosity correlations that are listed in Tab. 4.1 the model is consequently fully parametrized and the transient simulation of the increasing subcooling paths can be solved. All correlations from Tab. 4.1 that calculate the two-phase viscosity μ_{tp} are applied in the flow model one after another in order to predict the investigated increasing subcooling paths in Tab. A.2. This is done for the parametrization of the roughness e with Ra and Rz which includes the according parametrization of the entrance pressure drop coefficient ζ (ζ_{Ra} or xi_{Rz}).

[2]The content of this section is mainly adopted from (Gabrisch and Repke, 2020) and partly complemented

Tab. 5.1: *Statistical comparison between the experimental data and the predicted pressure drops of the* ***increasing subcooling paths*** *in the copper capillary applying different roughness measures and viscosity correlations (source: (Gabrisch and Repke, 2020)).*

		Predicted data within specified error bands		
Roughness e in m	**Applied viscosity correlation**	$\eta_{5\%}$ in %	$\eta_{10\%}$ in %	$\eta_{20\%}$ in %
0.101e-6 (Ra)	McAdams, Woods, and Heroman (1942)	18.1%	53.8%	84.4%
	Cicchitti et al. (1959)	22.5%	59.4%	88.1%
	Dukler, Wicks III, and Cleveland (1964)	17.5%	48.1%	81.9%
	Beattie and Whalley (1982)	32.5%	68.1%	95.0%
	Lin et al. (1991)	22.5%	58.1%	88.1%
	Fourar and Bories (1995)	27.5%	64.4%	90.6%
	Awad and Muzychka (2008)	21.9%	56.3%	86.3%
1.285e-6 (Rz)	McAdams, Woods, and Heroman (1942)	30.6%	55.6%	88.1%
	Cicchitti et al. (1959)	31.9%	60.6%	90.0%
	Dukler, Wicks III, and Cleveland (1964)	26.9%	53.8%	88.1%
	Beattie and Whalley (1982)	34.4%	66.3%	94.4%
	Lin et al. (1991)	31.9%	58.8%	90.0%
	Fourar and Bories (1995)	33.1%	61.9%	90.6%
	Awad and Muzychka (2008)	31.9%	58.1%	90.0%

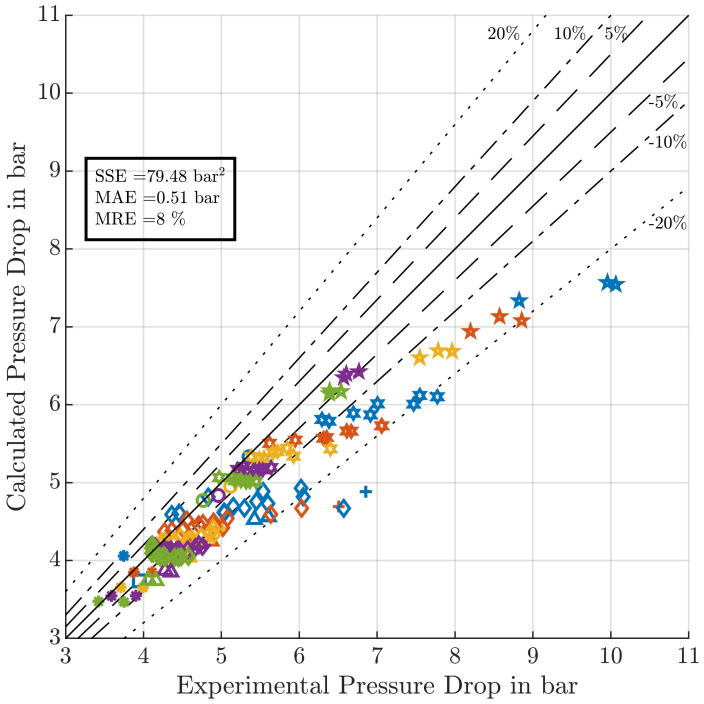

Fig. 5.3: *Comparison between the experimental pressure drops (DPR-1) of the increasing subcooling paths and the predicted pressure drops in the copper capillary using the viscosity correlation provided by Beattie and Whalley (1982) and the parametrization: e=Rz_{Copper} = 1.285e-6 m and ζ_{Rz} = 2.3475 (source: (Gabrisch and Repke, 2020)).*

As Tab. 5.1 reveals that applying the viscosity correlation provided by Beattie and Whalley (1982) delivers the best results concerning the prediction of the investigated increasing subcooling paths. The parametrization of e with Rz predicts 34.4 % of the experimental data within an error band of 5 %.

Fig. 5.3 illustrates the comparison between the experimental and predicted pressure drops of the investigated increasing subcooling paths and depicts the resulting SSE, mean absolute error (MAE) and mean relative error (MRE). The tendency of a higher deviation for higher resulting pressure drops especially for lower subcoolings becomes clear.

Fig. 5.4 highlights to which predicted void fraction at the outlet of the capillary the data in Fig. 5.3 correspond. It becomes obvious that the higher the outlet void fraction α_{out} the larger is the deviation between the predicted and experimental

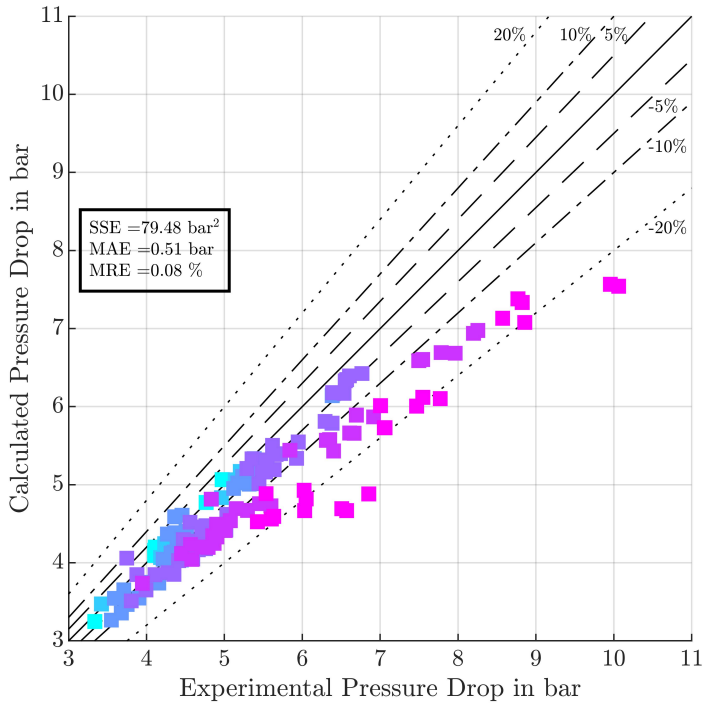

Fig. 5.4: *Comparison between the experimental pressure drops (DPR-1) of the increasing subcooling paths and the predicted pressure drops in the copper capillary using the viscosity correlation provided by Beattie and Whalley (1982) and the parametrization of e with Rz_{Copper}=1.285e-6 m and ξ_{Rz}=2.3475 (classified by the predicted void fraction α_{out} at the outlet of the capillary).*

pressure drops. Hence, it is reasonable to conclude that the prediction of the two-phase flow still shows potential for improvement.

5.1.3 Adaption of the two-phase viscosity correlation to propane

Fig. 5.4 indicates that the higher the ratio of two-phase flow in the capillary the more the pressure drop is underestimated by the flow model. As the viscosity correlation proposed by Beattie and Whalley (1982) shows the best results concerning the prediction of the overall pressure drops, the derivation of the correlation is examined in more detail in order to check if a modification that improves the match of the experimental data of propane is reasonable at some point. The proposed modification of the correlation of Beattie and Whalley (1982) is further referred to as *modified B&W viscosity correlation* and the effect of its application within the flow model is discussed with regard to the prediction quality of the model in the following. [3]

The viscosity correlation proposed by Beattie and Whalley (1982) takes into account the flow pattern of the refrigerant flow through the capillary. It is a hybrid approach which correlates the definition of the viscosity of bubble flow and annular flow:

$$\mu = \mu_l \cdot (1 + 2.5 \cdot \beta) \,(\text{bubble flow}) \tag{5.3}$$

$$\mu = \mu_l \cdot (1 - \beta) + \mu_v \cdot \beta \,(\text{annular flow}) \tag{5.4}$$

with

$$\beta = \frac{\rho_l \cdot x}{\rho_l \cdot x + \rho_v \cdot (1 - x)} \tag{5.5}$$

where β equals the homogeneous void fraction, see Eq. (4.18).

Beattie and Whalley (1982) state that their hybrid definition of the two-phase viscosity theoretically applies for any present flow pattern, i.e. is applicable without any prior knowledge about the present flow pattern. However, they indicate that the factor of 2.5 in Eq. (5.3) is presumably too low to cover void fractions above 20 %. In order to adapt their two-phase viscosity correlation to the gathered

[3] The content of this section is mainly adopted from (Gabrisch and Repke, 2020) and partly complemented

experimental data and better predict the larger pressure drops (see deviations in Fig. 5.3), the empirical factor ψ is introduced. The factor 2.5 in the two-phase viscosity correlation of Beattie and Whalley (1982) (see Tab. 4.1) is multiplied by the factor ψ in order to check whether a scaling yields better overall predictions of the experimental data of the increasing subcooling paths. The *modified B&W viscosity correlation* is presented in the following equation:

$$\mu_{tp} = \mu_l \cdot (1 - \beta) \cdot (1 + \psi \cdot 2.5 \cdot \beta) + \mu_v \cdot \beta \tag{5.6}$$

Fig. 5.5 illustrates the courses of the calculated two-phase viscosity predicted

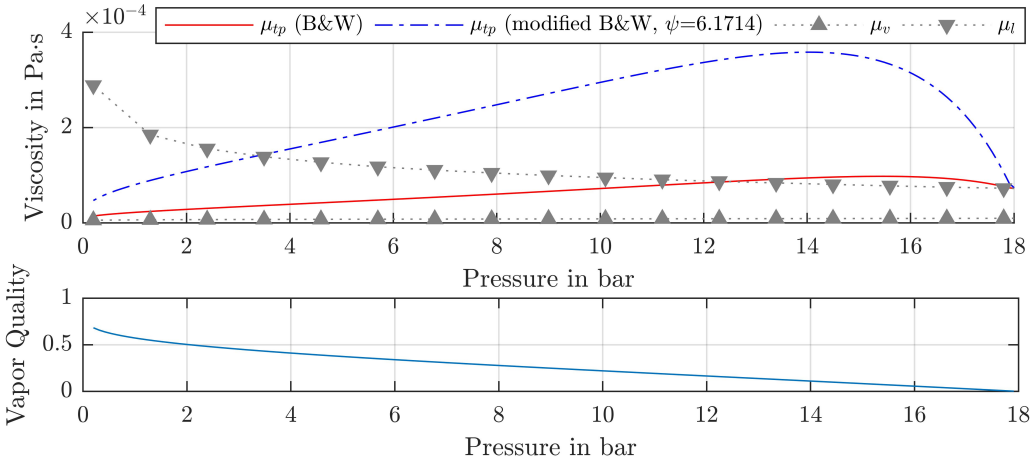

Fig. 5.5: *Theoretical courses of the two-phase viscosity μ_{tp} of propane using the viscosity correlation of Beattie and Whalley (1982) and the modified B&W viscosity correlation for an examplary isenthalpic throttling process from 18 bar and x=0 to 0.2 bar (source: (Gabrisch and Repke, 2020)).*

by the correlation of Beattie and Whalley (1982) and the *modified B&W viscosity correlation* for an exemplary (isenthalpic) pressure drop of propane from 18 bar and x=0 to 0.2 bar. In order to follow the throttling process, the diagrams need to be read from right to left. The viscosity correlations depend on the pressure and the vapour quality. The course of the vapour quality for the exemplary pressure drop is also depicted in Fig. 5.5. At 18 bar and x=0 the correlations correspond to the liquid viscosity μ_l. As the pressure decreases to very low pressures, the vapour quality increases and the calculated viscosities approach the vapour viscosity μ_v. The vapour viscosity is reached for x=1 (which becomes obvious when considering the correlation of Beattie and Whalley (1982) in Tab.4.1 and the *modified B&W*

viscosity correlation in Eq.(5.6)). The factor ψ in Eq. (5.6) scales the two-phase viscosity and shifts the maximum to higher vapour qualities, as can be seen in Fig. 5.5.

A parameter estimation based on the least square errors method is carried out in order to identify the parameter ψ. It is done using the nonlinear least-squares solver (lsqnonlin) in MATLAB which aims to minimize the error between the experimental and the numerical results of the pressure drops for the investigated increasing subcooling paths in Tab. A.2. Both, *Ra* and *Rz* are taken into consideration for the parameter estimation which implies the according parametrization of the entrance pressure drop coefficient ξ with either ξ_{Ra}=3.7526 or ξ_{Rz}=2.3475 . Fig. 5.6 exemplarily shows the comparison between the experimental pressure

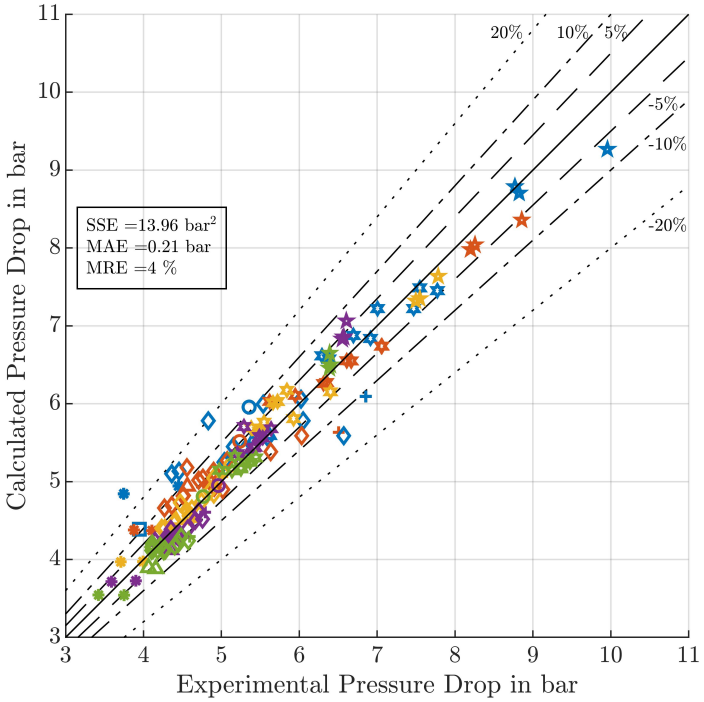

Fig. 5.6: *Comparison between the experimental pressure drops (DPR-1) of the increasing subcooling paths and the predicted pressure drops in the copper capillary using the modified B&W viscosity correlation in Eq.* (5.6) *and the parametrization: e=Rz$_{Copper}$=1.285e-6 m , ξ_{Rz}=2.3475 and the estimated ψ_{Rz}=6.1714 (source: (Gabrisch and Repke, 2020)).*

drop and the pressure drop predicted by the flow model applying the *modified B&W viscosity correlation* parametrized with *e=Rz*=1.285e-6 m and the estimated

Tab. 5.2: *Statistical comparison between the experimental database and the predicted pressure drops of the* ***increasing subcooling paths*** *in the copper capillary applying the viscosity correlation of Beattie and Whalley (1982) vs. applying the modified B&W viscosity correlation compared with different parametrizations of the roughness e (source: (Gabrisch and Repke, 2020)).*

Roughness e in m	**Viscosity correlation**	**Scaling factor** ψ	**Predicted data within specified error bands** $\eta_{5\%}$ in %	$\eta_{10\%}$ in %	$\eta_{20\%}$ in %	**Measure of precision** **SSE** in bar^2	**MAE** in bar	**MRE** in %
0.101e-6 (Ra)	B&W	-	32.5	68.1	95.0	80.04	0.51	8
	modified B&W	ψ_{Ra}=4.2097	75.6	92.5	98.8	13.22	0.22	4
1.285e-6 (Rz)	B&W	-	34.4	66.3	94.4	79.48	0.51	8
	modified B&W	ψ_{Rz}=6.1714	70.6	92.5	99.4	13.96	0.21	4

parameter ψ_{Rz}=6.1714 . It shows a huge improvement concerning the SSE, MAE and MRE, compared to the application of the viscosity correlation of Beattie and Whalley (1982) (see Fig. 5.3). The model parametrization with *Ra* instead of *Rz* leads to comparable results as can be seen in Tab. 5.2.

The *modified B&W viscosity correlation* better predicts the higher pressure drops that imply higher present void fractions than the original correlation of Beattie and Whalley (1982) does. Fig. D.2 shows that the MRE is rather normally distributed for the classified calculated outlet void fractions when applying the *modified B&W viscosity correlation*. The mean value of the depicted distribution in Fig. D.2 is around zero for all outlet void fractions and the error is mainly distributed between $\pm 15\,\%$. Hence, the application of the *modified B&W viscosity correlation* increased the prediction quality of the (two-phase) pressure drop. The positive effect of scaling the coefficient of 2.5 by the parameter ψ might be explainable due to different fluid properties of propane compared to the fluid that underlies the correlation of Beattie and Whalley (1982).

5.1.4 Estimation of the wetted surface roughness

In order to enable the prediction of the hysteresis effect, i.e. enable the prediction of ambiguous pressure drops within the flow model, the wetted surface roughness

$e_{wetted,Copper}$ needs to be parametrized as it is required to calculate the pressure drop of the two-phase flow along the capillary part that was previously wetted.[4]

For the identification of the effective wetted surface roughness e_{wetted}, a parameter estimation is conducted using the nonlinear least-squares solver (lsqnonlin) in MATLAB. The solver minimizes the square errors of the measured pressure drops of the decreasing subcooling paths compared with the predicted pressure drops, where the parameter e_{wetted} is the solution variable. The solver returns the value of e_{wetted} that leads to the minimal error between the experimental and numerical results of the pressure drop.

The flow model that is described in chapter 4 is generally not able to capture any collapses of metastable flow. Instead, the model assumes the maximum metastable flow which means that the full length of the capillary that was previously covered by liquid flow and now by two-phase flow is subject to the wetted surface roughness. The collapse of the metastable flow would mean that only part of this length is subject to the wetted surface roughness. Yet, it is unclear what evokes the collapse of the metastable flow and to which extend.

The listed experimental pressure drops for the decreasing subcooling paths in Tab. A.3 indicate some collapses of metastable flow when there are ambiguous steady-state pressure drops for the same flow condition. As the model is designed to capture the maximal metastable flow, only the lower resulting pressure drops are considered within the parameter estimation and the marked operating conditions in Tab. A.3 are excluded.

Yet, within the gathered experimental data, some of the courses of the decreasing subcooling paths indicate a collapse of metastable flow although there is no ambiguity in the gathered pressure drops. This was exemplarily discussed at Fig. 3.9 in terms of the "instability" of the metastable flow/hysteresis effect in section 3.3.2. The according operating conditions that indicate a collapse of metastable flow lead to a sudden disruption of the linear courses of the decreasing subcooling path. The operating conditions that were identified by this criteria of all decreasing subcooling paths (compare Fig. A.2) are listed in Tab. D.1 and are also excluded from the parameter estimation.

[4]The content of this section is mainly adopted from (Gabrisch and Repke, 2021) and partly complemented

Tab. 5.3: *Statistical comparison between the experimental database and predicted pressure drops of the* ***decreasing subcooling paths*** *in the copper capillary applying the modified B&W viscosity correlation and different roughness measures for e (Ra_{Copper} = 0.101e-6 m and e = Rz_{Copper} = 1.285e-6 m) and the according parametrization of ξ_{Ra} = 3.7526 or ξ_{Rz} = 2.3475 and ψ_{Ra} = 4.2097 or ψ_{Rz} = 6.1714 (source: (Gabrisch and Repke, 2021)).*

Roughness e in m	**Wetted surface roughness** $e_{wetted,Copper}$ in m	**Predicted data within specified error bands** $\eta_{5\%}$ in %	$\eta_{10\%}$ in %	$\eta_{20\%}$ in %	**Measure of precision** **SSE** in bar^2	**MAE** in bar	**MRE** in %
0.101e-6 (Ra)	1.009e-13	56.3	80.0	96.9	24.12	0.29	6
1.285e-6 (Rz)	3.5906e-10	70.0	95.0	99.4	10.78	0.21	4

The parameter estimation is conducted using the flow model and estimating the parameter e_{wetted} that suits the experimental data of the decreasing subcooling paths in Tab. A.3 without the above-mentioned exceptions. It is done twice: applying Ra_{Copper} and Rz_{Copper} for the parametrization of the roughness e, as both parametrizations lead to good results (see Tab. 5.2). The different parametrization of the roughness e implies the according parametrization of the entrance pressure drop with either ξ_{Ra}=3.7526 or ξ_{Rz}=2.3475 and the scaling factor with either ψ_{Ra}=4.2097 or ψ_{Rz}=6.1714 . The resulting wetted surface roughness of the copper capillary is therefore distinguished between $e_{wetted,Ra,Copper}$ and $e_{wetted,Rz,Copper}$. The two-phase viscosity μ_{tp} is calculated applying the *modified B&W viscosity correlation* in Eq. (5.6) with ψ_{Ra}=4.2097 and ψ_{Rz}=6.1714 , respectively.

Tab. 5.3 depicts the results of the parameter estimation of the wetted surface roughness $e_{wetted,Ra,Copper}$ and $e_{wetted,Rz,Copper}$ of the copper capillary as well as the statistical results of the comparison between experimental and predicted pressure drops of the decreasing subcooling paths for the different parametrization of the roughness e. It becomes obvious (see results depicted in Tab. 5.3) that the parametrization of the roughness measure e with Rz_{Copper} delivers better results than the parametrization with Ra_{Copper}. Probably, the effect of the wetted surface roughness is more significant given the rougher roughness measure Rz_{Copper}. The flow model with e=Rz_{Copper}=1.285e-6 m and the estimated wetted surface roughness $e_{wetted,Rz,Copper}$=3.5906e-10 m predicts 70.0 % of the experimental data of the decreasing subcooling paths within an error band of 5 %. The mean relative error with MRE=4 % is comparably low. Fig. 5.7 depicts the comparison between the

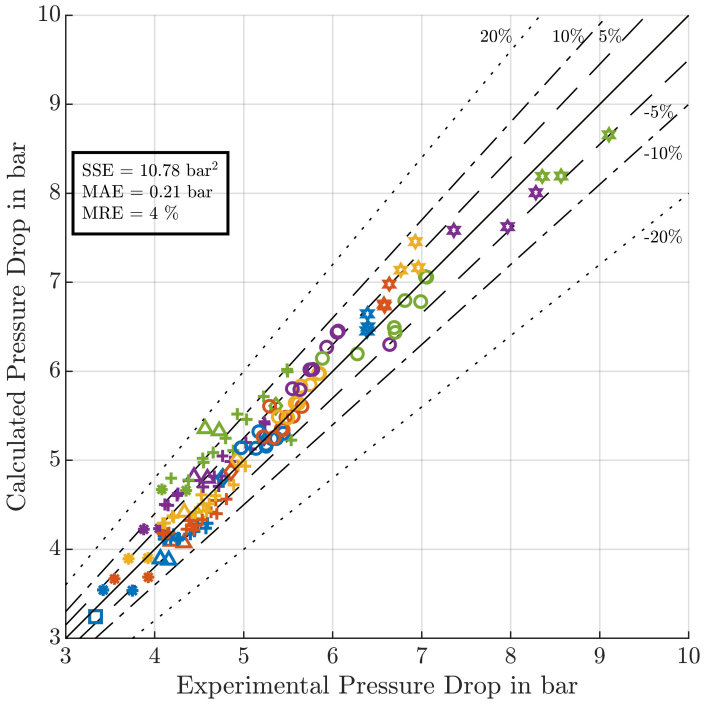

Fig. 5.7: *Comparison between the experimental pressure drops (DPR-1) of all measurement series and the predicted pressure drops in the copper capillary applying the modified B&W viscosity correlation in Eq.* (5.6) *with the following parametrization:* $e = Rz_{Copper} = 1.285\text{e-}6\,m$, $\zeta_{Rz} = 2.3475$, $\psi_{Rz} = 6.1714$ *and* $e_{wetted,Rz,Copper} = 3.5906\text{e-}10\,m$ *(source: (Gabrisch and Repke, 2021)).*

experimental and the predicted pressure drop of the decreasing subcooling paths in a parity plot. The experimental data that has been excluded from the parameter estimation (see Tab. D.1) is included in Tab. 5.3 and Fig. 5.7 as the statistical analysis of the prediction quality shall comprise the full decreasing subcooling paths. The ambiguous pressure drops (marked in Tab. A.3) are further excluded as the model is not designed to depict ambiguity/the collapse of metastable flow. Fig. 5.7 indicates that the predicted pressure drops according to their subcoolings are evenly distributed around the par values. Fig. D.3 shows that the mean relative errors of the predicted pressure drops of the decreasing subcooling paths classified by the outlet void fraction α_{out} are approximately normally distributed around 0 %. Hence, we can conclude that a high ratio of two-phase flow does not necessarily mean that the model does not predict the pressure drop in a good quality.

Tab. 5.4: *Validated parametrization of the flow model to predict the pressure drop of propane in the investigated copper capillary tube.*

Capillary material-specific parameters				**Geometry-specific parameter**	**Refrigerant-specific parameter**
Roughness	**Inner diameter**	**Length Length**	**Wetted surface roughness**	**Entrance pressure drop coefficient**	**Scaling factor Scaling factor**
d	e	L	e_{wetted}	ξ	ψ
1.1799e-3 m	1.285e-6 m (Rz)	1.0274 m	3.5906e-10 m ($e_{wetted,Rz}$)	2.3475 (ξ_{Rz})	6.1714 (ψ_{Rz})

5.1.5 Discussion of the numerical results

In this section[5], representative measurement series, i.e. the investigated increasing and decreasing subcooling paths in Tab. A.2 and Tab. A.3, are simulated applying the transient simulation of the flow model (following the algorithm in Fig. C.1 that describes the application of the flow model in chapter 4). The predicted hysteresis curves are compared to the experimental results. Further, all investigated measurement series comprising the full hysteresis curves (i.e. the experimental data from both Tab. A.2 and Tab. A.3) are compared to the according numerical results which is statistically evaluated.

The flow model is parametrized with the parameters listed in Tab. 5.4 which summarizes the refined and identified parameters of the flow model that have been derived following the systematic procedure in Fig. 5.1 and resulted in the best match between the experimental and numerical data. For the prediction of the investigated measurement series, the transient simulation is started with an initial wetting ratio of zero. Subsequently, the increasing subcooling and the decreasing subcooling paths are simulated.

The improvement yielded by the application of the *modified B&W viscosity correlation* and the model approach for the metastable flow is shown in Tab. 5.5 in comparison to the application of the viscosity correlation of Beattie and Whalley (1982) without modelling the metastable flow. Not modelling the metastable flow means that either the previous wetting ratio Θ^{-1} is set to zero or setting the wetted surface roughness e_{wetted} is set to the value of the "dry" roughness e (which is either Ra_{Copper} or Rz_{Copper}). Tab. 5.5 shows the improvement of prediction accuracy by applying the *modified B&W viscosity correlation* suggested by Gabrisch

[5]The content of this section is mainly adopted from (Gabrisch and Repke, 2021) and partly complemented

Tab. 5.5: *Statistical comparison between the experimental database and the predicted pressure drops of the* ***hysteresis curves*** *in the copper capillary applying the parameters in Tab. 5.4 accordingly but with different parameters for the wetted surface roughness e_{wetted} and different viscosity correlations as denoted (source: (Gabrisch and Repke, 2021)).*

		Predicted data within specified error bands			**Measure of precision**		
Viscosity correlation	**Wetted surface roughness** e_{wetted} in m	$\eta_{5\%}$ in %	$\eta_{10\%}$ in %	$\eta_{20\%}$ in %	**SSE** in bar^2	**MAE** in bar	**MRE** in %
B&W	1.285e-6	39.6	72.9	96.9	107.23	0.43	7
modified B&W	1.285e-6	59.4	84.4	98.3	38.62	0.28	5
modified B&W	3.5906e-10	69.1	93.1	99.3	23.99	0.22	4

and Repke (2020) and including the model assumptions for the development of metastable flow in the flow model. The model is parametrized with the parameters in Tab. 5.4 in each case - except the wetted surface roughness e_{wetted} which is parametrized as shown in Tab. 5.5 and the scaling factor ψ which does not apply for the viscosity correlation of Beattie and Whalley (1982). Applying the viscosity correlation of Beattie and Whalley (1982) and setting the wetted surface roughness e_{wetted} to Rz_{Copper}=1.285e-6 m (hence, not taking considering the development of metastable flow), the flow model predicts 39.6 % of the experimental data on all hysteresis curves in Tab. A.2 and Tab. A.3 within an error band of ± 5 % and results in an MRE of 7 %.

Applying the *modified B&W viscosity correlation* but still not considering the development of metastable flow, the model predicts 59.4 % of the experimental data within an error band of ± 5 % and results in an MRE of 5 %.

Finally, applying the *modified B&W viscosity correlation* together with the estimated wetted surface roughness e_{wetted}=3.5906e-10 m results in a prediction of 69.1 % of the data within an error band of ± 5 % and an MRE of only 4 %.

Consequently, the introduction of the *modified B&W viscosity correlation* together with the wetted surface roughness e_{wetted} yields 30 % more data being predicted within an error band of ± 5 % compared to the application of the original viscosity correlation of Beattie and Whalley (1982) and the disregard of the development of metastable flow in the model. The great improvement shows that it is worth to thoroughly distinguish the experimental investigations on the refrigerant flow through a capillary tube by the increasing and decreasing subcooling paths as

done in this work. Based on the increasing subcooling paths, the, in principle, matching viscosity correlation of Beattie and Whalley (1982) could be adapted to better fit the results of the investigated propane flow. The introduction of the model assumptions for the development of metastable flow enables the flow model to predict ambiguous pressure drops and thereby further improves the overall prediction quality of the propane flow through the capillary.

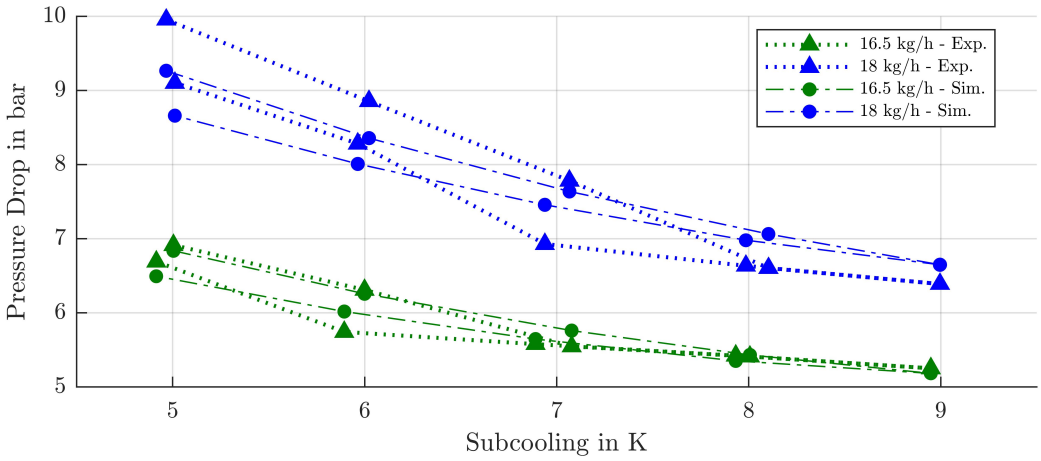

Fig. 5.8: *Experimental (Exp.) hysteresis curves resulting from increasing and decreasing subcooling paths at 23 bar inlet pressure (PRC-1) and different mass flows (FIRC-1) in the copper capillary compared to the according predicted hysteresis curves (Sim.) applying the modified B&W viscosity correlation applying the parameters in Tab. 5.4. The diagram shows the experimental pressure drops (DPR-1) vs. the simulated pressure drops over the change of the subcooling at the capillary inlet (mean values of the redundant measurements, source: (Gabrisch and Repke, 2021)).*

The resulting hysteresis curves at higher mass flows are generally very well predicted as Fig. 5.7 indicates. Fig. 5.8 shows the comparison of the experimental and the predicted pressure drops for exemplary mass flows at a constant inlet pressure of 23 bar for the investigated increasing and decreasing subcooling paths. Fig. 5.8 shows that the mathematical model is principally able to simulate a hysteresis curve on the pressure drop depending on the change in the subcooling at the inlet of the capillary. The course of the hysteresis curve at 16.5 kg/h mass flow is very well captured as well as the quantitative difference in pressure drop comparing the increasing and decreasing subcooling paths is well predicted. However, in order to improve the prediction quality, the prediction of the decreasing subcooling paths should yield lower pressure drops. It becomes visible considering Fig. 5.9

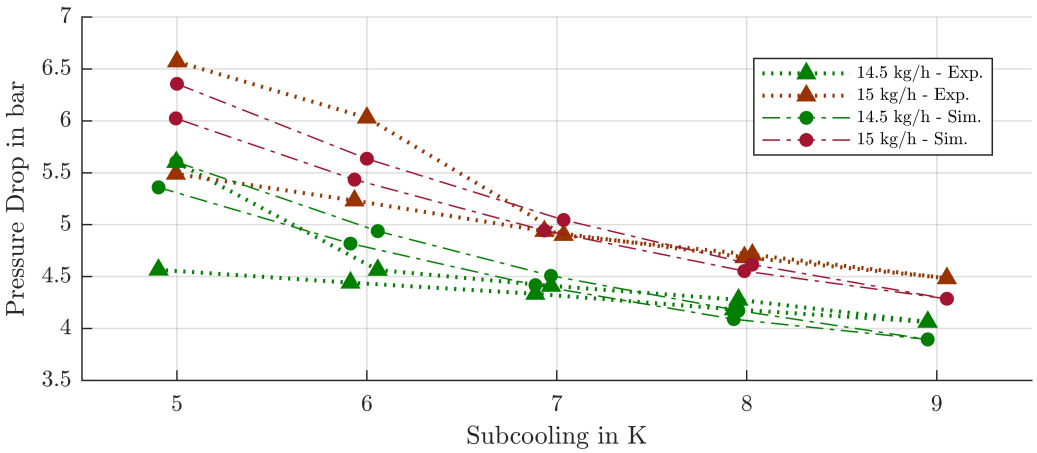

Fig. 5.9: *Experimental (Exp.) hysteresis curves resulting from increasing and decreasing subcooling paths at 16 bar inlet pressure (PRC-1) and different mass flows (FIRC-1) compared to simulated hysteresis curves (Sim.) applying the modified B&W viscosity correlation applying the parameters in Tab. 5.4. The diagram shows the experimental pressure drops (DPR-1) vs. the simulated pressure drops over the change of the subcooling at the capillary inlet (mean values of the redundant measurements, source: (Gabrisch and Repke, 2021)).*

that the predicted decreasing subcooling paths result in too large pressure drops compared to the experimental pressure drops. Fig. 5.9 depicts the experimental against the predicted pressure drops for exemplary mass flows at a constant inlet pressure of 16 bar for the investigated increasing and decreasing subcooling paths. It can be seen that the hysteresis effect captured by the experiments is more pronounced than the predicted hysteresis effect.

As a tendency it can be noted that the prediction of the decreasing subcooling paths should generally result in lower pressure drops for lower subcoolings (see Fig. 5.8 and Fig. 5.9). For a larger ratio of two-phase flow in the capillary (e.g. at lower subcoolings) the pressure drop for the decreasing subcoolings is rather overestimated. Fig. D.3, that shows the distribution of the mean relative errors of the prediction classified by the outlet void fraction α_{out}, supports this assumption. A possible optimization approach within the flow model may be modifying the determination of the wetting ratio Θ (see Eq. (4.26) in section 4.2). The wetting ratio Θ is determined by the length of the capillary ΔL_{liq} that is covered by pure liquid flow. However, it may be extended by taking into account the two-phase flow to a certain extend of vapour quality or void fraction, respectively. At low

void fractions, the gas bubbles of the two-phase flow are rather small and the liquid ratio dominates the two-phase flow. Consequently, the wetting ratio could be modified in the following way:

$$\Theta = \frac{(\Delta L_{liq} + \Delta L_{tp,\alpha_{crit}})}{L} \tag{5.7}$$

where $\Delta L_{tp,\alpha_{crit}}$ corresponds to the part of the capillary length that is covered with two-phase flow with a void fraction α below a critical value of α_{crit}. The critical value can be estimated by replacing Eq. (4.26) with Eq. (5.7) in the flow model and estimating the appropriate parameter α_{crit} within a parameter estimation as was analogously done in section 5.1.4 while keeping the wetted surface roughness $e_{wetted,Rz,Copper}$=1.285e-6 m at the estimated value.

5.2 Experimental and Numerical Results of the Steel Capillary Tube

The developed model of the flow in a capillary tube was compared against the experimental results of propane flow through a copper capillary tube and showed a high prediction quality (see section 5.1.5. The empirical scaling factor ψ of the *modified B&W viscosity correlation* that is related to the refrigerant propane was determined via parameter estimation based on the experiments in the copper capillary.

Now, the flow model is used to predict the investigated pressure drop of propane in a steel capillary tube. It serves to reveal whether the *modified B&W viscosity correlation* remains valid also in a different capillary design. More precisely, the investigations should show whether the estimated scaling factor ψ remains valid for independent experiments in a capillary tube different than the investigated copper capillary tube.

The evaluation is done using the parametrization of the roughness measure $e = Rz_{Steel}$ as section 5.1.4 revealed that the prediction of the flow (and especially the hysteresis effect) is best described using Rz as roughness measure.

However, neither the roughness measure Ra_{Steel} nor Rz_{Steel} were measured after having finished the experiments on the pressure drop in the steel capillary. Instead, the flow model presented in chapter 4 is used to determine the according roughness measure via parameter estimation based on the experiments of pure liquid flow of propane through the steel capillary tube (see Tab. A.4). In this way we benefit from the investigations in the capillary tube as the geometry of the copper and steel capillary and the refrigerant is the same. Hence, the entrance pressure drop coefficient ζ is already identified and the roughness values can instead be identified based on the liquid flow measurements. The identification of both - *Ra* and *Rz* - is presented in section 5.2.1.

In section 5.2.2 the measured increasing subcooling paths of the test plan in Tab. 3.6 exhibited in Tab. A.5 are predicted with the flow model. The prediction quality of applying the *modified B&W viscosity correlation* with the parameter ψ that was determined in section 5.1.3 is discussed.

In section 5.2.3, the wetted surface roughness e_{wetted} is identified via parameter estimation based on the experimental data of the decreasing subcooling paths in Tab. A.6. The wetted surface roughness is newly estimated since it is presumable that the value is related to the specific capillary material, hence, the surface quality.

The outlined steps for the parametrization of the flow model based on the experimental investigations of the propane flow in the steel tube are summarized in Fig. 5.10. Compared to the procedure depicted in Fig. 5.1 it can be seen that the extend of the parametrization work flow is reduced since the entrance pressure drop coefficient ζ and the appropriate two-phase viscosity correlation together with the scaling factor ψ have already been identified within the parametrization process of the flow model that refers to the copper capillary.

5.2.1 Estimation of the roughness

The entrance pressure drop coefficient is set to ζ_{Ra}=2.3475 or ζ_{Rz}=3.7526 , respectively, which corresponds to the estimated values in section 5.1.1. This is a simplification based on the minor deviation between the inner diameter of the copper

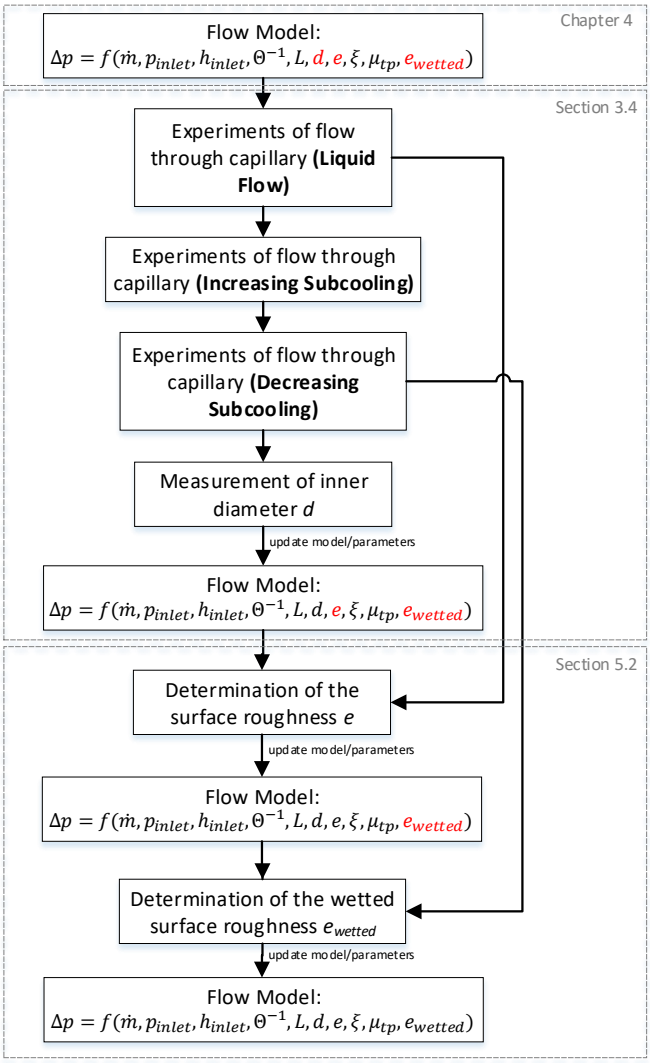

Fig. 5.10: *Systematic approach for the generation of an experimental database on the refrigerant flow in a capillary and the parametrization of the according flow model based on previous investigations and a partly parametrized flow model of the same refrigerant in a different capillary tube with the same geometry specifications.*

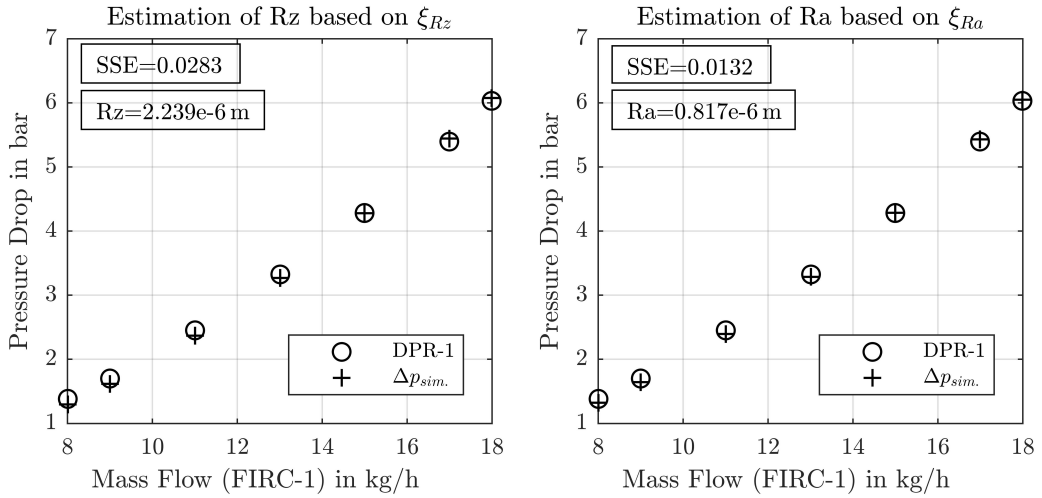

Fig. 5.11: *Estimation of the average roughness depth Rz and the average roughness value Ra of the steel capillary given the entrance pressure drop coefficients ξ_{Rz} and ξ_{Ra}. The diagram shows the resulting experimental pressure drop (DPR-1) vs. the simulated pressure drop ($\Delta p_{sim.}$) over the different measured mass flows (FIRC-1), see data in Tab. A.4. It further shows the resulting sum of square errors (SSE) and the resulting roughness measures Rz and Ra.*

capillary d_{Copper}=1.1799e-3 m and the steel capillary d_{Steel}=1.1749e-3 m . This implies that the pressure drop due to sudden contraction (coming from the larger cross-sectional area of the connection tube and entering the smaller cross-sectional area of the capillary) is approximately the same. Based on the determined diameter d_{Steel}=1.1749e-3 m (see section 3.4.3) and the entrance pressure drop coefficients ξ_{Rz}=3.7526 and ξ_{Rz}=2.3475 the according roughness measures Ra_{Steel} and Rz_{Steel} of the steel capillary are approximated via parameter estimation. The parameter estimation is conducted using the nonlinear least-squares solver (lsqnonlin) in MATLAB. The solver minimizes the sum of square errors of the measured pressure drops of pure liquid flow through the steel capillary compared with the predicted pressure drops using the flow model in chapter 4, where the parameter e is the solution variable. Since there is only liquid flow through the capillary tube, the parametrization of e_{wetted} is irrelevant in this case.

The result of the parameter estimation is: Ra_{Steel}=0.817e-6 m and Rz_{Steel}=2.239e-6 m as depicted in Fig. 5.11. Consequently, the investigated steel capillary is sig-

nificantly rougher than the copper capillary which explains the differences in the gathered pressure drops comparing section 3.3.2 and section 3.4.2.

5.2.2 Prediction of the increasing subcooling paths

The prediction of the increasing subcooling paths of the experimental investigations of the steel capillary (which are shown in Tab. A.5) is done applying the *modified B&W viscosity correlation* and parametrizing the flow model in chapter 4 with the following parameters:

- the measured diameter d_{Steel}=1.1749e-3 m (see section 3.4.3)
- the estimated roughness e=Rz_{Steel}=2.239e-6 m (see section 5.2.1)
- the length L=1.0274 m
- setting $e_{wetted,Steel}$=Rz_{Steel}=2.239e-6 m
- the estimated scaling factor ψ_{Rz}=6.1714 (see section 5.1.3)

The pressure drops are predicted using the transient calculation of the flow model (see solution algorithm in the appendix in Fig. C.1) which takes into account the history of previous inlet conditions. Hence, the transition of the investigated subcoolings from 5 to 9 K is calculated for the different investigated inlet pressures and mass flows. The initial wetting ratio Θ^0 is set to zero.

Fig. 5.12 depicts the comparison between the predicted and the experimental pressure drops of the increasing subcooling paths in the steel capillary. It shows a good agreement between the experimental and predicted pressure drops. The statistics that refer to the comparison between experimental and predicted pressure drops are added in Tab.5.6. It indicates that 72.7 % of the predicted pressure drops lie within an error band of 5 % compared to the experimental pressure drops. The MRE with 4 % is the same as for the prediction of the increasing subcooling paths in the copper capillary tube (see Tab. 5.2). Specifying the parameters related to the steel capillary and relying on the identified parameter ψ_{Rz}, the two-phase pressure drop in the steel capillary is well predicted. Consequently, the *modified*

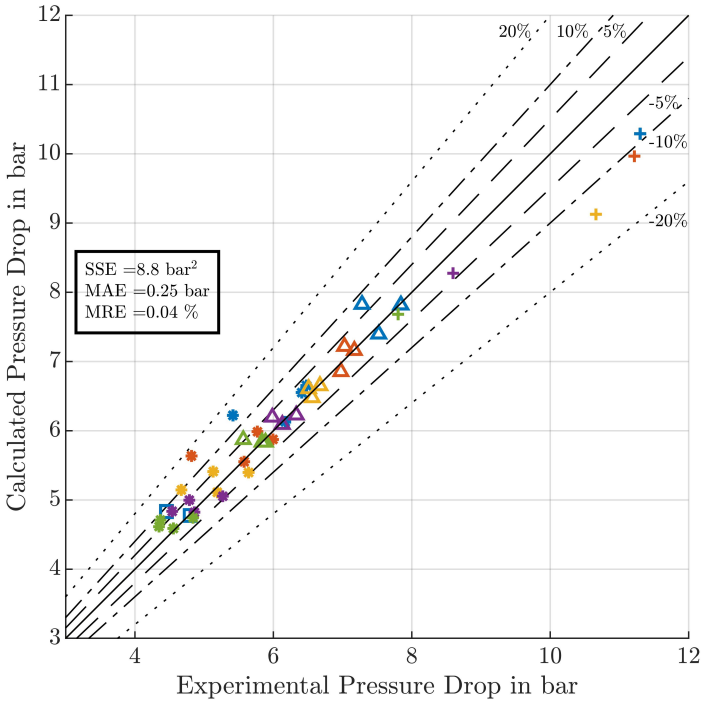

Fig. 5.12: *Comparison between the experimental pressure drops (DPR-1) of the increasing subcooling paths and the predicted pressure drops in the steel capillary using the modified B&W viscosity correlation in Eq.* (5.6) *with the parameters in Tab. 5.7 and* $e_{wetted,Steel}$=Rz_{Steel} *= 2.239e-6 m .*

B&W viscosity correlation with ψ_{Rz} is proven to be predictive independently from the investigated capillary materials.

5.2.3 Estimation of the wetted surface roughness

In order to identify the wetted surface roughness $e_{wetted,Rz,Steel}$, the flow model is parametrized with the same parameters as in section 5.2.2 to conduct a parameter estimation based on the experimental pressure drops of the decreasing subcooling paths in the steel capillary (shown in Tab. A.6).

The parameter estimation is done using the nonlinear least-squares solver (lsqnonlin) in MATLAB. The solver minimizes the sum square errors of the measured pressure drops through the steel capillary compared with the predicted pressure

Tab. 5.6: *Statistical comparison between the experimental database and the predicted pressure drops of the* ***increasing subcooling paths*** *in the steel capillary applying the modified B&W viscosity correlation in Eq.* (5.6) *with the parameters in Tab. 5.7 and* $e_{wetted,Steel} = Rz_{Steel}$ *= 2.239e-6 m .*

$\eta_{5\%}$	$\eta_{10\%}$	$\eta_{20\%}$	SSE	MAE	MRE
72.7	90.9	100.0	8.8	0.25	0.04

drops, where the parameter $e_{wetted,Rz,Steel}$ is the solution variable. The pressure drops are predicted using the transient calculation of the flow model which takes into account the history of previous inlet conditions (see solution algorithm in the appendix in Fig. C.1). Hence, the transition of the investigated subcoolings from 9 to 5 K is calculated for the different investigated inlet pressures and mass flows. The initial wetting ratio Θ^0 is set to zero which does not have an impact on the calculation of the pressure drop at 9 K subcooling because it is considered to result in the largest wetting ratio of the considered operating conditions in Tab. 3.5. The previous investigated subcoolings of the increasing subcooling path resulted in lower wetting ratios. For the calculation of the decreasing subcooling paths the actual value of the initial wetting ratio is not important as long as it is smaller than the wetting ratio that results at 9 K (i.e. the largest considered subcooling). The parameter estimation results in $e_{wetted,Rz,Steel}$=6.3903e-8 m .

Fig. 5.13 shows the comparison between the experimental and calculated pressure drops applying the *modified B&W viscosity correlation* and the parameters listed in Tab. 5.7 including the estimated parameter $e_{wetted,Rz,Steel}$. Tab. 5.7 summarizes the refined and identified parameters of the flow model that have been derived following the systematic procedure in Fig. 5.10 and resulted in the best match between the experimental and numerical data. The statistics related to the comparison are presented in Tab. 5.8. Consequently, 65.6 % of the experimental pressure drops are predicted within an error band of 5 % and the MRE is 5 % which is comparable to the results of predicting the experiments in the copper capillary in section 5.1.4.

5.2.4 Discussion of the numerical results

In order to analyse the benefit of applying the *modified B&W viscosity correlation* and the wetted surface roughness $e_{wetted,Rz,Steel}$ to predict the overall hysteresis

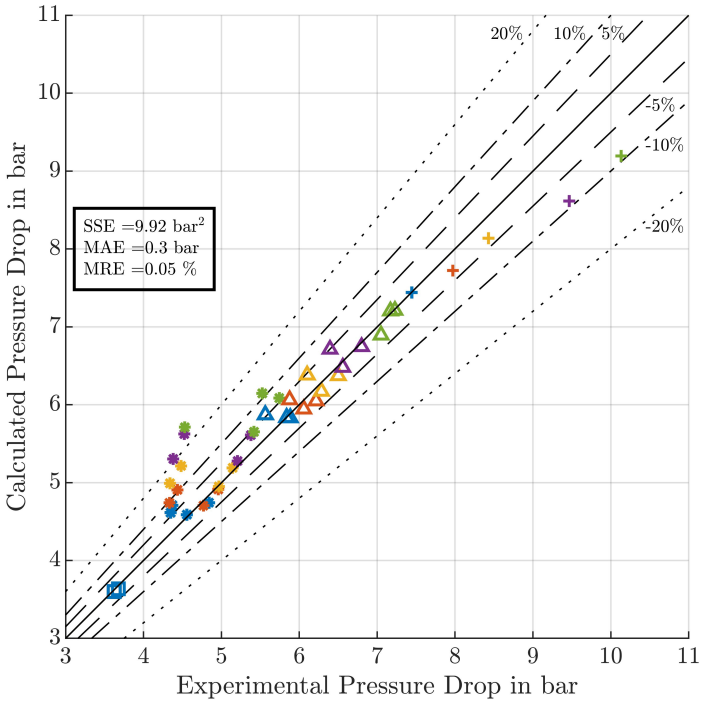

Fig. 5.13: *Comparison between the experimental pressure drops (DPR-1) of the decreasing subcooling paths and the predicted pressure drops in the steel capillary using the modified B&W viscosity correlation with the parameters in Tab. 5.7.*

Tab. 5.7: *Parametrization of the flow model to predict the pressure drop of propane in the investigated steel capillary tube.*

Capillary material-specific parameters				**Geometry-specific parameter**	**Refrigerant-specific parameter**
Roughness e	**Inner diameter** d	**Length Length** L	**Wetted surface roughness** e_{wetted}	**Entrance pressure drop coefficient** ξ	**Scaling factor Scaling factor** ψ
2.239e-6 m (Rz)	1.1749e-3 m	1.0274 m	6.3903e-8 m	2.3475 (ξ_{Rz})	6.1714 (ψ_{Rz})

Tab. 5.8: *Statistical comparison between the experimental database and the predicted pressure drops of the* ***decreasing subcooling paths*** *in the steel capillary applying the modified B&W viscosity correlation with the parameters in Tab. 5.7.*

Predicted data within specified error bands			**Measure of precision**		
$\eta_{5\%}$ in %	$\eta_{10\%}$ in %	$\eta_{20\%}$ in %	SSE in bar²	MAE in bar	MRE in %
65.6	83.6	94.5	9.92	0.3	5

curves investigated in the steel capillary, Tab. 5.9 compares different parametrizations of the wetted surface roughness and different viscosity correlations.

The first row of Tab. 5.9 denotes the application of the original viscosity correlation by Beattie and Whalley (1982) setting $e_{wetted,Rz,Steel}$=Rz_{Steel} (eliminating the impact of the wetted surface roughness in the flow model). This model setup predicts 32.2 % of the measured pressure drops of the hysteresis curves in the steel capillary within an error band of 5 % and results in an MRE of 8 %.

The second row in Tab. 5.9 shows the results of applying the *modified B&W viscosity correlation* but still neglecting the wetted surface roughness setting $e_{wetted,Rz,Steel} = Rz_{Steel}$. Applying the *modified B&W viscosity correlation*, thus, predicts 24.5 % more data within an error band of 5 % and enhances the MRE by 1 % compared to the application of the original viscosity correlation by Beattie and Whalley (1982).

Applying the *modified B&W viscosity correlation* together with the wetted surface roughness $e_{wetted,Rz,Steel}$ further increases the prediction quality as can be seen in the third row in Tab. 5.9. Compared with the first row of Tab. 5.9 this model setup predicts almost twice as much data within an error band of 5 % and results in an MRE of only 5 %. Consequently, the flow model gains significant prediction quality by applying the *modified B&W viscosity correlation* and the wetted surface roughness e_{wetted} as it takes into account the ambiguity of the pressure drop due to the present hysteresis effect.

Finally, it could be shown that the flow model parametrized with e=Rz, applying the *modified B&W viscosity correlation* and the wetted surface roughness e_{wetted} very well predicts the propane flow through both - the copper and steel capillary capturing the hysteresis effect. The introduction of the scaling factor ψ in order to adapt the viscosity correlation by Beattie and Whalley (1982) to the investigated refrigerant verifiably improved the prediction quality of the flow model as was already shown in section 5.1.3 for the investigations in the copper capillary. It was demonstrated that the scaling factor preserves its prediction quality for independent investigations in a steel capillary. The simple model approach by introducing the wetted surface roughness e_{wetted} and the wetting ration Θ in section 4.2 turns out to predict the hysteresis effect not only for copper capillaries but also for steel capillaries in a reasonable quality.

Tab. 5.9: *Statistical comparison between the experimental database and the predicted pressure drops of the* ***hysteresis curves*** *in the steel capillary applying the parameters in Tab. 5.7 accordingly but with different e_{wetted} and different viscosity correlations as denoted.*

		Predicted data within					
	Wetted surface roughness	specified error bands			**Measure of precision**		
Viscosity correlation	e_{wetted} in m	$\eta_{5\%}$ in %	$\eta_{10\%}$ in %	$\eta_{20\%}$ in %	**SSE** in bar^2	**MAE** in bar	**MRE** in %
B&W	2.239e-6 (set to Rz_{Steel})	32.2	66.7	96.6	61.3	0.58 bar	8 %
modified B&W	2.239e-6 (set to Rz_{Steel})	56.7	77.8	92.2	26.1	0.37 bar	7 %
modified B&W	6.3903e-8	65.6	84.4	96.7	18.3	0.30 bar	5 %

5.3 Model Uncertainty Analysis

In order to provide an estimation of the uncertainty of the predicted pressure drop by the presented flow model in chapter 4, an uncertainty analysis is carried out.[6] It is exemplarily done for the flow through the capillary tube applying the average roughness depth Rz_{Copper} as roughness measure e and the *modified B&W viscosity correlation* in the model. The model uncertainty analysis takes into account the uncertainties of the model parameters, namely the following:

- the inner diameter d_{Copper}=1.1799e-3 m with $\sigma_{d,Copper}$=0.01e-3 m
- the average roughness depth Rz_{Copper}=1.285e-6 m with $\sigma_{Rz,Copper}$=0.391e-6 m
- the entrance pressure drop coefficient ξ_{Rz}=2.3475
- the scaling coefficient ψ_{Rz}=6.1714 of the *modified B&W viscosity correlation*
- the wetted surface roughness $e_{wetted,Rz,Copper}$=3.5906e-10 m

The capillary length L is neglected as a parameter as the manufacturer tolerance of $\pm$=0.002 m has a negligible effect on the calculation of the pressure drop. Whereas the standard deviations of d_{Copper} and Rz_{Copper} have been determined within the measurements in section 3.3.4, the standard deviations of the entrance pressure drop coefficient ξ_{Rz}, the scaling coefficient ψ_{Rz} and the wetted surface roughness $e_{wetted,Rz,Copper}$ still have to be estimated.

[6] This section is taken from Gabrisch and Repke (2020)

The missing standard deviations are determined using the following approach:

$$\sigma_y = \sqrt{\sigma_{y,a}^2 + \sigma_{y,b}^2} \tag{5.8}$$

where y denotes a specific parameter. $\sigma_{y,a}$ is defined as the standard deviation of the parameter y which is **related to the parameter estimation** and includes the potential measurement errors of the input variables (inlet pressure, mass flow and subcooling) and the measured pressure drop as well as uncertainties of the model structure itself. $\sigma_{y,b}$ is defined as the standard deviation that is **derived from error propagation** considering the influence of uncertain parameters (as the inner diameter d and the roughness Rz but also the estimated parameters) that could not be considered within the parameter estimation. The standard deviation $\sigma_{y,a}$ is estimated via a method described by Müller et al. (2014) that uses the inverse Fisher Information Matrix (FIM). In order to obtain the FIM, first the sensitivity matrix S is approximated for each considered parameter:

$$S = \begin{pmatrix} \frac{\partial \Delta p_1}{\partial y} \\ \vdots \\ \frac{\partial \Delta p_n}{\partial y} \end{pmatrix} \tag{5.9}$$

where $\frac{\partial \Delta p_j}{\partial y}$ is the partial derivative of the calculated pressure drop Δp with respect to the parameter y (which in this work refers to one of the estimated parameters, e.g. the entrance pressure drop coefficient ζ) at a specific operating condition j. The partial derivatives are approximated using finite differences using the homogeneous flow model in chapter 4 and applying very small changes in the considered parameter.

The FIM is calculated by the following equation, see (Müller et al., 2014):

$$FIM = S' \cdot \frac{1}{\sigma_{DPR\,1}^2} \cdot S \tag{5.10}$$

where $\sigma_{DPR\,1}$ corresponds to the standard deviation of the differential pressure sensor DPR 1, which is set to $\sigma_{DPR\,1}$=0.01 bar, as the value of the sensor tolerance in Tab. 3.1 which is provided by the manufacturer is considered to be the value of

$3 \cdot \sigma$ and not σ. As only one parameter is considered at one time the FIM reduces to a scalar value.

The inverse of the FIM is defined as the variance of the respective estimated parameter while it is important to state that it is only an estimation of the lower bound of the variance. The uncertainty of the parameter, indeed, can be higher in reality. Consequently the square root of the inverse of the FIM is an estimation of the lower bound of the standard deviation $\sigma_{y,a}$ of the respective estimated parameter y:

$$\sigma_{y,a} = \sqrt{FIM^{-1}} \tag{5.11}$$

The sensitivity matrix S of each of the three considered parameters (ξ_{Rz}, ψ_{Rz} and e_{wetted}) is calculated for different experimental data sets. The sensitivity of ξ_{Rz} is evaluated against the experimental data of the input variables of the liquid flow experiments in Tab. A.1, the sensitivity of ψ_{Rz} is evaluated against the experimental data of the increasing subcooling paths in Tab. A.2 and the sensitivity of e_{wetted} is evaluated against the experimental data of the decreasing subcooling paths in Tab. A.3 as these are the experimental data sets on the basis of which the parameters have been estimated.

Estimation of the standard deviation of the entrance pressure drop coefficient $\sigma_{a,\xi_{Rz}}$

In order to estimate the standard deviation $\sigma_{a,\xi_{Rz}}$, the experimental data of the inlet pressure, mass flow and subcooling of the liquid flow experiments in Tab. A.1 is taken for the calculation of the sensitivity matrix S in Eq. (5.9) since ξ_{Rz} was estimated based on this experimental data (see section 5.1.1). For the calculation of the liquid flow, the previous wetting ratio Θ^{-1} and the wetted surface roughness $e_{wetted,Rz,Copper}$ are irrelevant. However, the wetting ratio is set to zero while $e_{wetted,Rz,Copper}$ is set to Rz within the calculations. The sensitivity matrix is calculated using finite differences setting $\Delta\xi_{Rz}$=1e-5$\cdot\xi_{Rz}$ and solving the flow model for the pressure drop Δp^{up} at ξ_{Rz}=ξ_{Rz}+$\Delta\xi_{Rz}$ and Δp^{down} at ξ_{Rz}=ξ_{Rz}-$\Delta\xi_{Rz}$ for all considered experimental data while parametrizing the rest of the parameters of the flow model with the parameters in Tab. 5.4 accordingly. Consequently, the

entries of the sensitivity matrix in Eq. (5.9) are approximated as follows:

$$\frac{\partial \Delta p_j}{\partial \xi_{Rz}} \approx \frac{\Delta p_j^{up} - \Delta p_j^{down}}{2 \cdot \Delta \xi_{Rz}} \tag{5.12}$$

Applying Eq. (5.10) and Eq. (5.11), the estimated standard deviation of ξ_{Rz}=2.3475 results to $\sigma_{a,\xi_{Rz}}$=0.0105 .

Estimation of the standard deviation of the scaling factor $\sigma_{a,\psi_{Rz}}$

For the estimation of $\sigma_{a,\psi_{Rz}}$ the experimental data of the inlet pressure, mass flow and subcooling of the increasing subcooling paths in Tab. A.2 is taken for the calculation of the sensitivity matrix S since ψ_{Rz} was estimated based on this experimental data (see section 5.1.3). Also for the calculation of the increasing subcooling paths, the previous wetting ratio Θ^{-1} and the wetted surface roughness $e_{wetted,Rz,Copper}$ are irrelevant (compare Fig. 4.2). Consequently the wetting ratio is set to zero and the wetted surface roughness $e_{wetted,Rz,Copper}$ is set to Rz within the calculations. The sensitivity matrix is calculated setting $\Delta\psi_{Rz}$=1e-5$\cdot\psi_{Rz}$ and solving the flow model for the pressure drop Δp^{up} at ψ_{Rz}=ψ_{Rz}+$\Delta\psi_{Rz}$ and Δp^{down} at ψ_{Rz}=ψ_{Rz}-$\Delta\psi_{Rz}$ for all considered experimental data while parametrizing the rest of the parameters of the flow model with the parameters in Tab. 5.4 accordingly. Consequently, the entries of the sensitivity matrix in Eq. (5.9) are approximated as follows:

$$\frac{\partial \Delta p_j}{\partial \psi_{Rz}} \approx \frac{\Delta p_j^{up} - \Delta p_j^{down}}{2 \cdot \Delta \psi_{Rz}} \tag{5.13}$$

Consecutively, Eq. (5.10) and Eq. (5.11) are applied and the standard deviation of ψ_{Rz}=6.1714 results to $\sigma_{a,\psi_{Rz}}$=0.2815 .

Estimation of the standard deviation of the wetted surface roughness $\sigma_{a,e_{wetted,Rz,Copper}}$

For the estimation of $\sigma_{a,e_{wetted,Rz,Copper}}$ the experimental data of the inlet pressure, mass flow and subcooling of the decreasing subcooling paths in Tab. A.3 is taken for the calculation of the sensitivity matrix S since $e_{wetted,Rz,Copper}$ was estimated based on this experimental data (see section 5.1.4). For the calculation of the decreasing subcooling paths, the previous wetting ratio Θ^{-1} is needed. The decreasing subcooling paths in Tab. A.3 are calculated using the transient simulation

of the flow model (see Fig. C.1) where the initial wetting ratio for the first subcooling of the decreasing subcooling path is set to zero. The sensitivity matrix is calculated setting $\Delta e_{wetted,Rz,Copper}$=1e-5·$e_{wetted,Rz,Copper}$ and solving the flow model for the pressure drop Δp^{up} at $e_{wetted,Rz,Copper}$=$e_{wetted,Rz,Copper}$+$\Delta e_{wetted,Rz,Copper}$ and $e_{wetted,Rz,Copper}$=Δp^{down} at $e_{wetted,Rz,Copper}$-$\Delta e_{wetted,Rz,Copper}$ for all considered experimental data while parametrizing the rest of the parameters of the flow model with the parameters in Tab. 5.4 accordingly. Consequently, the entries of the sensitivity matrix in Eq. (5.9) are approximated as follows:

$$\frac{\partial \Delta p_j}{\partial e_{wetted,Rz,Copper}} \approx \frac{\Delta p_j^{up} - \Delta p_j^{down}}{2 \cdot \Delta e_{wetted,Rz,Copper}} \tag{5.14}$$

The sensitivity matrix is zero for all entries (even for very small finite differences) which indicates that the parameter $e_{wetted,Rz,Copper}$ is not sensitive towards the calculated outlet pressure.

In order to estimate the standard deviation σ_b for the above mentioned parameters, an error propagation is carried out in the following.

Estimation of the standard deviation of the scaling factor $\sigma_{b,\xi_{Rz}}$

The standard deviation $\sigma_{b,\xi_{Rz}}$ of the parameter ξ_{Rz} is estimated based on one exemplary operating condition that has been experimentally investigated (PRC-1=20 bar, SC=29.6 K, FIRC-1=15.99 kg/h, DPR-1=4.39 bar, see Tab. A.1). Following the rules of error propagation the standard deviation, $\sigma_{b,\xi_{Rz}}$ is calculated depending on the standard deviation of the inner diameter $\sigma_{d,Copper}$=0.01e-3 m , the standard deviation of the roughness $\sigma_{Rz,Copper}$=0.391e-6 m and the derivatives $\frac{\partial \xi_{Rz}}{\partial d_{Copper}}$ and $\frac{\partial \xi_{Rz}}{\partial Rz_{Copper}}$:

$$\sigma_{b,\xi_{Rz}} = \sqrt{\left(\frac{\partial \xi_{Rz}}{\partial d_{Copper}}\right)^2 \cdot \sigma_{d,Copper}^2 + \left(\frac{\partial \xi_{Rz}}{\partial Rz_{Copper}}\right)^2 \cdot \sigma_{Rz,Copper}^2} \tag{5.15}$$

The derivates are determined applying finite differences. $\frac{\partial \xi_{Rz}}{\partial d_{Copper}}$ is approximated as follows:

$$\frac{\partial \xi_{Rz}}{\partial d_{Copper}} \frac{\approx \xi_{Rz}^{up} - \xi_{Rz}^{down}}{2 \cdot \Delta d_{Copper}} \tag{5.16}$$

setting Δd=1e-5$\cdot d_{Copper}$ and solving the flow model for the entrance pressure drop coefficient ξ_{Rz}^{up} at d_{Copper}=d_{Copper}+Δd and ξ_{Rz}^{down} at d_{Copper}=d_{Copper}-Δd at the considered exemplary operating condition while parametrizing the rest of the parameters of the flow model with the parameters in Tab. 5.4 accordingly. [7] Analogously $\frac{\partial \xi_{Rz}}{\partial Rz_{Copper}}$ is approximated. It follows $\sigma_{b,\xi_{Rz}}$=0.5317 and with Eq. 5.8 follows $\sigma_{\xi_{Rz}}$=0.5318 .

Estimation of the standard deviation of the entrance pressure drop coefficient $\sigma_{b,\psi_{Rz}}$

The standard deviation $\sigma_{b,\psi_{Rz}}$ of the parameter ψ_{Rz} is estimated based on one exemplary operating condition that has been experimentally investigated and results in a pressure drop that corresponds approximately to the average value of the experimentally investigated pressure drops (PRC-1=20 bar, SC=6 K, FIRC-1=16.49 kg/h, DPR-1=7.05 bar, see Tab. A.2). The standard deviation $\sigma_{b,\psi_{Rz}}$ is calculated including the standard deviation of the inner diameter $\sigma_{d,Copper}$=0.01e-3 m , the standard deviation of the roughness $\sigma_{Rz,Copper}$=0.391e-6 m , the standard deviation $\sigma_{\xi_{Rz}}$=0.5318 and the derivatives $\frac{\partial \psi_{Rz}}{\partial d_{Copper}}$, $\frac{\partial \psi_{Rz}}{\partial Rz_{Copper}}$ and $\frac{\partial \psi_{Rz}}{\partial \xi_{Rz}}$:

$$\sigma_{b,\psi_{Rz}} = \sqrt{\left(\frac{\partial \psi_{Rz}}{\partial d_{Copper}}\right)^2 \cdot \sigma_{d,Copper}^2 + \left(\frac{\partial \psi_{Rz}}{\partial Rz_{Copper}}\right)^2 \cdot \sigma_{Rz,Copper}^2 + \left(\frac{\partial \psi_{Rz}}{\partial \xi_{Rz}}\right)^2 \cdot \sigma_{\xi_{Rz}}^2} \tag{5.17}$$

The derivates are determined applying finite differences: $\frac{\partial \psi_{Rz}}{\partial d_{Copper}}$ is approximated setting Δd=1e-5$\cdot d_{Copper}$ and solving the flow model for the entrance pressure drop coefficient ψ_{Rz}^{up} at d_{Copper}=d_{Copper}+Δd and ψ_{Rz}^{down} at d_{Copper}=d_{Copper}-Δd (compare Eq. (5.16)) at the considered exemplary operating condition while parametrizing the rest of the parameters of the flow model with the parameters in Tab. 5.4 accordingly and setting the previous wetting ratio Θ^{-1} to zero. [8] Analogously $\frac{\partial \psi_{Rz}}{\partial Rz_{Copper}}$ and $\frac{\partial \psi_{Rz}}{\partial \xi_{Rz}}$ are approximated. It follows $\sigma_{b,\psi_{Rz}}$=5.7346 and with Eq. 5.8 it follows $\sigma_{\psi_{Rz}}$=5.7416 . It is obvious that the standard deviation $\sigma_{\psi_{Rz}}$ is very large. Thus, the error propagation of the inner diameter and the roughness is highly significant.

[7] The flow model is solved for ξ_{Rz} by means of the solver fsolve in MATLAB
[8] The flow model is solved for ψ_{Rz} by means of the solver fsolve in MATLAB

Estimation of the standard deviation of the wetted surface roughness $\sigma_{b,e_{wetted,Rz,Copper}}$

The standard deviation $\sigma_{b,e_{wetted,Rz,Copper}}$ is approximated analogously as described above using finite differences:

$$\sigma^2_{b,\xi_{Rz}} = \frac{\partial e_{wetted,Rz,Copper}}{\partial d_{Copper}}^2 \cdot \sigma^2_{d,Copper} + \frac{\partial e_{wetted,Rz,Copper}}{\partial Rz_{Copper}}^2 \cdot \sigma^2_{Rz,Copper} + \frac{\partial e_{wetted,Rz,Copper}}{\partial \xi_{Rz}}^2 \cdot \sigma^2_{\xi_{Rz}} + \frac{\partial e_{wetted,Rz,Copper}}{\partial \psi_{Rz}}^2 \cdot \sigma^2_{\psi_{Rz}} \tag{5.18}$$

However, as the parameter $e_{wetted,Rz,Copper}$ is not sensitive, all approximated derivatives in Eq. 5.18 equal zero and hence, the standard deviation $\sigma_{b,e_{wetted,Rz,Copper}}$ can not be identified.

Given the estimated uncertainties of the considered parameters of the flow model, the uncertainty of the calculated pressure drop $\sigma_{\Delta p}$ is calculated following the rules of error propagation:

$$\sigma^2_{\Delta p} = \left(\frac{\partial \Delta p}{\partial d} \cdot \sigma_d\right)^2 + \left(\frac{\partial \Delta p}{\partial e} \cdot \sigma_e\right)^2 + \left(\frac{\partial \Delta p}{\partial \xi_{Rz}} \cdot \sigma_{\xi_{Rz}}\right)^2 + \left(\frac{\partial \Delta p}{\partial \psi_{Rz}} \cdot \sigma_{\psi_{Rz}}\right)^2 \tag{5.19}$$

Eq. (5.19) is approximated via finite differences (analogously as described above for the determination of $\sigma_{b,\xi_{Rz}}$ and $\sigma_{b,\psi_{Rz}}$) at an exemplary operating condition that was experimentally investigated and results in a pressure drop that corresponds approximately to the average value of the experimentally investigated pressure drops (PRC-1=20 bar, SC=6 K, FIRC-1=16.49 kgh^{-1}, DPR-1=7.1 bar, see Tab. A.2). The estimated uncertainty of the calculated pressure drop results to $\sigma_{\Delta p}$=0.8505 bar. Eq. (5.19) applies for the uncertainty of the calculated pressure drop using the flow model and applying the *modified B&W viscosity correlation*. In the case that the original viscosity correlation of Beattie and Whalley, 1982 is applied Eq. (5.19) is reduced by the term $\frac{\partial \Delta p}{\partial \psi_{Rz}} \cdot \sigma_{\psi_{Rz}}$ and the uncertainty of the calculated pressure drop results to $\sigma_{\Delta p}$=0.8456 bar. The major influence on the uncertainty of the calculated pressure drop bear the uncertainties of the inner diameter and the roughness.

All in all, it is evident that the uncertainty of the parameters that were considered in the uncertainty analysis (see itemization at the top of this section) significantly

contribute to the overall uncertainty of the flow model. It has to be stated that the outlined standard deviations are only lower bounds and that only one representative operating condition was considered for the analysis of the error propagation (determination of $\sigma_{b,\xi_{Rz}}$ and $\sigma_{b,\psi_{Rz}}$). Further, the deviation of the wetted surface roughness is not considered as it is not identifiable. Hence, the standard deviation of each parameter and thereby the uncertainty of the flow model may be even larger. Against this background, it is noticeable how precise the flow model predicts the overall database of the experiments in the copper and steel capillary (see Tab. 5.5 and Tab. 5.9). The parameter estimation of ψ_{Rz} might cover any deviations of the parametrized inner diameter and the roughness from the actual values of the investigated capillary. Anyway the predictions of the experiments in the steel capillary that rely on the estimation of ψ_{Rz} still show very good results. Consequently, it is conclusive that the flow model is well parametrized as the mean error for both - the predictions of the experiments in the copper and steel capillary - indicate a mean absolute error of only 0.2-0.3 bar which is much below the above quantified standard deviation of the pressure drop $\sigma_{\Delta p}$=0.8505 bar.

5.4 Further Numerical Investigations and Predictions

This section treats further transient simulations of different series of changing flow conditions at the capillary inlet and discusses the resulting predictions of the pressure drop in the capillary. The series of different flow conditions is in each case simulated consecutively following the solution algorithm for the transient simulation of the flow model attached in the appendix (see Fig. C.1). The flow model presented in chapter 4 is parametrizted following the listed parameters in Tab. 5.4 by applying the *modified B&W viscosity correlation*. The initial wetting ratio is set to zero unless it is stated differently.

Up to this point, only one increasing subcooling path which is followed by one decreasing subcooling path was investigated numerically. Fig. 5.14 shows the course of the predicted pressure drop that results from the simulation of the depicted alternation of the subcooling at a fixed inlet pressure of 16 bar and mass flow of 15 kg/h. The first simulated flow condition is at a subcooling of 3 K with an initial wetting ratio that is set to zero. It results in the comparably highest

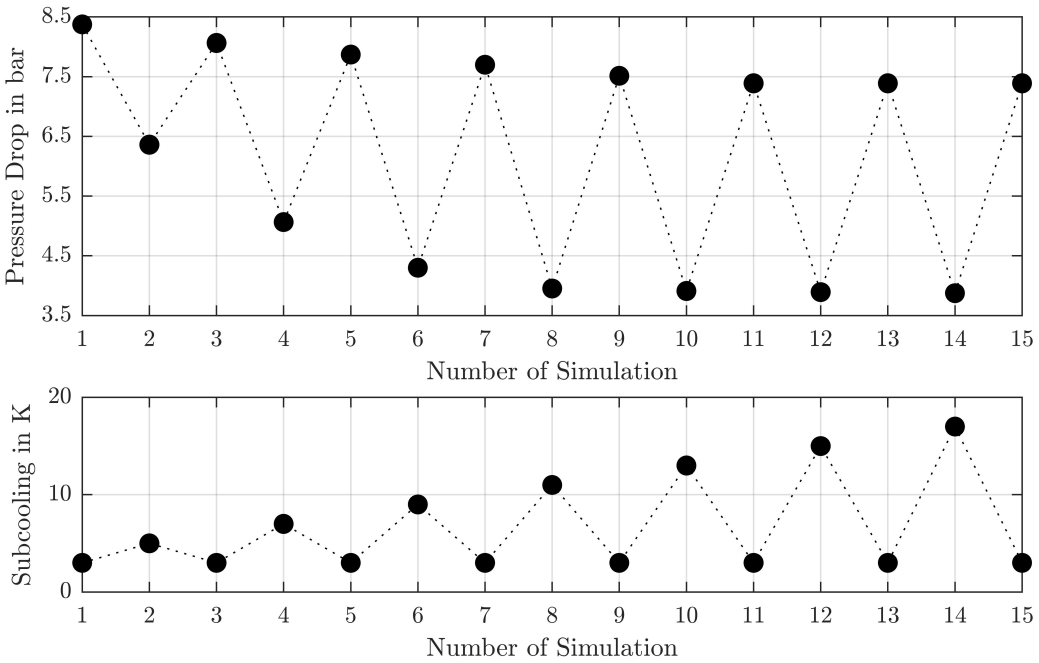

Fig. 5.14: *Simulated hysteresis effect on the pressure drop evoked by the alternation of the subcooling at a constant inlet pressure of 16 bar and mass flow of 15 kg/h using the flow model in chapter 4 and the parametrization in Tab. 5.4. The horizontal axis displays the number of simulation, i.e. indicates a new flow condition (change of the subcooling).*

pressure drop of the simulated subcooling alternation. Changing to a subcooling of 5 K and than back to 3 K results in a lower pressure drop for the 3 K subcooling than was simulated at the beginning. The higher the previous subcooling is when changing back to 3 K subcooling the lower is the pressure drop at 3 K subcooling. However, for previous subcoolings higher than 11 K there is no further impact on the pressure drop at 3 K - this is where the wetting ratio becomes 1. If the initial wetting ratio at the beginning of the transient simulation of the subcooling alternation is set to 1 instead of 0, no impact of the alternation on the pressure drop is seen at all. Than the calculated pressure drop is at the constant level of around 7.5 bar. Consequently, the previous or initial wetting ratio when simulating the flow through a capillary is of great importance. For the design of a capillary which is derived from the operation of the capillary it may therefore also be valuable to know the initial wetting condition of the capillary.

The hypothesis for the occurrence of a hysteresis effect that impacts the flow through a capillary tube that underlies this work, is that metastable flow is developed when two-phase flow passes a wetted capillary part. Hence, the assumption is that the pressure drop is lower for two-phase flow passing a wetted capillary than passing a dry capillary (see section 3.3.3) which was implemented within the flow model (see section 4.2).

Consequently, it is not the change of subcooling, actually, (i.e. increasing vs. decreasing subcooling) as it was mainly investigated in this work, but actually the change of the wetting ratio. However, a change of the wetting ratio can be evoked by different changes of the inlet conditions other than the subcooling; also a change of the inlet pressure by constant subcooling and mass flow as well as a change of the mass flow by constant subcooling and inlet pressure has an impact on the wetting ratio.

Fig. 5.15 depicts the hysteresis effect on the pressure drop that is evoked by the change of the mass flow at a constant inlet pressure of 25 bar and a constant subcooling of 5 K. The mass flow is varied from 19 kg/h to 11 kg/h and back in 1 kg/h-steps. Fig. 5.15 sketches the course of the resulting wetting ratio of the subsequently calculated flow conditions. As a high mass flow results in a higher pressure drop concerning both - the liquid and two-phase flow - the length of the capillary that is covered by liquid flow is smaller for higher mass flows than for low mass flows. Consequently, the wetting ratio is lower at higher mass flows than at lower mass flows. Due to the underlying model assumptions a hysteresis effect on the pressure drop is evoked which has the highest impact at the highest simulated mass flow of 19 kg/h. At this point, the difference between the decreasing and increasing mass flow path amounts approximately 11 % in the resulting pressure drops of the decreasing and increasing mass flow paths. Logically, the hysteresis effect is lower for higher subcoolings as there is generally less two-phase flow and, the assumption of the wetted surface roughness only affects the two-phase flow.

Fig. 5.16 depicts the hysteresis effect on the pressure drop that is evoked by the change of the inlet pressure at a constant mass flow of 16 kg/h and a constant subcooling of 5 K. The inlet pressure is varied from 16 bar to 32 bar and back in 3 bar-steps. The series of different inlet pressure is simulated analogously as

above for the series of mass flows. As can be seen in Fig. 5.16 the change of the inlet pressure evokes a change in the resulting wetting ratio and thereby the resulting hysteresis effect on the pressure drop. The largest discrepancy between the pressure drops of the increasing and decreasing inlet pressure paths is at the lowest simulated inlet pressure of 16 bar and amounts to a difference of about 4 %.

As could be demonstrated, the flow model provided in this work is able to not only capture a hysteresis effect in the pressure drop that is evoked by changing the subcooling at the inlet of the capillary but also by changing the inlet pressure and the mass flow in the capillary. The effects may certainly superpose each other: the wetting ratio increases even more when the increasing of the subcooling is accompanied by a decreasing of the mass flow for example. Depending on how the heat pump is operated and which operating conditions the capillary goes through, the hysteresis effect that is evoked by changes in the wetting ratio of the capillary may have a significant influence on the heat pump operation as we see a high impact on the resulting pressure drop in the capillary. The proposed flow model, thus, offers the opportunity to test the impact by implementing it as a capillary model within an overall heat pump model

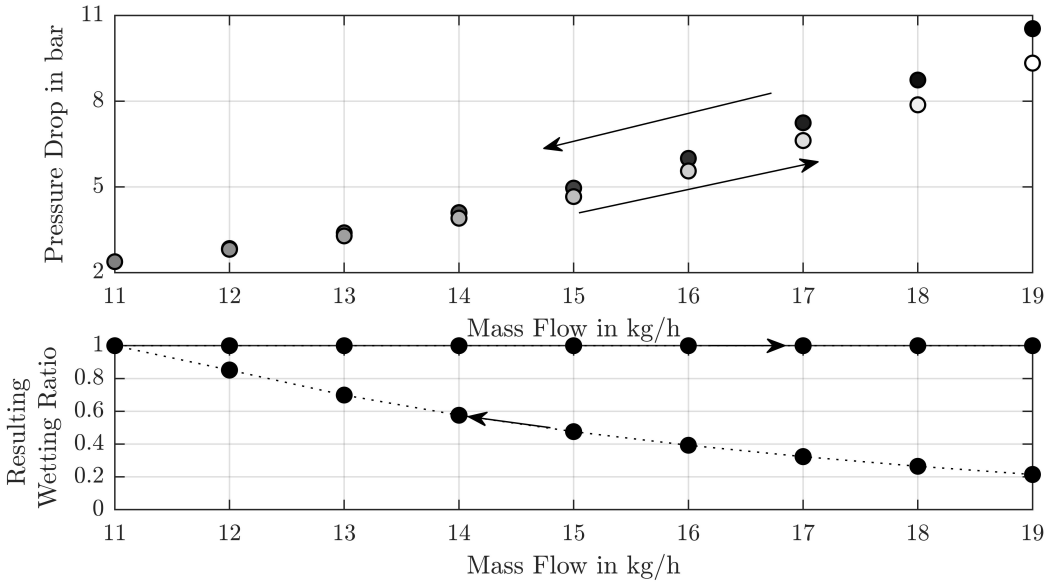

Fig. 5.15: *Simulated hysteresis on the pressure drop evoked by the change of the mass flow from high mass flow to low mass flow to high mass flow at a constant inlet pressure of 25 bar and constant subcooling of 5 K using the flow model in chapter 4 and the parametrization in Tab. 5.4.*

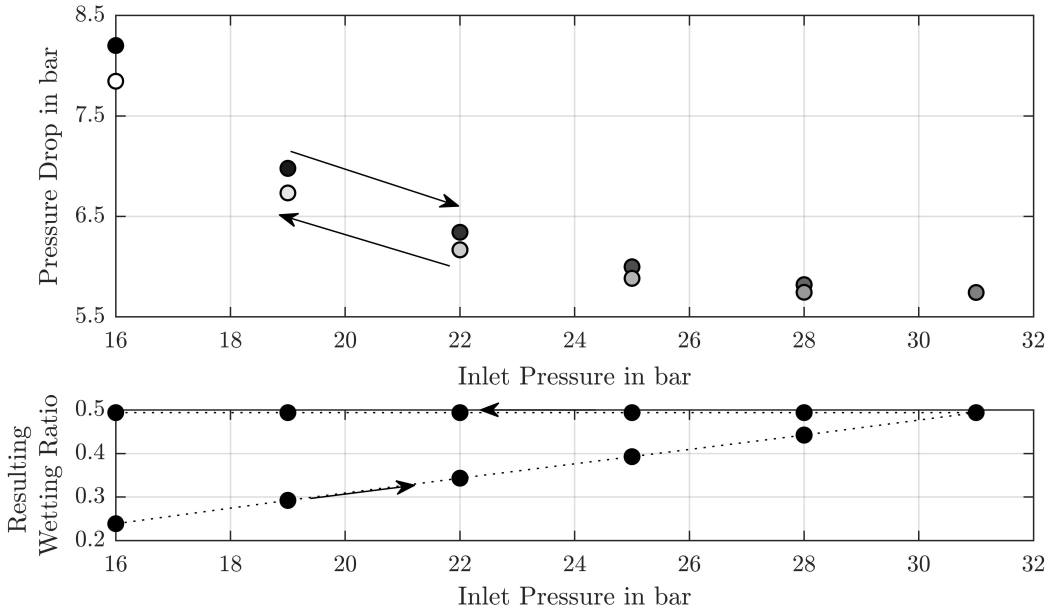

Fig. 5.16: *Simulated hysteresis on the pressure drop evoked by the change of the inlet pressure from low inlet pressure to high inlet pressure to low inlet pressure at a constant mass flow of 16 kg/h and constant subcooling of 5 K using the flow model in chapter 4 and the parametrization in Tab. 5.4.*

6 Conclusion and Future Directions

The model-based development or optimization of technical systems is a time-efficient and cost-effective method. In order to derive reliable solutions, a valid and predictive simulation of the considered system is an indispensable prerequisite. Regarding the model-based optimization of a heat pump operation, valid and predictive models of each components of the heat pump are required. Controlling the refrigerant mass flow in the system, the capillary tube as expansion device is a component that decisively influences the overall heat pump performance. All the more, it is important to refer to a reliable model that is able to cover the operation range of a heat pump and capture the physical behaviour of the refrigerant that flows through the capillary tube.

In the present thesis, extensive investigations on the propane flow in a copper and a steel capillary were carried out which serve as a validation basis for a developed flow model that serves to predict the flow of refrigerants in capillary tubes. The experimental or validation range, respectively, is shown in Tab. 6.1. It comprises inlet pressures from 16 to 25 bar, subcoolings from 5 to 9 K and mass flows from 13.5 kg/h to 18 kg/h. The experimental database on the propane flow in the copper capillary covers a larger number of investigated flow conditions. The experiments on the flow in the steel capillary mainly served as a further validation base in order to check whether the flow model that has been adapted to the experiments on the copper capillary are still predictive with respect to

Tab. 6.1: *Range of validity for the modified B&W viscosity correlation.*

		Capillary Specification				**Flow Conditions**				
	Material	d	L	Ra	Rz	Inlet Temperature	SC	Inlet Pressure	Mass Flow	Mass Flux
Refrigerant	in m	in m	in m	in m	in m	in °C	in K	in bar	in kg/h	kg/m²s
Propane	Copper	1.1799e-3	1.0274	0.101e-6	1.285e-6	33-63	5-9	16-25	13.5-18	3430-4573
	Steel	1.1749e-3	1.0274	0.817e-6	2.239e-6	33-63	5-9	16-25	13.5-18	3430-4573

the steel capillary. Generally, the steel capillary evoked a higher pressure drop than the copper capillary for the same inlet conditions which is traced back to the higher roughness of the inner surface of the steel capillary. The experiments capture the hysteresis effect depending on the variation of the subcooling at the capillary inlet. Quantitative and qualitative differences concerning the hysteresis effect in the copper and steel capillary were worked out. The hysteresis effect is more pronounced in the steel capillary than in the copper capillary.

From the extensive experiments on the propane flow in the copper capillary a hypothesis for the cause and the interrelation between the metastable flow and hysteresis effect of the refrigerant flow has been derived. The conducted experiments support the studies of Guobing and Yufeng (2006) who observed that the metastable flow phenomena is more prominent starting with a high subcooling and subsequently decreasing the subcooling than starting with a low subcooling and subsequently increasing the subcooling. From systematic experiments it is assumed that the wetting of the capillary entails a metastable flow. However, the expression "metastable flow" needs to be differentiated from the common reference in the literature. Generally, researchers describe the observation of refrigerant flow that remains subcooled at pressures below the actual saturation pressures as metastable flow. Differently in this work, metastable flow is considered to be two-phase flow that passes a previously wetted capillary surface and therefore in this area is subject to less friction than in areas that have not been wetted by liquid refrigerant flow, yet. Consequently, a hysteresis effect is induced as the pressure drop is higher for increasing subcoolings starting with a low wetting ratio of the capillary than vice versa. This assumption was transferred into a model approach that supplements the common homogeneous flow approach by the required input variable of the previous wetting ratio Θ^{-1} and the model parameter e_{wetted} that specifies the (effective) wetted surface roughness of the considered capillary which is estimated according to the database on the decreasing subcooling measurements. Together with a proposed modification of the two-phase viscosity correlation of Beattie and Whalley (1982) the developed flow model predicts 69.1 % of the experimental data of the propane flow including ambiguous data due to the hysteresis effect in the copper capillary within an error band of 5 % and results in a mean relative error of 4 %. Further, it predicts the flow of propane in the steel capillary in a comparable accuracy (see section 5.2.4) which supports

the overall prediction quality of the flow model. Based on the flow model it is predicted that not only the variation of the subcooling entails a hysteresis effect but also a change in the inlet pressure or the mass flow since the change in the wetting ratio is the cause of the hysteresis effect.

The systematic experimental investigations and the model adaptions in section 5.1 and section 5.2 have been transferred into a systematic procedure for the adaption of the proposed flow model to the refrigerant and capillary (see Fig. 5.1 and Fig. 5.10). The systematic procedure is a proposal for future investigations on the flow of refrigerants in capillary tubes to thoroughly capture the occurence of a hysteresis effect and provide reliable experimental data that serve as a validation basis for according flow models. Investigating the same refrigerant in a different capillary, yet with the same geometry with respect to the inner diameter and length of the capillary, the systematic procedure is reduced in its extent. Further, it is possible to save expensive measurements of the surface roughness for the secondly investigated capillary tube following and relying on the proposed systematic procedure.

The difference in the investigated pressure drops due to the observed hysteresis effect reaches values higher than 20 % (see section 3.3.2). Therefore, it is reasonable to assume that the hysteresis effect may have an impact on the heat pump performance if a hysteresis curve (e.g. increasing subcooling followed by decreasing subcooling trajectory at the capillary inlet) is passed through within the heat pump operation. It is worth to investigate possible impacts within an overall heat pump simulation as Meyer and Dunn (1998) already suggested. However, up to now, to the best of the author's knowledge, no model was available that captured the hysteresis effect of the refrigerant flow in capillaries. Hence, the model that was proposed in this work (see chapter 4) can now be included within an overall heat pump model and the consequences of the hysteresis on the heat pump performance can be evaluated.

As an alternative approach of adapting the homogeneous flow model for a better prediction of the experimental results of the propane flow, the correlation of the friction factor by Colebrook (1939) or its approximation of Serghides (1984) could be questioned. As it is desirable, to reduce the amount of empirical parameters within a physical model, sticking to the proposed *modified B&W viscosity correlation*,

a possible physical meaning of the scaling factor ψ (see Eq. (5.6) in section 5.1.3 can be explored. Investigating different refrigerants following the proposed systematic procedure and comparing the resulting parameter ψ for each refrigerant could provide information on the physical meaning of ψ. The results could be related to different molecule sizes of the refrigerant for example.

In order to gain a deeper understanding of the development of metastable flow, more fundamental research on the two-phase flow of refrigerants along wetted and dry surfaces is recommended. It is conceivable that the in this work simply considered parameter of the wetted surface roughness e_{wetted} is an interplay between the surface profile of the capillary and e.g. the surface tension of the refrigerant in reality. Thorough experiments with different refrigerants and different surface qualities of the capillary could reveal a possible correlation. Still, a simple parameter characterizing the wetted surface roughness yields computational benefits when modelling the flow of refrigerants in a capillary tube. Therefore, it might be possible to find a correlation between the roughness of the capillary and/or the surface tension of the refrigerant. Any reduction of empirical parameters within the flow model increases the overall applicability of the model as the experimental investigations for the identification of the parameters are not needed in advance. Furthermore, a broad investigation of different refrigerants and capillary tubes should generally be used in order to verify the overall prediction quality of the developed flow model. Extended experiments on the collapse of metastable flow are advised in order to understand what circumstances favour the collapse. The findings can then be supplemented into the flow model so that it gains further prediction quality on the development of metastable flow and the resulting hysteresis effect.

Appendix A

Experimental Data

A.1 Experimental Data of the Propane Flow Through the Copper Capillary Tube

Tab. A.1: *Experimental data of the pressure for the liquid flow through the steel capillary given the operating conditions in Tab. 3.2 (SC = Subcooling, source: (Gabrisch and Repke, 2020)).*

PRC-1 in bar	FIRC-1 in kg/h	SC in K	DPR-1 in bar
16.1	12.04	19.5	2.70
15.92	14.94	19.1	3.91
16.01	18.02	19.6	5.40
20.02	13.01	29.7	3.10
19.99	14.00	29.6	3.50
19.99	14.99	29.6	3.95
20.01	15.98	29.6	4.39
20.02	16.95	29.7	4.77
24.08	11.99	38.7	2.68
24.00	18.01	33	5.51
23.99	21.98	32.9	7.83

Tab. A.2: *Experimental data of the pressure drop for the increasing subcooling paths given the operating conditions in Tab. 3.3 in the copper capillary (SC = Subcooling, source: (Gabrisch and Repke, 2020)).*

PRC-1 in bar	FIRC-1 in kg/h	SC in K	DPR-1 in bar
16	13.5	4.9	3.95
16	13.5	6	3.8
16	13.5	7	3.68
16	13.5	8	3.55
16	13.5	9	3.34
16	14	5	4.45
16	14	6	3.88
16	14	7.1	3.71
16	14	8	3.59
16	13.99	8.9	3.42
15.99	13.95	5	3.75
16	14.02	6.1	4.11
16	13.99	7.1	3.99
16	14	8	3.9
16	13.99	9	3.75
16	14.5	5	5.6
16	14.5	6.1	4.56
15.99	14.5	7	4.41
15.99	14.52	8	4.28
16	14.5	9	4.06
16	14.49	5	5.42
16	14.49	6	4.87
16	14.5	7	4.58
16	14.5	8	4.35
16	14.49	9	4.16
16	14.85	5.1	6.85
16	15	6	6.51
16	15	7	5.01
16	15	8	4.79

Continued on next page

Tab. A.2 (continued).

PRC-1 in bar	FIRC-1 in kg/h	SC in K	DPR-1 in bar
16	14.99	9	4.59
16	15	5	6.57
16	15	6	6.03
16	15	7	4.9
16	15	8	4.71
16.01	15	9	4.48
17	14.96	5	5.54
17	15	6.2	5.07
17	15	7.1	4.9
17	15.01	8	4.76
17	15.02	9	4.58
17	15	5	6.02
17	14.99	6	5.63
17	15	7	4.85
17	15	8	4.66
17	15	9	4.45
18	15.01	5	4.83
18	15	6	4.56
18	15	7	4.47
18	15	8	4.35
18	15.01	9	4.21
18	15	5	6.05
18	15	6	4.9
18	15	7	4.74
18	15	8	4.57
18	15	8.9	4.4
19	15	5	5.6
19	15	6	4.71
19	15	7	4.57
19	15	8.1	4.42

Continued on next page

Tab. A.2 (continued).

PRC-1 in bar	FIRC-1 in kg/h	SC in K	DPR-1 in bar
19	14.99	9	4.27
19	15	4.9	5.45
19	15	6	4.76
19	15	6.9	4.62
19	15	8	4.46
19	15	9.1	4.28
20	15	4.9	5.15
20	15	6	4.91
20	15	7	4.62
20	15	8.1	4.31
20	15	9	4.18
20	14.99	5	5.3
20	15	6	5.02
20	14.99	6.9	4.58
20	15	8	4.44
20	14.99	9	4.26
21	14.99	5	5.04
21	15	6	4.51
21	15	7.1	4.39
21	15	8	4.26
21	15	9	4.1
21	15	5	5.03
21	15	6	4.51
21	15	7	4.4
21	15	8	4.28
21	15	8.9	4.12
23	15.01	4.9	4.46
23.01	14.99	6	4.36
23.01	14.99	7	4.27
23	14.99	8	4.15

Continued on next page

Tab. A.2 (continued).

PRC-1 in bar	FIRC-1 in kg/h	SC in K	DPR-1 in bar
23	15	8.9	4.1
23	15.01	5	4.36
23	14.99	6	4.27
23	14.98	7	4.23
23	15	8	4.15
23	15	9	4.11
25	16	5.1	5.36
25	16	6.1	5.23
25	16	7	5.12
24.99	16	8	4.96
25	16	8.9	4.77
20	16.49	5	7.55
20	16.49	6	7.05
20	16.49	7	6.4
20	16.49	7.9	5.29
20	16.49	9	5.17
20	16.5	5.1	7.77
20	16.5	6	7.06
20	16.5	7	5.84
20	16.5	8	5.64
20.01	16.5	9.1	5.44
20.99	16.49	5	7.47
21.01	16.5	6	6.67
20.99	16.5	7	5.72
21	16.5	8.1	5.53
21	16.5	9	5.37
21	16.49	5	7
21	16.5	6	6.61
21	16.5	7	5.66
21	16.5	8	5.49

Continued on next page

Tab. A.2 (continued).

PRC-1 in bar	FIRC-1 in kg/h	SC in K	DPR-1 in bar
21	16.49	9	5.32
23	16.49	5	6.91
23	16.5	6	6.31
23	16.5	7.1	5.55
23	16.5	8	5.41
23	16.5	9	5.25
23	16.51	5	6.69
23	16.51	6	6.35
23	16.5	7	5.93
23	16.5	9	5.43
23	16.49	9	5.25
25	16.5	5	6.29
25	16.5	5.9	5.95
25	16.51	7	5.38
25	16.5	8	5.2
25	16.49	9	4.97
25	16.5	5	6.38
25	16.5	6.1	5.62
25	16.5	7.1	5.49
25	16.5	8.1	5.33
25.01	16.5	9.1	5.14
23	17.99	5	10.06
23	18.01	5.9	8.57
23	18	7.1	7.96
23	18	8	6.77
23.01	18	9	6.54
23	18	5	9.96
23	18	6	8.86
23	18	7.1	7.78
23	18.01	8.1	6.6

Continued on next page

Tab. A.2 (continued).

PRC-1 in bar	FIRC-1 in kg/h	SC in K	DPR-1 in bar
23	18	9	6.39
25	18	5	8.82
25	18	6	8.2
25	18	7.1	7.55
25	18	8.1	6.57
24.98	18	9.1	6.39
24.99	18	4.9	8.77
25	18	5.9	8.25
25	18	7.1	7.5
25	18	8.1	6.55
25	18	9	6.4

Tab. A.3: *Experimental data of the pressure drop for the decreasing subcooling paths given the operating conditions in Tab. 3.3 in the copper capillary. (The *-marked operating conditions are excluded from the parameter estimation of the wetted surface roughness by analysing Fig. A.2 and picking out pressure drops that are probably affected by a metastable collapse), (SC = Subcooling, source: (Gabrisch and Repke, 2021)).*

PRC-1 in bar	FIRC-1 in kg/h	SC in K	DPR-1 in bar
16	13.5	9	3.34
16	13.5	8	3.35
16	13.5	7	3.36
16	13.5	6	3.39
16	13.5	5	3.42
16	13.99	8.9	3.42
16	14	8	3.55
16	14	7	3.71
16	13.99	6	3.88
16	14	5	4.08
16	13.99	9	3.75
16	14.02	7.9	3.93
16.01	14	7	3.93

Continued on next page

Tab. A.3 (continued).

PRC-1 in bar	FIRC-1 in kg/h	SC in K	DPR-1 in bar
16.01	14.01	6	4.05
16	14.03	5.1	4.35
16	14.5	9	4.06
16	14.5	7.9	4.19
16	14.51	6.9	4.33
16	14.5	5.9	4.44
16	14.5	4.9	4.57
16	14.49	9	4.16
16	14.5	8	4.33
16	14.51	7	4.48
16	14.53	6	4.59
16	14.51	5	4.73
16	14.99	9	4.59
16	15	7.9	4.81
16	15	7	5.02
16	15	6	5.24
16.01	15.01	5	5.49
16.01	15	9	4.48
16	15	8	4.69
16	15	6.9	4.94
16	15	5.9	5.23
16	15	5	5.49
17	15.02	9	4.58
17	14.96	8	4.7
17	15	7	4.89
17	15	6.1	5.08
17	14.93	5.1	5.36
17	15	9.1	4.45
17	15	8	4.63
17	15	6.9	4.84
17	15	5.9	5.02

Continued on next page

Tab. A.3 (continued).

PRC-1 in bar	FIRC-1 in kg/h	SC in K	DPR-1 in bar
17	15	5	5.23
18	15.01	9	4.21
18	15	8	4.39
18	15.03	7	4.53
18	15.05	5.9	4.76
18	15.01	4.9	4.93
18	15	8.9	4.4
18	14.99	7.9	4.54
18	15	7	4.68
18	15	6	4.85
18	15.01	5	5.03
19	14.99	9	4.27
19	15	8	4.42
19	15	6.9	4.55
19	15	6	4.67
19	15	5	4.8
19	15	9	4.28
19	15	7.9	4.46
19	15	6.9	4.61
19	15	6	4.75
19	15	5	5.53
20	15	9	4.18
20	15	7.9	4.36
20	15	7	4.46
20	15	6	4.55
20	15	5	4.66
20	14.99	9	4.26
20	15.01	8	4.44
20	15	6.9	4.58
20	15	6	4.72

Continued on next page

Tab. A.3 (continued).

PRC-1 in bar	FIRC-1 in kg/h	SC in K	DPR-1 in bar
20	15	5	4.88
20	16.49	9	5.17
20.01	16.5	7.9	5.29
20	16.5	7	5.84
20	16.5	6	6.05
20	16.5	5	7.04
20*	16.51*	5*	7.59*
20.01	16.5	9.1	5.44
20	16.5	7.9	5.65
20	16.5	7	5.85
20	16.5	6	6.06
20	16.5	5	7.06
21	15	9	4.1
21	15	8	4.15
21	15	6.9	4.2
21	15	6	4.25
21	15.01	5	4.55
21	15	8.9	4.12
21	15	8	4.16
21	15	7	4.21
21	15	5.9	4.26
21	15.02	4.9	4.54
21	16.5	9	5.37
21	16.5	7.9	5.56
21	16.5	6.9	5.75
21.01	16.5	6	5.93
21.02	16.5	5	6.81
21*	16.5*	5*	7.19*
21	16.49	9	5.32
21	16.5	8	5.48
21	16.5	7	5.64

Continued on next page

Tab. A.3 (continued).

PRC-1 in bar	FIRC-1 in kg/h	SC in K	DPR-1 in bar
21	16.51	5.9	6.64
21	16.5	5.1	6.99
23	15	8.9	4.1
23	15.01	7.9	4.09
23	15	6.9	4.09
23	15	5.9	4.11
23	15	4.9	4.19
23*	15.01*	4.9*	4.4*
23	15	9	4.11
23	15.01	8	4.1
23.01	15.01	6.9	4.12
23	15	5.9	4.15
23	15	5	4.38
23	16.5	9	5.25
23	16.5	7.9	5.42
23	16.5	6.9	5.58
23	16.5	5.9	5.74
23	16.5	4.9	6.69
23	16.49	9	5.25
23	16.5	7.9	5.44
23	16.51	6.9	5.61
23	16.5	5.9	5.78
23	16.51	5	6.7
23.01	18	9	6.54
23	18	8	6.77
23	18	6.9	7.18
23	17.99	6	8.52
23	17.99	5	9.08
23	18	9	6.39
23	18	8	6.64
23	18	6.9	6.93

Continued on next page

Tab. A.3 (continued).

PRC-1 in bar	FIRC-1 in kg/h	SC in K	DPR-1 in bar
23	18	6	8.28
23	18	5	9.1
25	16	8.9	4.77
25	16	7.9	4.86
25	16	7.1	4.93
25	16	6.1	5.23
25	16	5	5.36
25	16.49	9	4.97
25	16.5	8	5.22
25	16.5	6.9	5.39
25	16.5	5.9	5.55
25	16.5	5	6.28
25.01	16.5	9.1	5.14
25	16.5	8	5.34
25	16.5	7	5.5
25	16.5	5.9	5.63
25	16.5	5.1	5.88
24.98	18	9.1	6.39
25.01	18	8	6.58
25	18	6.9	6.96
25	18	6	7.97
25	18	5	8.57
25	18	9	6.4
25	18	8	6.58
25	18	7	6.77
25	18	6	7.36
25.01	18	5	8.36

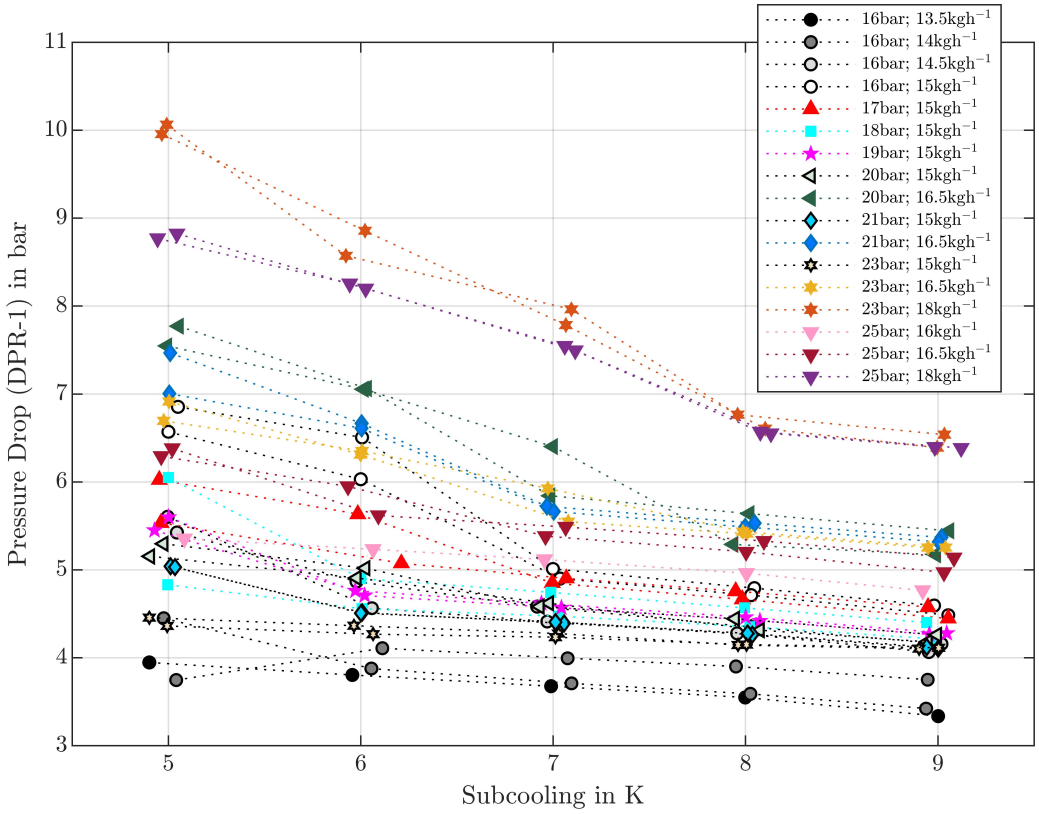

Fig. A.1: *Diagram of all experimentally gathered increasing subcooling paths in Tab. A.2 in the copper capillary. The legend shows the different investigated inlet pressures (PRC-1) and the mass flows (FIRC-1). The diagram shows the resulting pressure drop (DPR-1) over the change of the subcooling at the capillary inlet, source: (Gabrisch and Repke, 2020).*

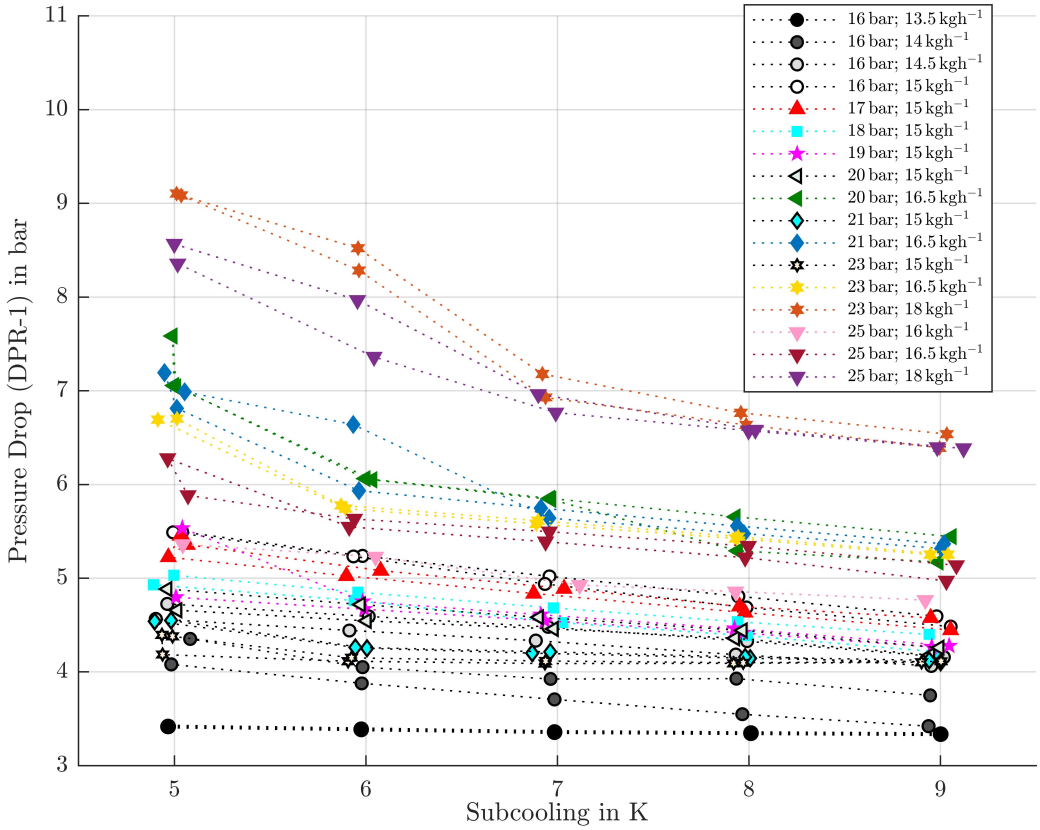

Fig. A.2: *Diagram of all experimentally gathered decreasing subcooling paths in Tab. A.3 in the copper capillary. The legend shows the different investigated inlet pressures (PRC-1) and the mass flows (FIRC-1). The diagram shows the resulting pressure drop (DPR-1) over the change of the subcooling at the capillary inlet, source: (Gabrisch and Repke, 2021).*

A.2 Experimental Data of the Propane Flow Through the Steel Capillary Tube

Tab. A.4: *Experimental data of the pressure drop for the liquid flow through the steel capillary given the operating conditions in Tab. 3.5, SC = Subcooling.*

PRC-1 in bar	FIRC-1 in kg/h	SC in K	DPR-1 in bar
15.01	8.01	9.2	1.38
15.01	9	9.4	1.7
16	11	11.4	2.45
16.5	13.01	11.8	3.32
18.03	14.99	16.6	4.28
18.53	16.99	17.8	5.4
19.04	17.99	19	6.03

Tab. A.5: *Experimental data of the pressure drop for the increasing subcooling paths given the operating conditions in Tab. 3.6 in the steel capillary (SC = Subcooling).*

PRC-1 in bar	FIRC-1 in kg/h	SC in K	DPR-1 in bar
18	15	5	6.48
18	15	6	5.77
18	15	7.1	5.13
18	15	8.1	4.79
18	15	9	4.37
18	15	5.1	6.41
18	15	6.2	5.99
18	15	7.1	5.64
18	15	7.9	5.27
18	15	8.9	4.84
23.01	16.5	5.1	7.84
23	16.49	6	7.17
23	16.49	7.1	6.51
23	16.5	8	5.98

Continued on next page

Tab. A.5 (continued).

PRC-1 in bar	FIRC-1 in kg/h	SC in K	DPR-1 in bar
23	16.5	9.1	5.56
23.03	16.49	5	7.28
23	16.5	6	7.03
23.01	16.5	7	6.67
23	16.5	8	6.33
23.01	16.48	9.1	5.89
25.02	16.51	5.2	7.52
25	16.5	6.2	6.97
25	16.5	7	6.56
25	16.5	8	6.13
24.95	16.49	8.9	5.84
25	18	4.9	10.88
25	18	5.9	9.81
25	18	7.1	8.71
25	18	8.1	8.01
25	17.99	9.1	7.44
20	15.02	5	5.42
20	15	6	4.82
20	15	7.1	4.67
20	15	8.1	4.54
20	14.99	9	4.35
20	15.01	5.1	6.17
20	15	6.1	5.58
20	15	7.2	5.19
20	15	8.1	4.86
20	14.99	9.1	4.56
23	17.78	5	11.3
23	18.09	6	11.22
23	18.09	7	10.66
23	18	8	8.6

Continued on next page

Tab. A.5 (continued).

PRC-1 in bar	FIRC-1 in kg/h	SC in K	DPR-1 in bar
23	17.99	9	7.8
16.01	13.49	5.2	4.46
16	13.49	6.1	4.29
16.01	13.5	7.1	4.07
16	13.5	8.1	3.86
16.01	13.5	9	3.62
16	13.5	5.3	4.8
16	13.51	6.2	4.55
16	13.5	7.1	4.15
16.01	13.5	8	3.91
16	13.49	8.8	3.68

Tab. A.6: *Experimental data of the pressure drop for the decreasing subcooling paths given the operating conditions in Tab. 3.6 in the steel capillary (SC = Subcooling).*

PRC-1 in bar	FIRC-1 in kg/h	SC in K	DPR-1 in bar
18	15	9	4.37
18	15	8	4.44
18	15	7	4.48
18	15	5.9	4.52
18	15	4.9	5.52
18	15	8.9	4.84
18	15	8	4.96
18.01	14.99	7	5.14
18	15	6	5.38
18	15	5	5.74
23	16.5	9.1	5.56
23	16.5	8	5.88
23	16.5	6.9	6.1
23	16.5	6	6.39
23	16.51	5	7.17

Continued on next page

Tab. A.6 (continued).

PRC-1 in bar	FIRC-1 in kg/h	SC in K	DPR-1 in bar
23.01	16.48	9.1	5.89
23	16.5	8	6.22
23	16.5	6.9	6.5
23	16.5	5.9	6.8
23	16.51	4.9	7.23
24.95	16.49	8.9	5.84
25.01	16.5	8	6.06
25	16.5	7.1	6.28
25	16.5	6	6.56
25	16.5	5	7.05
25	17.99	9.1	7.44
25	18	8	7.97
25	18	7	8.43
25	17.99	6	9.47
25	18	5	10.13
20	14.99	9	4.35
20	15	8	4.33
20	15	6.9	4.34
20	15	5.9	4.38
20	15	4.9	4.53
20	14.99	9.1	4.56
20	15	8.1	4.77
20	15	7	4.97
20	15	5.9	5.21
19.99	14.98	4.9	5.42
23	17.99	9	7.8
23	18	7.9	8.53
23	18	6.9	9.08
23	18	5.9	9.62
23	17.85	5	10.31
16.01	13.5	9	3.62

Continued on next page

Tab. A.6 (continued).

PRC-1 in bar	FIRC-1 in kg/h	SC in K	DPR-1 in bar
16	13.5	8	3.68
16	13.5	7	3.73
16	13.5	6	3.78
16	13.5	5	3.83
16	13.49	8.8	3.68
16	13.5	8	3.83
16	13.5	7	4
16	13.51	6.1	4.16
16	13.51	5.2	4.32

Tab. A.7: *Comparison of the experimental data in the copper and steel capillary tube for the measurement series in Tab. 3.6, SC = Subcooling, DPR-1$_{\text{diff}}$=(DPR-1$_{\text{Steel}}$-DPR-1$_{\text{Copper}}$)/DPR-1$_{\text{Copper}}$. Positive values of DPR-1$_{diff}$ mean that the pressure drop in the steel capillary is higher than in the copper capillary (mean values of the redundant measurement series).*

Copper				Steel				
PRC-1 in bar	FIRC-1 in kg/h	SC in K	DPR-1 in bar	PRC-1 in bar	FIRC-1 in kg/h	SC in K	DPR-1 in bar	DPR-1$_{\text{diff}}$ in %
16	13.5	5	3.95	16.01	13.49	5.2	4.46	12.91
16	13.5	6	3.8	16	13.49	6	4.29	12.89
16	13.5	7	3.68	16.01	13.5	7.1	4.07	10.6
16	13.5	8	3.55	16	13.5	8.1	3.86	8.73
16	13.5	9	3.34	16.01	13.5	9	3.62	8.38
16	13.5	8	3.35	16	13.5	8	3.68	9.85
16	13.5	7	3.36	16	13.5	7	3.73	11.01
16	13.5	6	3.39	16	13.5	6	3.78	11.5
16	13.5	5	3.42	16	13.5	5	3.83	11.99
18	15	5	5.4	18	15	5.1	6.45	18.57
18	15	6	4.73	18	15	6.1	5.88	24.31
18	15	7	4.61	18	15	7.1	5.39	16.92
18	15	8	4.46	18	15	8	5.03	12.78

Continued on next page

Tab. A.7 (continued).

Copper				Steel				
PRC-1 in bar	FIRC-1 in kg/h	SC in K	DPR-1 in bar	PRC-1 in bar	FIRC-1 in kg/h	SC in K	DPR-1 in bar	$DPR\text{-}1_{diff}$ in %
18	15	9	4.31	18	15	9	4.61	6.96
18	14.99	8	4.46	18	15	8	4.7	5.38
18	15.01	7	4.6	18	15	7	4.81	4.57
18	15.03	6	4.81	18	15	6	4.95	2.91
18	15.01	4.9	4.98	18	15	5	5.63	13.05
20	15	4.9	5.22	20	15.01	5	5.79	10.92
20	15	6	5	20	15	6.1	5.2	4.84
20	15	7	4.6	20	15	7.1	4.93	7.17
20	15	8	4.38	20	15	8.1	4.7	7.31
20	14.99	9	4.22	20	14.99	9.1	4.45	5.45
20	15	8	4.4	20	15	8.1	4.55	3.41
20	15	6.9	4.52	20	15	6.9	4.65	2.88
20	15	6	4.63	20	15	5.9	4.79	3.46
20	15	5	4.77	20	14.99	4.9	4.97	4.19
23	16.5	5	6.8	23.02	16.49	5	7.56	11.18
23	16.51	6	6.33	23	16.5	6	7.1	12.16
23	16.5	7	5.74	23	16.49	7	6.59	14.81
23	16.5	8	5.42	23	16.5	8	6.16	13.65
23	16.5	9	5.25	23.01	16.49	9.1	5.72	8.95
23	16.5	7.9	5.43	23	16.5	8	6.05	11.42
23	16.5	6.9	5.6	23	16.5	6.9	6.3	12.5
23	16.5	5.9	5.76	23	16.5	5.95	6.6	14.58
23	16.51	5	6.7	23	16.51	5	7.2	7.46
25	16.5	5	6.34	25.02	16.51	5.2	7.52	18.61
25	16.5	6	5.78	25	16.5	6.2	6.97	20.59
25	16.5	7	5.43	25	16.5	7	6.56	20.81
25	16.5	8.1	5.27	25	16.5	8	6.13	16.32
25	16.49	9.1	5.05	24.95	16.49	8.9	5.84	15.64
25	16.5	8	5.28	25.01	16.5	3	6.06	14.77

Continued on next page

Tab. A.7 (continued).

Copper				Steel				
PRC-1 in bar	FIRC-1 in kg/h	SC in K	DPR-1 in bar	PRC-1 in bar	FIRC-1 in kg/h	SC in K	DPR-1 in bar	$DPR\text{-}1_{diff}$ in %
25	16.5	7	5.44	25	16.5	7.1	6.28	15.44
25	16.5	5.9	5.59	25	16.5	6	6.56	17.35
25	16.5	5	6.08	25	16.5	5	7.05	15.95
23	18	5	10.01	23	17.78	5	11.3	12.89
23	18	6	8.71	23	18.09	6	11.22	28.82
23	18	7.1	7.87	23	18.09	7	10.66	35.45
23	18	8	6.69	23	18	8	8.6	28.55
23	18	9	6.46	23	17.99	9	7.8	20.74
23	18	8	6.7	23	18	7.9	8.53	27.31
23	18	6.9	7.05	23	18	6.9	9.08	28.79
23	18	6	8.4	23	18	5.9	9.62	14.52
23	18	5	9.09	23	17.85	5	10.31	13.42
25	18	5	8.8	25	18	4.9	10.88	23.64
25	18	6	8.23	25	18	5.9	9.81	19.2
25	18	7.1	7.52	25	18	7.1	8.71	15.82
25	18	8.1	6.56	25	18	8.1	8.01	22.1
24.99	18	9.1	6.39	25	17.99	9.1	7.44	16.43
25.01	18	8	6.58	25	18	8	7.97	21.12
25	18	7	6.86	25	18	7	8.43	22.89
25	18	6	7.66	25	17.99	6	9.47	23.63
25	18	5	8.46	25	18	5	10.13	19.74

Appendix B

Investigation of the Inner Diameter and the Roughness

Tab. B.1: *Statistical results of the measurements of the inner diameter of the copper capillary test samples.*

Sample	Diameter 1 in µm	Diameter 2 in µm	Diameter 3 in µm	Diameter 4 in µm	Diameter 5 in µm	Mean Value in µm	Standard Deviation in µm
Inlet	1235.3	1273.4	1178.2	1203.8	1205.6	1219.2	32.6
Outlet	1295.4	1299.9	1289.3	1282.3	1279.7	1289.3	7.6
D-1	1147.1	1151.8	1156.8	1147.8	1148.1	1150.3	3.6
D-2	1134.3	1120.1	1128.5	1123.0	1128.4	1126.8	4.9
D-3	1114.8	1115.3	1120.7	1108.9	1108.9	1113.7	4.4

Appendix B Investigation of the Inner Diameter and the Roughness

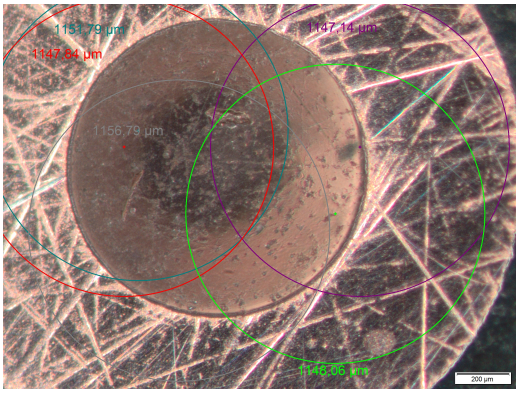

Fig. B.1: *Exemplary measurements of the inner diameter of a test sample (D-1) under the light microscope.*

Fig. B.2: *Preparation of half-pipes of the capillary test samples for the investigation of the roughness of the inner surface.*

Tab. B.2: *Statistical results of the measurement of the roughness of the inner surface of the copper capillary test samples.*

	Ra		Rz	
Sample	**Mean Value in µm**	**Standard Deviation in µm**	**Mean Value in µm**	**Standard Deviation in µm**
R1	0.099	0.013	1.200	0.380
R2	0.100	0.018	1.400	0.394
R3	0.103	0.018	1.260	0.398
R4	0.102	0.016	1.280	0.391

Tab. B.3: *Statistical results of the measurements of the inner diameter of the steel capillary test samples.*

Sample	Diameter 1 in µm	Diameter 2 in µm	Diameter 3 in µm	Diameter 4 in µm	Diameter 5 in µm	Mean Value in µm	Standard Deviation in µm
Inlet	1180.0	1183.6	1173.2	1189.9	1180.6	1181.5	5.4
Outlet	1137.9	1073.4	1160.2	1148.0	1156.8	1150.7	31.9
D-1	1180.0	1183.6	1173.2	1189.9	1180.6	1181.5	5.4
D-2	1176.1	1177.7	1176.1	1182.3	1184.9	1179.4	3.5
D-3	1185.1	1177.3	1181.5	1184.5	1178.2	1181.3	3.2

Appendix C

Transient Simulation of the Flow Model

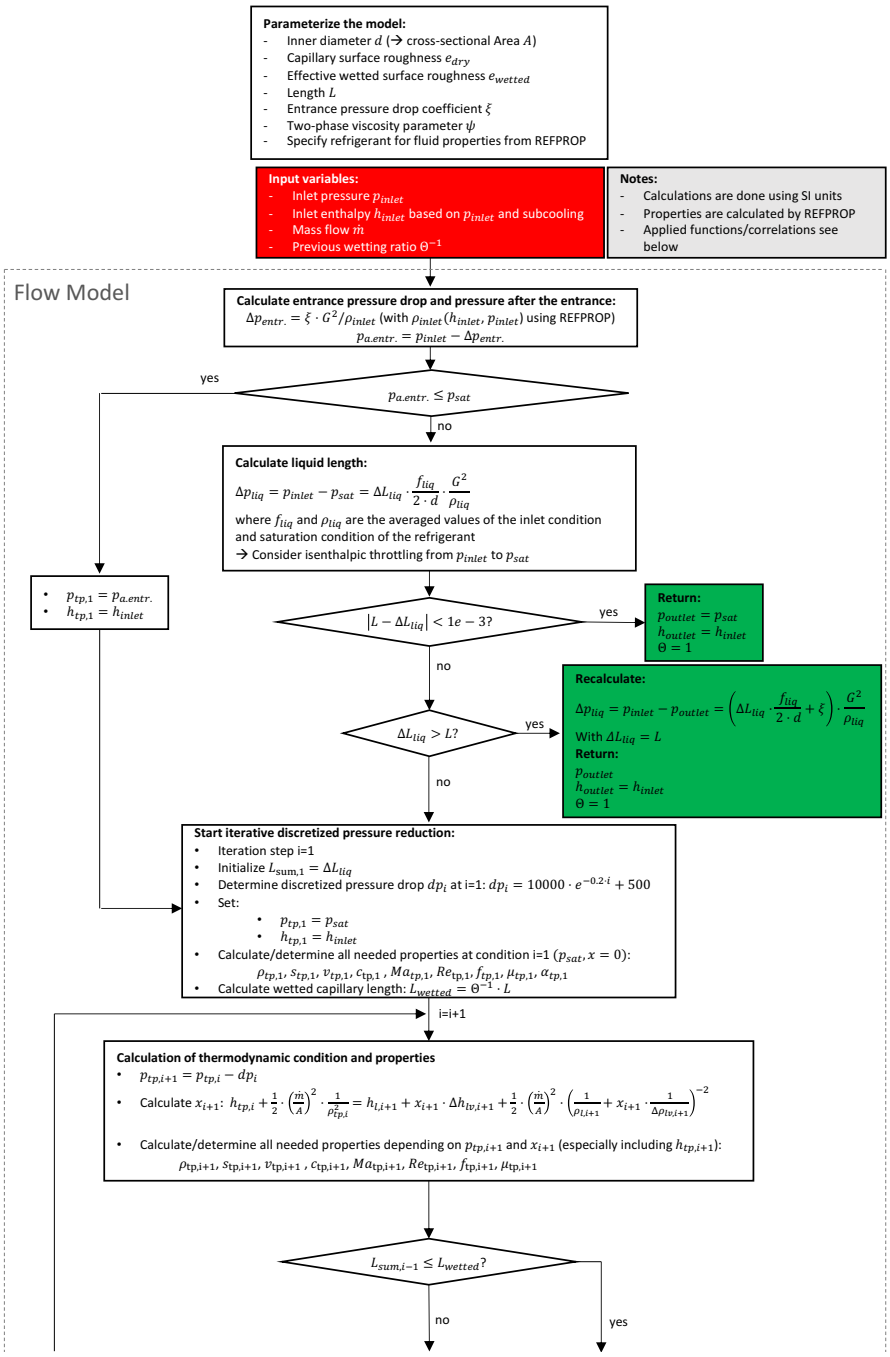
Parameterize the model:
- Inner diameter d (→ cross-sectional Area A)
- Capillary surface roughness e_{dry}
- Effective wetted surface roughness e_{wetted}
- Length L
- Entrance pressure drop coefficient ξ
- Two-phase viscosity parameter ψ
- Specify refrigerant for fluid properties from REFPROP
Input variables:
- Inlet pressure p_{inlet}
- Inlet enthalpy h_{inlet} based on p_{inlet} and subcooling
- Mass flow $\dot{m}$
- Previous wetting ratio Θ^{-1}
Notes:
- Calculations are done using SI units
- Properties are calculated by REFPROP
- Applied functions/correlations see below
Flow Model
Calculate entrance pressure drop and pressure after the entrance:
$\Delta p_{entr.} = \xi \cdot G^2/\rho_{inlet}$ (with $\rho_{inlet}(h_{inlet}, p_{inlet})$ using REFPROP)
$p_{a.entr.} = p_{inlet} - \Delta p_{entr.}$
$p_{a.entr.} \leq p_{sat}$
yes
no
Calculate liquid length:
$\Delta p_{liq} = p_{inlet} - p_{sat} = \Delta L_{liq} \cdot \frac{f_{liq}}{2 \cdot d} \cdot \frac{G^2}{\rho_{liq}}$
where f_{liq} and ρ_{liq} are the averaged values of the inlet condition and saturation condition of the refrigerant
→ Consider isenthalpic throttling from p_{inlet} to p_{sat}
$p_{tp,1} = p_{a.entr.}$
$h_{tp,1} = h_{inlet}$
$|L - \Delta L_{liq}| < 1e-3$?
yes
Return:
$p_{outlet} = p_{sat}$
$h_{outlet} = h_{inlet}$
$\Theta = 1$
no
$\Delta L_{liq} > L$?
yes
Recalculate:
$\Delta p_{liq} = p_{inlet} - p_{outlet} = \left(\Delta L_{liq} \cdot \frac{f_{liq}}{2 \cdot d} + \xi\right) \cdot \frac{G^2}{\rho_{liq}}$
With $\Delta L_{liq} = L$
Return:
p_{outlet}
$h_{outlet} = h_{inlet}$
$\Theta = 1$
no
Start iterative discretized pressure reduction:
- Iteration step i=1
- Initialize $L_{sum,1} = \Delta L_{liq}$
- Determine discretized pressure drop dp_i at i=1: $dp_i = 10000 \cdot e^{-0.2 \cdot i} + 500$
- Set:
  - $p_{tp,1} = p_{sat}$
  - $h_{tp,1} = h_{inlet}$
- Calculate/determine all needed properties at condition i=1 ($p_{sat}, x = 0$):
  $\rho_{tp,1}$, $s_{tp,1}$, $v_{tp,1}$, $c_{tp,1}$, $Ma_{tp,1}$, $Re_{tp,1}$, $f_{tp,1}$, $\mu_{tp,1}$, $\alpha_{tp,1}$
- Calculate wetted capillary length: $L_{wetted} = \Theta^{-1} \cdot L$
i=i+1
Calculation of thermodynamic condition and properties
- $p_{tp,i+1} = p_{tp,i} - dp_i$
- Calculate x_{i+1}: $h_{tp,i} + \frac{1}{2} \cdot \left(\frac{\dot{m}}{A}\right)^2 \cdot \frac{1}{\rho^2_{tp,i}} = h_{l,i+1} + x_{i+1} \cdot \Delta h_{lv,i+1} + \frac{1}{2} \cdot \left(\frac{\dot{m}}{A}\right)^2 \cdot \left(\frac{1}{\rho_{l,i+1}} + x_{i+1} \cdot \frac{1}{\Delta p_{lv,i+1}}\right)^{-2}$
- Calculate/determine all needed properties depending on $p_{tp,i+1}$ and x_{i+1} (especially including $h_{tp,i+1}$):
  $\rho_{tp,i+1}$, $s_{tp,i+1}$, $v_{tp,i+1}$, $c_{tp,i+1}$, $Ma_{tp,i+1}$, $Re_{tp,i+1}$, $f_{tp,i+1}$, $\mu_{tp,i+1}$
$L_{sum,i-1} \leq L_{wetted}$?
no
yes

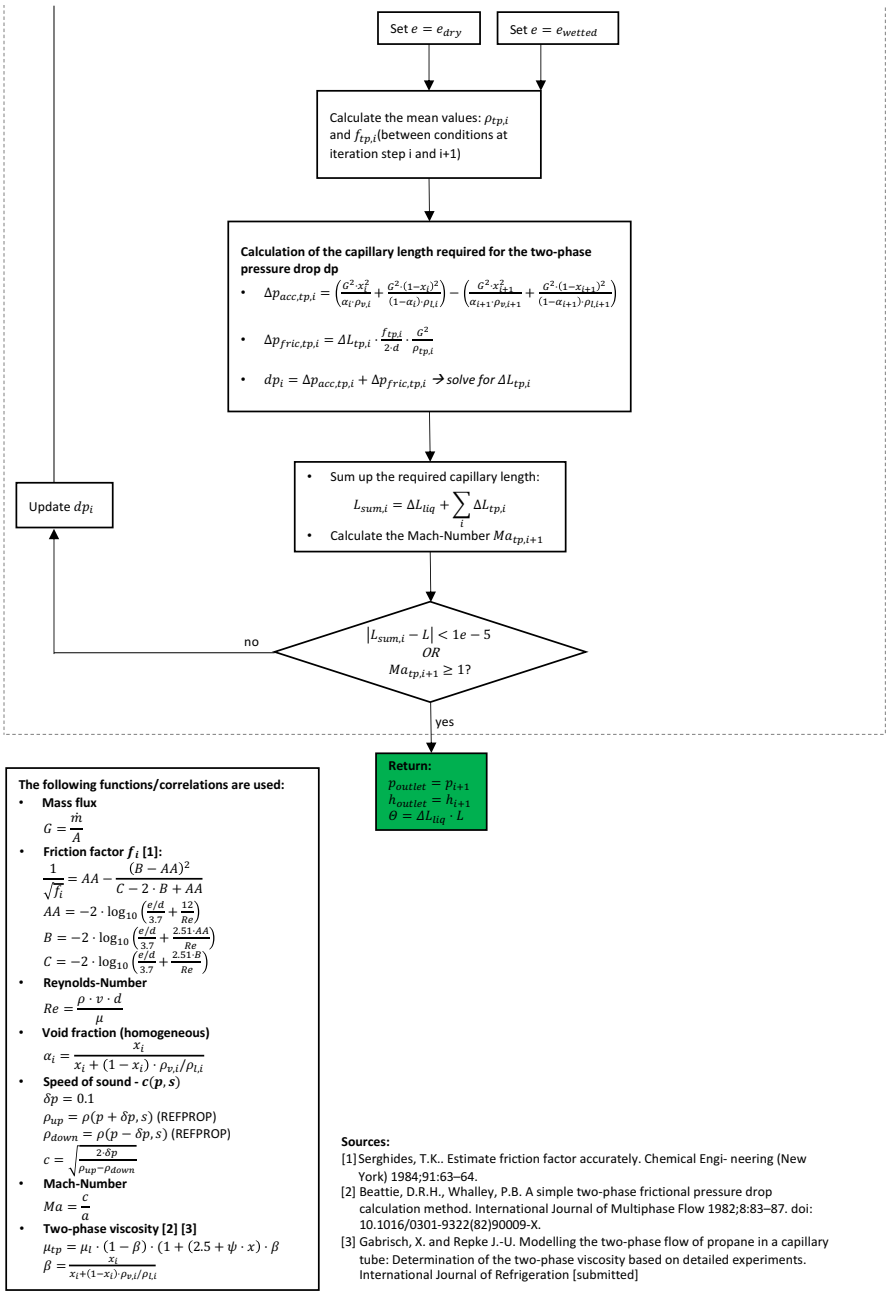

Fig. C.1: *Solution algorithm of the transient flow model simulation (Source: (Gabrisch and Repke, 2021)).*

Appendix D

Comparison between Experimental and Numerical Results

Fig. D.1 classifies the calculated pressure drops according to their corresponding void fraction at the capillary outlet. The histogram shows how the percentage shares of the classified void fractions distribute across the relative error of the pressure drop prediction. It shows that the higher the outlet void fraction (i.e. the higher the ratio of the two-phase flow), the more the model underestimates the pressure drop and the higher is the deviation from the measured pressure drop. Flow conditions that end up in a void fraction of up to 55 % are predicted with a relative error of ± 10 %.

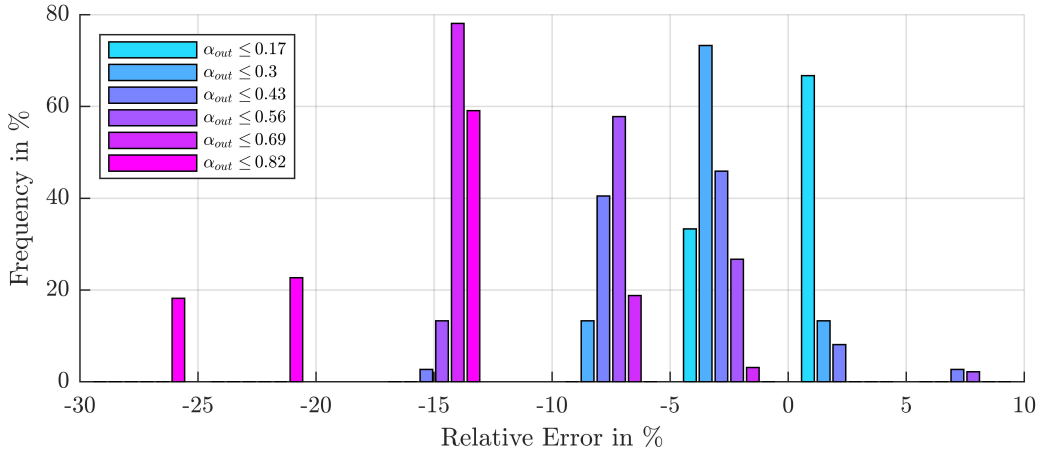

Fig. D.1: *Histogram of the deviation of the predicted pressure drops from the measured pressure drops (DPR-1) in the copper capillary for the increasing subcooling paths applying the viscosity correlation of Beattie and Whalley (1982) and the parametrization: e=Rz_{Copper}=1.285e-6 m , ξ_{Rz}=2.3475 and ψ_{Rz}=6.1714 .*

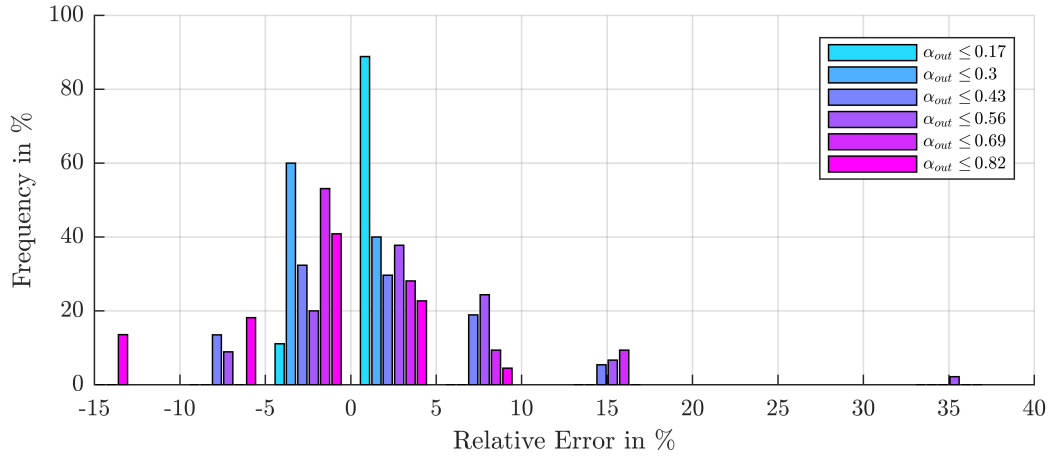

Fig. D.2: *Histogram of the deviation of the predicted pressure drops from the measured pressure drops (DPR-1) in the copper capillary for the increasing subcooling paths applying the modified B&W viscosity correlation and the parametrization: e=Rz_{Copper}=1.285e-6 m , ξ_{Rz}=2.3475 and ψ_{Rz}=6.1714 .*

Tab. D.1: *Operating conditions from Tab. A.3 that are excluded from the parameter estimation of* e_{wetted}.

Inlet Pressure in bar	**Mass Flow** in kg/h	**Subcooling** in K	
20	15	5.01	4.66
20	15	4.96	4.88
20	16.5	5.01	7.04
20	16.5	5	7.06
20	16.5	6.03	6.05
20	16.5	6	6.06
21	16.5	5.01	6.81
21	16.5	5.05	6.99
23	16.5	4.91	6.69
23	16.5	5.01	6.7
23	17.99	5.04	9.08
23	18	5.01	9.1
23	17.99	5.96	8.52
23	18	5.96	8.28
25	16	5.04	5.36
25	16.5	4.96	6.28
25	16.5	5.07	5.88
25	18	5	8.57
25.01	18	5.02	8.36
25	18	5.96	7.97
25	18	6.04	7.36

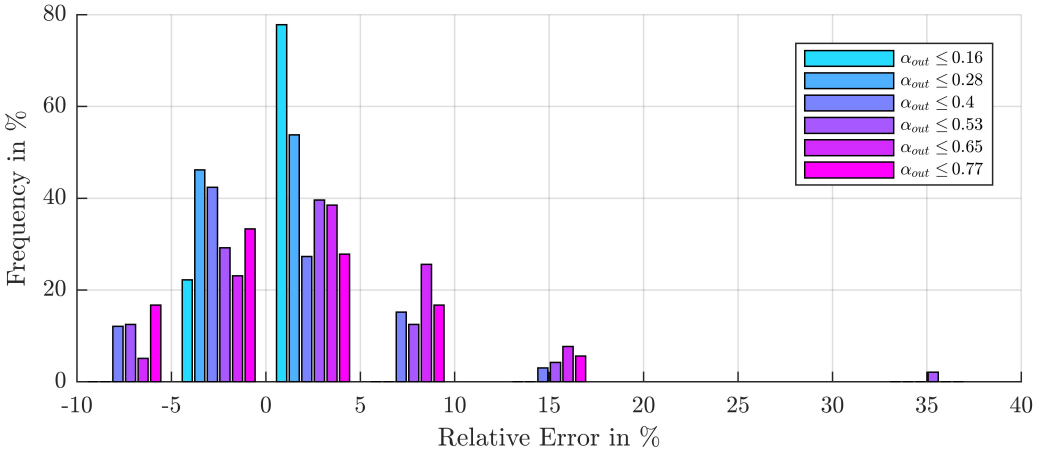

Fig. D.3: *Histogram of the deviation of the predicted pressure drops from the measured pressure drops (DPR-1) for the decreasing subcooling paths applying the modified B&W viscosity correlation and the parametrization: e = Rz_{Copper} = 1.285e-6 m , ξ_{Rz} = 2.3475 , ψ_{Rz} = 6.1714 and $e_{wetted,Rz,Copper}$ = 3.5906e-10 m (classified by the predicted void fraction α_{out} at the outlet of the capillary).*

List of References

Asker, M., O. E. Turgut, and M. T. Coban (2014): A review of non iterative friction factor correlations for the calculation of pressure drop in pipes. *Journal of Science and Technology* 4 (1), 1–8. DOI: 10.17678/beujst.90203 (cit. on p. 59).

Awad, M. M. and Y. S. Muzychka (2008): Effective property models for homogeneous two-phase flows. *Experimental Thermal and Fluid Science* 33 (1), 106–113. DOI: 10.1016/j.expthermflusci.2008.07.006 (cit. on pp. 16, 62, 73).

Bansal, P. K. and G. Wang (2004): Numerical analysis of choked refrigerant flow in adiabatic capillary tubes. *Applied Thermal Engineering* 24, 851–863. DOI: 10.1016/j.applthermaleng.2003.10.010 (cit. on p. 11).

Beattie, D. R. H. and P. B. Whalley (1982): A Simple Two-Phase Frictional Pressure Drop Calculated Method. *International Journal of Multiphase Flow* 8, 83–87. DOI: 10.1016/0301-9322(82)90009-X (cit. on pp. 60, 62, 69, 73–77, 79, 83–85, 95, 102, 110, 144).

Bittle, R. R., J. A. Carter, and J. V. Oliver (2001): Extended insight into the metastable liquid region behavior in an adiabatic capillary tube. *HVAC and R Research* 7 (2), 107–123. DOI: 10.1080/10789669.2001.10391266 (cit. on p. 21).

Chang, S. D. and S. T. Ro (1996): Experimental and numerical studies on adiabatic flow of HFC mixtures in capillary tubes. In: *International Refirgeration and Air Condition Conference*, 83–87 (cit. on pp. 20–22).

Chen, Z. H., R. Y. Li, and Z. Y. Chen (1990): A correlation for metastable flow of refrigerant 12 through capillary tubes. *ASHRAE Transactions* 96 (1), 550–554 (cit. on pp. 2, 3, 20, 22).

Cicchitti, A., C. Lombardi, M. Silvestri, G. Soldaini, and R. Zavattarelli (1959): Two-phase cooling experiments: Pressure drop, heat transfer and burnout measurements. *Energia Nucleare* 7 (cit. on pp. 62, 73).

Colebrook, C. F. (1939): Turbulent flow in pipes, with particular reference to the transition region between the smooth and rough pipe laws.. *Journal of the Institution of Civil Engineers* 11 (4), 133–156. DOI: 10.1680/ijoti.1939.13150 (cit. on pp. 15, 59, 111).

Collier, J. G. and J. R. Thome (1994a): Introduction. In: *Convective boiling and condensation*. 3rd ed. New York: Oxford University Press Inc. Chap. 1, 1–33 (cit. on pp. 17, 18).

Collier, J. G. and J. R. Thome (1994b): The basic models. In: *Convective Boiling and Condensation*. New York: Oxford University Press Inc. Chap. 2, 34–83 (cit. on pp. 16, 17).

Cooper, L., C. K. Chu, and W. R. Brisken (1957): Simple selection method for capillaries derived from physical flow conditions. *Refrigerating Engineering* (cit. on pp. 2, 20).

Del Col, D., M. Bortolato, and S. Bortolin (2014): Comprehensive experimental investigation of two-phase heat transfer and pressure drop with propane in a minichannel. *International Journal of Refrigeration* 47, 66–84. ISSN: 01407007. DOI: 10.1016/j.ijrefrig.2014.08.002. URL: http://dx.doi.org/10.1016/j.ijrefrig.2014.08.002 (cit. on p. 23).

Dinçer, I. and M. Kanoglu (2010): *Refrigeration systems and applications*. 2nd ed. John Wiley & Sons, Inc., 168–169 (cit. on p. 10).

Dirik, E., A. A. S. C. Inan, A. A. S. M. Y. Tanes, E. Dirik, C. Inan, and M. Yal˜m (1994): Numerical and Experimental Studies on Adiabatic and Nonadiabatic Capillary Tubes with HFC-134a. In: *International Refrigeration and Air Condition Conference*, 365–370 (cit. on pp. 20, 57).

Dubba, S. K. and R. Kumar (2017): Flow of refrigerants through capillary tubes: A state-of-the-art. *Experimental Thermal and Fluid Science* 81, 370–381. DOI: 10.1016/j.expthermflusci.2016.09.012 (cit. on pp. 1, 3, 19, 20, 29).

Dukler, A. E., M. Wicks III, and R. G. Cleveland (1964): Frictional pressure drop in two-phase flow: B. An approach through similarity analysis. *AIChE Journal* 10 (1), 44–51. DOI: 10.1002/aic.690100118 (cit. on pp. 62, 73).

Feburie, V., M. Giot, S. Granger, and J. Seynhaeve (1993): A model for choked flow through cracks with inlet subcooling. *Internation Journal of Multiphase Flow* 19 (4), 541–562 (cit. on pp. 3, 21).

Fiorelli, F. A., C. A. Silva, and A. A. Huerta (2013): Metastable flow of R-410A in capillary tubes. *Applied Thermal Engineering* 51, 1181–1190. ISSN: 13594311. DOI: 10.1016/j.applthermaleng.2012.09.037 (cit. on p. 23).

Fourar, M. and S. Bories (1995): Experimental study of air-water two-phase flow through a fracture (narrow channel). *International Journal of Multiphase Flow* 21 (4), 621–637. DOI: 10.1016/0301-9322(95)00005-I (cit. on pp. 62, 73).

Gabrisch, X., T. Grunert, and J.-U. Repke (2017): Dynamische Modellierung einer Kältemittel-Luft-Wärmepumpe - Analyse des Einflusses der Drosselmodellierung auf die Betriebspunktsimulation. In: *Deutsche Kälte- und Klimatagung*. Ed. by X. Gabrisch, T. Grunert, and J.-U. Repke. Bremen: Deutscher Kälte- und Klimatechnischer Verein (cit. on pp. 27, 32, 60).

Gabrisch, X. and J.-U. Repke (2020): Modelling the two-phase flow of propane in a capillary tube: Determination of the two-phase viscosity based on detailed experiments. *International Journal of Refrigeration* 118, 427–442. ISSN: 0140-7007. DOI: https://doi.org/10.1016/j.ijrefrig.2020.05.018. URL: https://www.sciencedirect.com/science/article/pii/S0140700720302279 (cit. on pp. 19, 26, 57, 69, 71–74, 76–79, 83, 96, 113, 114, 125).

Gabrisch, X. and J.-U. Repke (2021): Modelling the two-phase flow of propane in a capillary tube: Investigating and modelling the metastable flow and hysteresis effect. *International Journal of Refrigeration* 121, 126–135. ISSN: 0140-7007. DOI: https://doi.org/10.1016/j.ijrefrig.2020.10.030. URL: https://www.sciencedirect.com/science/article/pii/S0140700720304497 (cit. on pp. 19, 43, 44, 57, 64, 80–86, 119, 126, 141).

Gao, L., H. Eguchi, and Y. Tatara (2015): ID : 697 Effects of Boiling Hysteresis on Metastable Two-phase Flow of Refrigerant in a Straight Adiabatic Capillary

Tube. In: *ICR*. DOI: S1050-6411(08)00010-2[pii]\r10.1016/j.jelekin.2008.01.003[doi] (cit. on pp. 2, 22, 57).

García-Valladares, O. (2007): Numerical simulation of non-adiabatic capillary tubes considering metastable region. Part I: Mathematical formulation and numerical model. *International Journal of Refrigeration* 30 (4), 642–653. DOI: 10.1016/j.ijrefrig.2006.08.015 (cit. on pp. 20, 22).

Guobing, Z. and Z. Yufeng (2006): Experimental investigation on hysteresis effect of refrigerant flowing through a coiled adiabatic capillary tube. *Energy Conversion and Management* 47 (18-19), 3084–3093. DOI: 10.1016/j.enconman.2006.03.007 (cit. on pp. 2, 3, 20, 22, 23, 29, 41, 68, 110).

Kim, L. S., K. D. Son, D. Sarker, J. H. Jeong, and S. H. Lee (2011): An assessment of models for predicting refrigerant characteristics in adiabatic and non-adiabatic capillary tubes. *Heat and Mass Transfer/Waerme- und Stoffuebertragung* 47 (2), 163–180. ISSN: 09477411. DOI: 10.1007/s00231-010-0697-0 (cit. on pp. 21, 22).

Lee, W. J. and J. H. Jeong (2019): Evaluation of the constituent correlations for predicting the refrigerant flow characteristics in adiabatic helically coiled capillary tubes. *Journal of Mechanical Science and Technology* 33 (5), 2123–2136. ISSN: 19763824. DOI: 10.1007/s12206-019-0415-x (cit. on pp. 21, 23).

Lemmon, E. W., I. H. Bell, M. L. Huber, and M. O. McLinden (2013): *NIST Standard Reference Database 23: Reference Fluid Thermodynamic and Transport Properties-REFPROP, Version 9.1, National Institute of Standards and Technology*. DOI: http://dx.doi.org/10.18434/T4JS3C. URL: https://www.nist.gov/srd/refprop (cit. on p. 23).

Lemmon, E. W., M. O. McLinden, and W. Wagner (2009): Thermodynamic properties of propane. III. A reference equation of state for temperatures from the melting line to 650 K and pressures up to 1000 MPa. *Journal of Chemical and Engineering Data* 54 (12), 3141–3180. DOI: 10.1021/je900217v (cit. on p. 24).

Li, R.-Y., S. Lin, Z.-Y. Chen, and Z.-H. Chen (1990): Metastable flow of R12 through capillary tubes. *International Journal of Refrigeration* 13 (3), 181–186. ISSN: 01407007. DOI: 10.1016/0140-7007(90)90073-6 (cit. on pp. 19, 20).

Lillo, G., R. Mastrullo, A. W. Mauro, and L. Viscito (2018): Flow boiling heat transfer, dry-out vapor quality and pressure drop of propane (R290): Experiments and assessment of predictive methods. *International Journal of Heat and Mass Transfer* 126, 1236–1252. DOI: https://doi.org/10.1016/j.ijheatmasstransfer.2018.06.069 (cit. on p. 23).

Lin, S., C. C. K. Kwok, R.-Y. Li, Z.-H. Chen, and Z.-Y. Chen (1991): Local frictional pressure drop during vaporization of R-12 through capillary tubes. *International Journal of Multiphase Flow* 17 (1), 95–102. DOI: https://doi.org/10.1016/0301-9322(91)90072-B (cit. on pp. 62, 73).

Longo, G. A., S. Mancin, G. Righetti, and C. Zilio (2017): Hydrocarbon refrigerants HC290 (Propane) and HC1270 (Propylene) low GWP long-term substitutes for HFC404A: A comparative analysis in vaporisation inside a small-diameter horizontal smooth tube. *Applied Thermal Engineering* 124, 707–715. ISSN: 13594311. DOI: 10.1016/j.applthermaleng.2017.06.080. URL: http://dx.doi.org/10.1016/j.applthermaleng.2017.06.080 (cit. on p. 23).

Maqbool, M., B. Palm, and R. Khodabandeh (2013): Investigation of two phase heat transfer and pressure drop of propane in a vertical circular minichannel. *Experimental Thermal and Fluid Science* 46, 120–130. DOI: 10.1016/j.expthermflusci.2012.12.002 (cit. on p. 23).

McAdams, H. W., W. K. Woods, and L. C. Heroman (1942): Vaporization inside horizontal tubes II-benzene-oil mixtures. *Trans. ASME* 64 (3), 193–200 (cit. on pp. 62, 73).

Melo, C., C. B. Neto, R. T. S. Ferreira, and R. H. Pereira (1998): Constitutive Equations for Capillary Tube Modeling. In: *International Refrigeration and Air Condition Conference*, 431–436 (cit. on pp. 20, 21).

Meyer, J. J. and W. E. Dunn (1998): New insights into the behavior of the metastable region of an operating capillary tube. *HVCR&R* 4 (1), 105–115 (cit. on pp. 2, 3, 20, 21, 23, 37, 111).

Mittal, M. K., R. Kumar, and A. Gupta (2009): Numerical analysis of adiabatic flow of refrigerant through a spiral capillary tube. *International Journal of Thermal*

Sciences 48 (7), 1348–1354. DOI: 10.1016/j.ijthermalsci.2009.01.003 (cit. on p. 21).

Müller, D., E. Esche, D. C. López C., and G. Wozny (2014): An algorithm for the identification and estimation of relevant parameters for optimization under uncertainty. *Computers and Chemical Engineering* 71, 94–103. DOI: 10.1016/j.compchemeng.2014.07.007 (cit. on p. 97).

Nikuradse, J. (1933): Laws of flow in rough pipes. *Forschung auf dem Gebiete des Ingenieurwesens* 4. DOI: 10.1016/s0016-0032(36)90073-x (cit. on p. 15).

Novianto, S., A. S. Pamitran, R. Koestoer, and K. Saito (2018): Two-phase Frictional Pressure Drop of Propane with Prediction Methods of Viscosity and Density in 500 μm Diameter Tube. *IOP Conference Series: Materials Science and Engineering* 316. ISSN: 1757899X. DOI: 10.1088/1757-899X/316/1/012058 (cit. on p. 23).

Pamitran, A. S., K. I. Choi, J. T. Oh, and P. Hrnjak (2010): Characteristics of two-phase flow pattern transitions and pressure drop of five refrigerants in horizontal circular small tubes. *International Journal of Refrigeration* 33 (3), 578–588. ISSN: 01407007. DOI: 10.1016/j.ijrefrig.2009.12.009. URL: http://dx.doi.org/10.1016/j.ijrefrig.2009.12.009 (cit. on p. 23).

Pohlmann, W. (2010): *Pohlmann Taschenbuch der Kältetechnik : Grundlagen, Anwendungen, Arbeitstabellen und Vorschriften*. VDE Verlag, 373–374. ISBN: 9783800733934. URL: https://books.google.de/books?id=iSOqlAEACAAJ (cit. on p. 10).

Quiñones-Cisneros, S. E. and U. K. Deiters (2006): Generalization of the friction theory for viscosity modeling. *Journal of Physical Chemistry B* 110 (25), 12820–12834. DOI: 10.1021/jp0618577 (cit. on p. 24).

Rasti, M. and J. H. Jeong (2018): A generalized continuous empirical correlation for predicting refrigerant mass flow rates through adiabatic capillary tubes. *Applied Thermal Engineering* 139 (April), 47–60. ISSN: 13594311. DOI: 10.1016/j.applthermaleng.2018.04.111. URL: https://doi.org/10.1016/j.applthermaleng.2018.04.111 (cit. on pp. 21, 23).

Ribatski, G. (2013): A critical overview on the recent literature concerning flow boiling and two-phase flows inside micro-scale channels. *Experimental Heat*

Transfer 26 (2-3), 198–246. DOI: 10.1080/08916152.2012.737189 (cit. on pp. 3, 19, 23).

Sauer, H. J. and R. H. Howell (1983): *Heat Pump Systems*. John Wiley & Sons, Inc., 116 (cit. on pp. 7, 10).

Schade, H. and E. Kunz (2007a): Rohrhydraulik. In: *Strömungslehre*. Ed. by F. Kameier and C. O. Paschereit. 3rd ed. de Gruyter. Chap. 5, 102–103 (cit. on pp. 15, 63).

Schade, H. and E. Kunz (2007b): Rohrhydraulik. In: *Strömungslehre*. Ed. by F. Kameier and C. O. Paschereit. 3rd ed. de Gruyter. Chap. 5, 106 (cit. on p. 58).

Sempértegui-Tapia, D. F. and G. Ribatski (2017): Two-phase frictional pressure drop in horizontal micro-scale channels: Experimental data analysis and prediction method development. *International Journal of Refrigeration* 79, 143–163. DOI: 10.1016/j.ijrefrig.2017.03.024 (cit. on p. 19).

Serghides, T. K. (1984): Estimate friction factor accurately. *Chemical Engineering (New York)* 91, 63–64 (cit. on pp. xii, 59, 111).

Simon Fries, Severin Skusa, A. L. (2019): Heat transfer and pressure drop of condensation of hydrocarbons in tubes. *Heat and Mass Transfer* 55 (1), 33–40. DOI: https://doi.org/10.1007/s00231-018-2318-2 (cit. on p. 23).

Wang, J., F. Cao, Z. Wang, Y. Zhao, and L. Li (2012): Numerical simulation of coiled adiabatic capillary tubes in CO 2 transcritical systems with separated flow model including metastable flow. *International Journal of Refrigeration* 35 (8), 2188–2198. DOI: 10.1016/j.ijrefrig.2012.07.012 (cit. on p. 22).

Wang, S., M. Q. Gong, G. F. Chen, Z. H. Sun, and J. F. Wu (2014): Two-phase heat transfer and pressure drop of propane during saturated flow boiling inside a horizontal tube. *International Journal of Refrigeration* 41, 200–209. ISSN: 01407007. DOI: 10.1016/j.ijrefrig.2013.03.019 (cit. on p. 23).